THE TRANSITION FROM THE TURBULENT TO THE LAMINAR REGIME FOR INTERNAL CONVECTIVE FLOW WITH LARGE PROPERTY VARIATIONS

by

Carlos Weldon Coon, Jr.

A Dissertation Submitted to the Faculty of the

DEPARTMENT OF AEROSPACE AND MECHANICAL ENGINEERING
WITH A MAJOR IN MECHANICAL ENGINEERING

In Partial Fulfillment of the Requirements
For the Degree of

DOCTOR OF PHILOSOPHY

In the Graduate College

THE UNIVERSITY OF ARIZONA

1968

THE UNIVERSITY OF ARIZONA

GRADUATE COLLEGE

I hereby recommend that this dissertation prepared under my direction by Carlos Weldon Coon, Jr.

entitled The Transition from the Turbulent to the Laminar Regime for Internal Convective Flow with Large Property Variations

be accepted as fulfilling the dissertation requirement of the degree of Doctor of Philosophy

H. C. Perkins	4/19/68
Dissertation Director	Date

After inspection of the final copy of the dissertation, the following members of the Final Examination Committee concur in its approval and recommend its acceptance:*

H. C. Perkins	4/19/68
D. M. McElwain	19 April 1968
E. R. Parker	4/19/68
Leon Glicksman	4/23/68
L. C. McIntyre Jr.	4/26/68

*This approval and acceptance is contingent on the candidate's adequate performance and defense of this dissertation at the final oral examination. The inclusion of this sheet bound into the library copy of the dissertation is evidence of satisfactory performance at the final examination.

STATEMENT BY AUTHOR

This dissertation has been submitted in partial fulfillment of requirements for an advanced degree at The University of Arizona and is deposited in the University Library to be made available to borrowers under rules of the Library.

Brief quotations from this dissertation are allowable without special permission, provided that accurate acknowledgment of source is made. Requests for permission for extended quotation from or reproduction of this manuscript in whole or in part may be granted by the head of the major department or the Dean of the Graduate College when in his judgment the proposed use of the material is in the interests of scholarship. In all other instances, however, permission must be obtained from the author.

SIGNED: Carlos W. Coon Jr.

ACKNOWLEDGMENTS

The author would like to express sincere appreciation to the many individuals and institutions that contributed to the success of this venture. Professor H. C. Perkins has been singularly helpful throughout all phases of the project. Professor D. M. McEligot provided the basis of the definition of momentum thickness for a tube along with numerous other suggestions during the course of the work. Lt. Col. Joseph Spitler, U. S. Army, was responsible for a considerable portion of the computer program used for data reduction. Mr. Larry Cooper, Mr. John Heiny, and Mr. James Wharrie assisted in the construction of the apparatus and in the accumulation of data, and Mr. Kenneth Bauer applied the touch of a true craftsman to delicate portions of the apparatus.

Financial assistance during the course of the project was received from the National Science Foundation through an Initiation Grant (Gk-247) awarded to Professor Perkins and from the U. S. Army Research Office (Durham). The National Aeronautics and Space Administration provided funds for equipment through the NASA Educational Allowance Committee of the Graduate College of The University of Arizona, and the National Science Foundation provided summer salary funds for the author through the NSF

Institutional Fund of the Research Coordinator of The University of Arizona. The author also received financial support from the Engineering Experiment Station and from the Aerospace and Mechanical Engineering Department of The University of Arizona. The Parker Seal Company donated the seals used to secure the test section flange.

TABLE OF CONTENTS

TABLE OF CONTENTS--Continued

LIST OF ILLUSTRATIONS

LIST OF ILLUSTRATIONS--Continued

LIST OF ILLUSTRATIONS--Continued

LIST OF TABLES

ABSTRACT

The results of a primarily experimental study of the transition from turbulent flow to laminar flow as a consequence of high heating rates are presented. Results are reported for hydrodynamically fully developed, low Mach number flows of air and helium through a vertical, electrically heated, circular tube at entering Reynolds numbers from 1700 to 40000 and wall-to-bulk temperature ratios to 4.4.

The experimental results for flow situations involving mild heating exhibit good agreement in comparison to generally accepted heat transfer and friction correlation relationships for both turbulent and laminar flow. At high heating rates, the departure from the turbulent correlations for initially turbulent flows is pronounced; in extreme cases the laminar correlations provide an accurate representation of the heat transfer and friction parameters in the downstream region of the tube. The laminar characteristics of the flow in the downstream region of the tube for high heating rates are graphically demonstrated by superposition of the experimental data points on the analytical thermal entry length solution for laminar flow in a circular tube with constant wall heat flux; experimental runs are classified as laminar, turbulent, or transitional on the basis of

these graphs. Reasonable agreement is demonstrated between the classification of experimental runs in the present work and the classification schemes suggested by McEligot, Ormand, and Perkins and by Bankston, Sibbitt, and Skoglund.

As a means of predicting the occurrence of a transition from turbulent flow to laminar flow, the experimental results are compared to the acceleration parameter suggested by Moretti and Kays and to a modified form of the parameter that is appropriate to a circular tube. It is suggested that the turbulent flow correlations do not provide acceptable predictions of the Nusselt number and the friction factor if the value $\frac{4 \mu q''}{G^2 D T c_p} \approx 1.5 \times 10^{-6}$ based on bulk properties, is exceeded for an initially turbulent flow situation.

It is further suggested that Nusselt numbers and friction factors at locations downstream from the point

$$\left(\frac{x}{D}\right)_{critical} \approx 2 \times 10^{-8} \left(T_{inlet}\right) \left(Re_{b,inlet}\right)^2 \left(\frac{T_w}{T_b}\right)_{max}^{-1}$$

for bulk temperatures in degrees Rankine, may be obtained from the laminar correlation equations even though the flow is initially turbulent.

CHAPTER I

INTRODUCTION

The problem of reverse transition, defined in this study as a transition from a turbulent flow to a laminar flow, is of interest both for practical reasons, ie., in the design of nuclear rocket engines, and for fundamental reasons, ie. as a possible contribution to the nature of the transition process. This study is concerned with a primarily experimental investigation of the reverse transition process in a circular tube. The reverse transition is caused by the action of large heating rates which in turn cause significant transport property variations, especially in the viscosity. The viscosity increases such that the Reynolds number based on tube diameter decreases sufficiently for the flow to undergo a transition from turbulent to laminar.

It is well known that flow situations can be classified in different regimes according to the motion of the fluid particles in the system. The laminar and turbulent regimes, and the transition region between them, have been the object of considerable investigation since the time of Osborne Reynolds. The area of laminar flow has received the most thorough investigation since the

governing equations can be solved either exactly or numerically for almost every situation. The turbulent regime has been attacked by many schemes, and some models, such as the use of the eddy diffusivity, have produced good results. The usual transition region is more elusive; it is usually described as a situation during which a laminar flow becomes unstable and undergoes a change into a turbulent flow. Rotta, according to Schlichting (1960), has depicted the situation in the transition region as an alternating flow with each cycle having a portion that is almost entirely laminar and a portion that is almost entirely turbulent. As reported by Schlichting (1960), criteria have been developed that will predict the onset of turbulence in a laminar external flow; thus, all of the usual flow situations can be analyzed with some degree of accuracy for some situations.

Although the occurrence of transition can be predicted for simple flow situations, there are numerous conditions that can be imposed on the flow that will alter the attitude of the system with respect to transition. For example, it has been found that the onset of turbulence in a circular tube will occur at a Reynolds number of about 2300 for a simple flow situation, but a roughened surface or a trip wire will initiate turbulent flow at a somewhat lower Reynolds number while a quiescent fluid and an

extremely smooth channel can be used to sustain laminar flow at much higher Reynolds numbers. In addition, as will be discussed in the next chapter, there are various other effects, such as rotation, channel configuration (pressure gradient), and heat transfer that can affect the occurrence of laminar or turbulent flow. Of particular interest in this investigation is the use of a large heat flux to vary the properties of the fluid; it is expected that a turbulent-to-laminar transition for tube flow can be effected in this manner.

The phenomenon of transition from a turbulent flow to a laminar flow due to a variation in gas properties has achieved interest by virtue of the proposed use of gas cooled nuclear reactors as space propulsion systems. The operating requirements of such devices are such that accurate design information is frequently not available, and the use of accepted correlations for heat transfer and friction parameters that were obtained for less strenuous situations can lead to erroneous results. For example, an acceptable gas cooled nuclear propulsion system must be capable of repeated on-off cycles; if the coolant supply is limited, then the required cooling portion of the cycle should be as economical as possible. A precise knowledge of the capability of energy transfer to the gas will allow the coolant flow to be minimized while still maintaining

safe operating temperatures in the core and nozzle. However, an unexpected transition from turbulent to laminar flow in the cooling tubes would cause a sharp decrease in the energy transfer to the gas and a subsequent rise in the wall temperature causing possible failure of the tubes. As is the case in numerous other areas, the demands of current technology require a deeper investigation of a physical phenomenon; the object of this work is to fulfill that need.

It is the goal of the present study to investigate the form of turbulent-to-laminar transition described above for gas flow at low Mach number through a tube; the phenomenon can be described in terms of the usual transition parameter, the Reynolds number, if that quantity is written in the following form:

$$Re = \frac{\rho D \bar{u}}{\mu} = \frac{4\dot{m}}{\pi \mu D}$$

In this expression, since the mass flow rate and the diameter are constant, the Reynolds number is a function only of the viscosity. For a gas, the viscosity increases as the temperature increases; the temperature extremes in this experiment correspond to an increase in the viscosity along the tube of about 500 percent. The nature of the experiment is such that a flow of gas with a low bulk temperature is suddenly subjected to a hot tube wall, so

that the viscosity near the wall can be on the order of four times the viscosity at the centerline. It is hypothesized that the result of this viscosity gradient, as described in later sections, is to reduce the turbulence generated near the wall. The flow then begins to exhibit laminar characteristics, and after the existing turbulence dies out, it can no longer be distinguished from a truly laminar flow. In this study the presence of laminar flow is detected primarily by temperature and pressure measurements; local values of heat transfer parameters and friction parameters are presented as evidence that the transition does in fact occur. In addition, a criterion for the onset of laminar flow is described; it is thought to be of value in design situations involving flow configurations of this nature.

It should be noted that the effect of heat transfer in this case is opposite to the accepted result for external flow. Schlichting (1960), for example, in a discussion of external boundary layers, quite bluntly states that heat transfer from the wall to a gas is a de-stabilizing influence if other factors are unchanged; it should increase the tendency of the flow toward turbulence. However, the relatively large changes in viscosity that are encountered in the present study are beyond the scope of the stability discussion as presented by

Schlichting. It should also be noted that, for external flow, the Reynolds number is based on the variable that represents distance from the leading edge of the body while for tube flow the Reynolds number is based on the diameter which remains constant. Furthermore, it is of particular significance that heat transfer from the wall to a gas is designated as a de-stabilizing influence without consideration of the effect of acceleration on the boundary layer. Both Moretti and Kays (1964) and Back and Seban (1967) have discussed the heat transfer characteristics of accelerated external flow situations, and it has been observed that the heat transfer coefficients in regions of strong acceleration are much lower than the values that would be typical of turbulent flow. The measured velocity profiles presented by Back and Seban reveal "laminar-like" behavior near the wall while corresponding temperature profiles indicate a reduction of the eddy transport near the wall. The implication of these experimental results is that, in the presence of free stream acceleration, heat transfer from the wall to the gas can exert a stabilizing influence on the flow.

The acceleration effect resulting from the presence of a heat flux from the wall to the gas is more pronounced for internal flow than for external flow. As the temperature of the gas increases, the density

decreases; and since the mass flow rate must remain constant, the result is an increase in velocity. In addition, the presence of friction in the tube creates a favorable pressure gradient. On the basis of these arguments, it would appear that a stabilizing influence is provided by a heat flux from the wall to a gas for internal flow situations; Bankston (1965) reported that this was indeed the case. In addition, the results to be presented later in this work show that the external flow parameters, such as those suggested by Moretti and Kays (1964), provide a good indication of the transition from turbulent to laminar flow for internal flow situations.

CHAPTER II

PREVIOUS INVESTIGATIONS

Several previous investigations have been conducted into the general situation of turbulent to laminar transition. Although the mechanism for creating transition in several cases has been different from that employed in the present work, reference is made to them in the interest of completeness.

The completely adiabatic work of Sibulkin (1962) involved the transition from turbulent flow to laminar flow by virtue of a change in the diameter of the surrounding tube. Gas flowing with a low turbulent Reynolds number through a small tube was allowed to expand into a larger tube; the Reynolds number was thus decreased by the ratio of the diameters. Hot wire anemometer measurements were used to confirm the presence of laminar flow in the larger tube. An outgrowth of the anemometer measurements was the discovery that the rate of decay of turbulence level was most rapid near the centerline and near the wall; the higher turbulence intensity in the middle region was attributed either to lower rates of diffusion minus production or to diffusion of turbulence energy from the other regions.

Several authors have investigated laminar boundary layers that have appeared under somewhat surprising conditions in various flow situations. Sergienko and Gretsov (1959) have described the occurrence of a laminar boundary layer in a supersonic nozzle that was supplied with a fully developed turbulent flow and was exhausting at a Mach number of 2.6. Measurements were made only at the inlet and outlet of the nozzle; in the opinion of the authors, the transition occurred in the converging section. Sternberg (1954) has investigated the case of a cone with a following attached cylinder in supersonic flow; it was discovered that a laminar boundary layer could exist on the cylinder while a turbulent boundary layer was maintained on the cone. In addition, the work of Wisniewski and Jack (1961) and of Richards and Stollery (1966) has shown that the laminar to turbulent transition point for a cooled body in hypersonic flow is sensitive to the wall-to-adiabatic wall temperature ratio; there is a range of temperature ratios for which the transition is withheld, and laminar flow persists for a much longer duration.

During the investigation of the boundary layer in a turbine nozzle cascade, Senoo (1958a, 1958b) found that a laminar boundary layer was present on the end-wall at the nozzle throat even though the upstream boundary layer

was turbulent. A three dimensional laminar boundary layer analysis was employed to predict the behavior of the flow, and since it was found that the upstream turbulent boundary layer had little effect on the end-wall boundary layer in the nozzle, the analysis provided good agreement with measurements obtained from a model of the cascade. In the discussion of the work of Senoo, Kline (1967) expressed an interest in the apparent transition from turbulent flow to laminar flow and suggested that the effect might be caused by the large favorable pressure gradient present in the turbine nozzle.

There is evidence to support the fact that both laminar and turbulent flow can exist simultaneously in the cross section of a closed channel. In a brief note submitted to report on the initial examination of the phenomenon, Eckert and Irvine (1956) stated that investigations with a triangular tube having a small apex angle indicated that the flow near the apex could be laminar while the flow near the base was turbulent. The flow pattern was maintained throughout the tube length for a wide range of Reynolds numbers. In a later paper (1960) the same authors report heat transfer measurements lower than those that would be expected from circular tube information, and Cremers and Eckert (1962) confirmed a

lower value of turbulent transport in the direction of the duct height.

The work of Cannon (1965) also serves as an example of simultaneous turbulent and laminar flow across a channel. In that case, the rotation of a cylindrical tube caused an initially turbulent flow of water to break down into a non-rotating, turbulent inner core, characterized by a structure of decaying turbulence, and a rotating outer ring of fluid with a laminar structure. The heat transfer experiments, conducted with air for both heating and cooling, showed that the heat transfer to the fluid flowing in the rotating tube was depressed considerably below the values that would be expected for non-rotating turbulent flow. Since the author conducted exhaustive visual and photographic studies of the flow mechanism, a statistical description of the transition phenomenon was possible. The reason for the existence of the combined laminar and turbulent flow mentioned above was speculative; the author reasoned that turbulent bursts were retarded by a combination of forces that arose because of the rotation and these affected the radial pressure flow field.

The investigation due to Launder (1964) provides one of the first reasonably thorough examinations of the appearance of an adiabatic laminar-type flow due to a strong favorable pressure gradient. Experiments were

conducted with the boundary layer on a flat plate; a deliberate attempt was made to insure initial turbulence through the use of screens at the leading edge of the plate. The author employed a shape factor defined as the ratio of displacement thickness to momentum thickness, and it was found that measurements which indicated laminarization corresponded to rapid increases in this quantity. In this same region, a thickening of the sublayer was also noticed, along with a departure from the law of the wall. In an attempt to describe the mechanism of the process, the author employs a one-parameter correlation for natural transition, due to Persh (1956), which allows recognition of some of the trends. An even more emphatic indication of departure from turbulent flow was obtained by plotting the data on coordinates composed of $Re_\theta . C_f$ and $\frac{\theta^2}{\nu} \frac{du}{dx}$. As a further refinement, the data points were also displayed on $Re_\theta . C_f$ versus $\frac{\theta}{u} \frac{du}{dx} . Re_\theta^{1/4}$ coordinates in order to provide a unique path for laminarization process. When the critical stability curve proposed by Schlichting and Ulrich (1942) was placed on these coordinates along with the data points which represented the observed occurrence of laminarization, a smooth curve was obtained which was considered to be an incipient laminarization boundary. The graph depicted three distinct regions that represented (a) turbulent boundary layers that stay turbulent,

(b) turbulent boundary layers that become laminar,
(c) turbulent boundary layers that begin laminarization and then revert to a turbulent condition.

The general topic of heat transfer in rocket nozzles has provided another source of information concerning the appearance of laminar regions in otherwise turbulent streams. Back, Massier, and Gier (1964), in referring to the work done by Back for his Ph.D. Thesis, noted that heat transfer measurements indicated a departure from fully turbulent flow through a converging-diverging nozzle operated at low stagnation pressures. In their work the same trends were reported, and it was suggested that these results were due to the presence of a large favorable pressure gradient. The boundary layer turbulence energy equation was manipulated to arrive at the following parameter used to describe the flow:

$$\chi = \frac{22\nu_e \, (du_e/dx)}{(\tau_w/\rho_e)}$$

where the subscript "e" refers to conditions at the edge of the boundary layer. The quantity χ can be evaluated for various stagnation pressures; increasing values of χ correspond to reduction of the net production of turbulent kinetic energy, presumably due to acceleration. The

variation of χ through the nozzle was reported to follow the same trend as did the depressed heat transfer.

The investigation of the heat transfer to a turbulent boundary layer on a flat plate by Moretti and Kays (1965) provided another source of information concerning the transition from turbulent to laminar flow. The authors coined appropriate terms for use in the description of the transition process; it is convenient to reproduce them here in the interest of completeness. The word "laminarescent" describes a boundary layer that has previously been turbulent and may contain residual turbulence, but which is no longer generating new turbulence, and the word "relaminar" describes a boundary layer which has completed the process of transition and which no longer exhibits the effects of former turbulence. The term "laminar", then, simply describes a flow that is not generating turbulence.

In their experimental work the authors found that the heat transfer in cases with strong acceleration had a tendency to approach laminar values following a delay, of length about 200 times the momentum thickness, which was attributed to the time required for decay of turbulence. The physical situation was essentially flow over a flat plate to which a variety of pressure gradients and heating or cooling rates could be applied. The above mentioned

decay period was also noticed by Schraub and Kline (1965) in visual studies using water; the effect of acceleration was a decrease in, and the ultimate termination of, the formation of eddies.

The quantity chosen by Moretti and Kays (1965) for prediction of reverse transition was the "acceleration parameter"

$$K = \frac{\nu}{u_\infty^2} \frac{du_\infty}{dx}$$

which is similar to the parameters employed by Back, Massier, and Gier (1964) and by Launder (1964). The authors argue that the relevance of the Reynolds number (based on momentum thickness) to the acceleration parameter is probably small, and the stated critical value of K for the occurrence of reverse transition is $K_c \approx 3 \times 10^{-6}$. This value was obtained from analysis of the experimental data, but it can be justified by examination of the momentum integral equation as explained by Kays (1966). Laminar analysis is suggested for situations where K_c is exceeded for large distances. It is interesting to note that the critical value of K was confirmed by Schraub and Kline (1965) in connection with the water table studies mentioned above.

Velocity profiles in situations involving accelerated flow have been reported by Moretti and Kays (1964) and by Boldman, Schmidt and Ehlers (1967). Moretti and Kays expressed considerable doubt about the applicability of the law of the wall to flow situations involving a pressure gradient, and it was stated that the "layer techniques" (ie. sublayer, buffer layer, etc.) that have resulted from this assumption are probably good only for flow with a constant value of K. The heat transfer results that were presented were couched in terms of an Ambrok (1957) solution that was modified to fit the experimental data. Significant among the modifications was the use of the skin friction coefficient to introduce a delay in the effect of the acceleration parameter; it was also found that the quantity K/St provided an acceptable correlation for the heat transfer results.

The analytical work of Hatton (1965) involved the use of the law of the wall for prediction of the heat transfer to turbulent boundary layers with moderate pressure gradients. The author encountered difficulty in the solution for large Reynolds numbers and negative pressure gradients; it was suggested that this occurrence had some relation to the reverse transition described by Moretti and Kays (1964).

In further experiments Back, Massier, and Cuffel (1966) reiterated the statement that the heat transfer in a rocket nozzle can be decreased by acceleration; the results indicated that a large angle of convergence enhanced the process of reverse transition. The criterion used for estimating the degree of turbulence reduction due to acceleration was the K parameter of Moretti and Kays (1965). The values of K were obtained for various axial positions along the nozzle, and it was again found that large values of K corresponded to regions of maximum departure of the heat transfer from the turbulent prediction. The results showed that the maximum reduction in heat transfer occurred downstream from the point of maximum K, but it was pointed out that the intervening distance could be a region of viscous dissipation of residual turbulence.

In a review of earlier results presented recently, Back and Seban (1967) confirmed the findings of Moretti and Kays with respect to reduction of the heat transfer coefficient in accelerated flow. The authors found that, for acceleration parameters in excess of 2×10^{-6}, the heat transfer coefficients could be reduced by as much as 40 percent compared to typical values for fully turbulent flow. It was further stated, in agreement with Moretti and Kays, that although the velocity profiles became

laminar-like near the wall, the temperature profiles still exhibited some effects of eddy transport. It was reported that an earlier turbulent boundary layer prediction by the same authors, based on a Karman sublayer model, could be modified to yield good heat transfer results by forcing it to agree with experimental momentum thickness, Reynolds numbers and friction coefficients.

McEligot (1963), during an investigation that was primarily devoted to turbulent flow in tubes, obtained some data in the transition region and presented a correlation equation for the transition results. The first published investigation mentioning turbulent-to-laminar transition for tube flow was that due to Perkins and Worsoe-Schmidt (1965). The authors examined the local heat transfer and friction factors for gas flow in a tube with wall-to-bulk temperature ratios as high as seven; it was noticed that the effects of variable properties were in some cases sufficient to cause an apparent transition to laminar flow. This tendency was observed even though the bulk Reynolds number did not come near the critical value; it was suggested that the conditions at the wall might be appropriate for correlation purposes. The experimental data points for which transition occurred were not correlated by the expressions that were presented, but some of them were displayed on the curves to

indicate the departure from predicted values. It was found that the friction factors, based on bulk properties, could be advantageously normalized by an isothermal friction factor correlation evaluated at the same wall Reynolds number; the wall Reynolds number, designated as the "modified wall Reynolds number", was defined as

$$Re_w = \frac{4\dot{m}}{\pi D \mu_w} \left(\frac{T_b}{T_w} \right)$$

The heat transfer data were well correlated on both bulk and wall properties, but an attempt at correlation with film properties met with little success. Both the friction and heat transfer correlations were provided with an entry correction; it was found that the data required a large correction at small x/D and large T_w/T_b. The authors suggested that the transition to laminar-like flow was evidenced by the departure of the friction and heat transfer results from the turbulent correlations. A technique for categorizing the experimental results as laminar, transitional, or turbulent according to the departure from turbulent correlations was presented by McEligot, Ormand, and Perkins (1966), and the results thus classified were displayed on a plot of the wall to bulk temperature ratio versus the wall Reynolds number.

During the study of the parallel channel stability problem associated with gas cooled nuclear reactor

cores, Bankston, Sibbitt, and Skoglund (1966) and Bankston (1965) encountered the phenomenon of transition from turbulent flow to laminar flow. An experiment was conducted using a tube with almost simultaneous hydrodynamic and thermal entry lengths; therefore, the effect of heating on the usual laminar-to-turbulent transition could be investigated. It was found that the transition point was quite sensitive to heating rate and axial location; the general effect of heating was to increase the bulk Reynolds number at which transition occurred. The maximum wall-to-bulk temperature ratio reported was 2.25, and it was found that the resulting variable properties effects caused a slight decrease in the friction factor for fully developed turbulent flow. The sensitivity of Nusselt numbers to radial property variations was found to be small in the laminar regime.

The authors employed hot wire anemometer probes to obtain evidence of turbulent to laminar transition. The probes were calibrated on the basis of isothermal flow runs, and it was found that the turbulent intensities were greatly reduced from their turbulent flow values during certain test runs with heating. The classification scheme presented by McEligot, Ormand, and Perkins (1966), using the modified wall Reynolds number, was used to obtain boundaries for the laminar, transition, and

turbulent regimes; it was found that the divisions could also be represented by the parameter

$$Y = Re_b \left(\frac{T_b}{T_w} \right)^2$$

The quantity Y was then used to obtain correlations for the transition region, and existing correlations were employed in the fully laminar and fully turbulent regions.

It appears that one of the most significant contributions at the present time would be an improved definition of the boundaries between the flow regimes. Bankston (1965), Moretti and Kays (1965), and Bankston, Sibbitt, and Skoglund (1966) all suggest that values of the friction factor and the heat transfer coefficient for the transition region can be obtained by some sort of interpolation between the laminar and turbulent regions, but this technique requires that the boundaries be clear and precise.

CHAPTER III

EXPERIMENTAL APPARATUS

The experimental apparatus constructed for this study was basically a tube in which the flow conditions typical of gas cooled nuclear rocket engines could be approximated. The test assembly was composed of a test section that was resistively heated in order to provide an approximate constant wall heat flux boundary condition, a vacuum system that was used to minimize both the heat loss from the test section and the oxidation of the test section at high temperature, and a liquid nitrogen system that was used to precool the gas prior to heating in order that high wall-to-bulk temperature ratios could be achieved with conventional test section materials. Auxiliary systems allowed the control and measurement of the test section heating power, the control and measurement of the mass flow rate of gas, the measurement of appropriate temperatures, and the measurement of axial pressure drops in the test section. The following sections describe the components of the test assembly in detail.

Test Section

The test section was constructed from drawn, seamless Inconel 600 tubing with a nominal outside diameter of 0.250 inches and a nominal wall thickness of 0.010 inches. A detailed description of the composition and the dimensions of the test section is provided in Table I. The composition values were provided by the Superior Tube Company for the particular heat from which the tubing was fabricated. The values presented in Table I for the test section diameters represent the quantities selected from the results of several different measuring techniques. An assortment of micrometers, diameter gauges, and a metallurgical microscope were used to measure the test section diameters.

The selection of Inconel 600 as the test section material was based on the need for a metal with a high melting point that was amenable to electrical heating. Certain other metals, such as platinum, will withstand higher temperatures and have superior radiation emittance characteristics, but these features are overshadowed by the low electrical resistivity and high thermal conductivity that are characteristic of such materials. Inconel has the further advantages of relative low cost and ease of fabrication; the construction difficulty alone makes materials such as tungsten undesirable.

Table I Test Section Data

Description of Test Section Composition:

Nickel	76.24 percent	Manganese	0.26 percent
Chromium	15.81	Sulfur	0.007
Iron	7.29	Silicon	0.25
Titanium	0.25	Copper	0.08
Carbon	0.04	Aluminum	0.06

Dimensions:

Heated Length Thermocouple Number	Unheated $\frac{x}{D}$
1	0.445
2	1.232
3	4.057
4	7.455
5	11.768
6	18.290
7	23.451
8	35.621
9	47.877
10	61.469
11	74.358
12	87.616
13	100.488
14	107.960

Pressure Tap Number	Unheated $\frac{x}{D}$
1	2.046
2	15.329
3	28.107
4	41.433
5	54.237
6	67.580
7	80.478
8	93.744
9	106.727

Unheated Length Thermocouple Number	$\frac{x}{D}$
1	-48
2	-16
3	- 1

Overall Heated Length = 25.047 inches
Outside Diameter = 0.250 inches
Inside Diameter = 0.230 inches

Nine pressure taps, made of 0.0625 inch outside diameter by 0.052 inch inside diameter Inconel tubing, were attached to the test section at the locations indicated in Table I with Nioro, a nickel-gold eutectic brazing alloy manufactured by the Western Gold and Platinum Company. An attempt was made to minimize the size of the braze fillet in order to prevent excessive temperature depression at the tap location due to increased area for current flow. A special jig was constructed to hold the pressure tap tube perpendicular to the test section during the brazing operation. The static pressure tap holes in the test section wall were drilled, subsequent to the brazing operation, by means of the electrical discharge process described in Appendix D.

Twenty-three Chromel-Alumel thermocouples made of 0.005 inch diameter premium grade wire were attached to the test section at the locations shown in Table I. Each of the two wire ends for every thermocouple was separately spot welded directly to the test section, as shown in Figure 1, in order to provide an assurance that the temperature measuring junction was not separated from the wall by the thickness of a wire. A junction between the thermocouple wires at a point removed from the test section wall would cause erroneous readings due to the

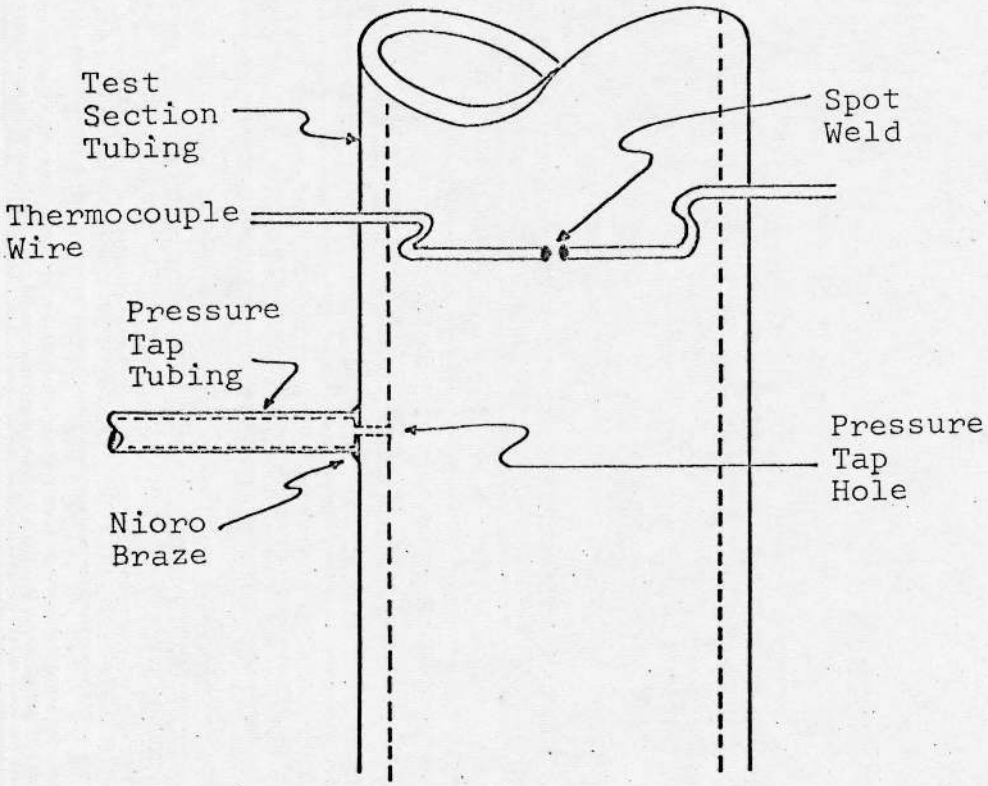

Figure 1. Detail of Thermocouple and Pressure Tap Attachment.

temperature drop between the wall and the junction; these errors in temperature measurement were discussed by Hess (1965). The axial locations of both the thermocouples and the pressure taps were obtained by means of a Gaertner precision cathetometer after the test section installation was completed; the zero point for the measurements was the upper surface of the lower electrode. The measuring operation also provided an opportunity for the evaluation of the misalignment of the individually welded thermocouple wires; the misalignment was generally no greater than one thermocouple wire radius. The thermocouple junctions were considered to be located midway between the centerlines of the two thermocouple wires, and the pressure taps were considered to be located at the centerlines of the pressure tap tubes.

The overall length of the test section was about 50 inches; the above mentioned thermocouples and all of the pressure taps were concentrated in half of this length. The tube was brazed into a 0.125 inch thick stainless steel disk at its midpoint; this disk, two inches in diameter, had previously been furnace brazed into the central portion of an eight inch outside diameter by 0.500 inch thick stainless steel vacuum system flange. The disk served as one electrode for the test section heating current, and the portion of the tube that had no pressure

taps served as a 100 diameter entry length for the gas flow. The beginning of the entry length was sealed into a double-reversing mixer that was provided with two sheathed, ungrounded, Chromel-Alumel thermocouple probes. The tip of one probe was exposed to the flow stream; the tip of the other probe was within a tubular shield that was open to the flow stream at one end.

The upper end of the heated section was attached to a mixer which also served as the high potential electrode for the heating current, Figure 2. The upper mixer contained a perforated copper slug through which the heated gas was forced; the slug was isolated from its surroundings in a radial direction by a 0.015 inch gap. The portion of the mixer that contained the copper slug was provided with a gold plated radiation shield in order to minimize the heat loss from the mixer to the surroundings. Thermocouples were imbedded in the copper slug; in operation the copper was heated to the gas exit bulk temperature, and this temperature was measured by the thermocouples. Subsequent comparison of the measured exit bulk temperature with the value calculated by the data reduction program indicated agreement to within five percent for runs during which the heat loss calculations could be considered reliable.

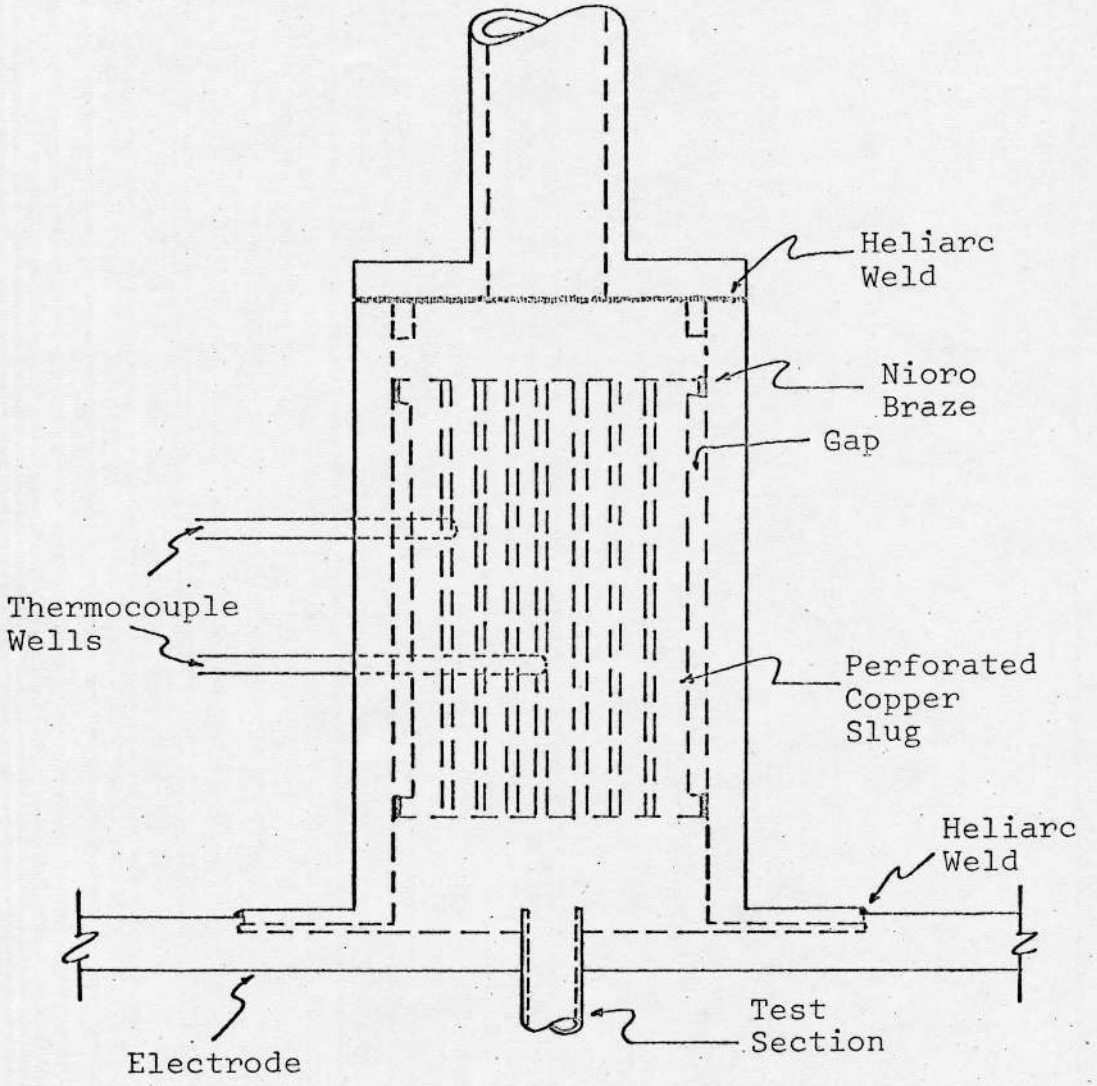

Figure 2. Detail of Exit Gas Mixer.

That part of the exit mixer located above the copper slug was held in a vertical position by lubricated, spring loaded positioning feet that allowed the test section to elongate when heated. The exhaust line from the mixer was provided with a flexible section for the same purpose.

The possible buckling of the test section at high temperature was prevented through the use of a spring which supplied a constant tensile force in the axial direction along the test section. The spring was oriented in a manner such that the spring force decreased as the length of the test section increased, and the initial spring tension was set, prior to the final brazing of the test section to the lower electrode, so that the spring force balanced the weight of the test section, the mixer, and the exhaust line in the unheated condition.

The test section was polished after the brazing process, and it was cleaned with trichloroethylene and ethyl alcohol during the assembly of the vacuum system. It was hoped that pressure levels of the order of 10^{-5} torr would be sufficient to prevent oxidation of the test section and a possible corresponding change in emittance, but after a brief period of operation at approximately 1000°F it was noticed that some discoloration had occurred. When the change of color began the test section became

quite dark; but, as the time at high temperature increased, it lightened to an almost golden hue. The change of emittance, which was somewhat less than ten percent, had severe implications insofar as the validity of the heat loss calibration runs was concerned, and a procedure was developed that would partially compensate for the emittance change. It would be possible to reduce the problem of emittance change either through the use of more exotic materials, such as platinum, or through the use of a low emittance plating, such as gold, that would prevent oxidation of the Inconel at high temperatures. Preliminary experiments were conducted to determine the feasibility of gold plating future test sections with an immersion gold solution. It was found that the high chromium content of Inconel made this process impossible unless the test section was first covered with a thin coating of nickel. The test section used in the present work was not gold plated, but a discussion of the plating techniques developed for Inconel has been presented by Cooper (1967).

Vacuum System

The primary reason for operating the test section in an evacuated environment was to control the energy loss from the tube so that the energy transfer to the gas could

be obtained with a high degree of accuracy. At sufficiently low pressures, the energy transfer by molecular conduction can be ignored, and energy loss from the test section to the surroundings occurs only by radiation. Hottel and Sarofim (1967) have specified that the effect of molecular conduction is negligible if the mean free path in the surrounding medium is large compared to a characteristic dimension of the system. The mean free path at the usual operating pressure was of the order of ten meters; therefore, it was assumed that radiation was the only significant mode of energy transfer between the test section and the surroundings. The energy loss from the test section could also be reduced through the use of solid insulation, but a much longer time would be required for the attainment of thermal equilibrium prior to each experimental run. The high response time offered by the vacuum system made the use of helium as a test gas relatively economical. A disadvantage of the vacuum environment was the requirement placed on the surface finish of the tube; oxidation at high temperatures could change the emittance of the surface and consequently change the heat loss calibration.

The base of the vacuum system was a 26 inch square by 1-1/4 inch thick plate supported by a steel frame; connections between the vacuum system and the atmosphere

were accomplished by means of fittings sealed to this plate. The plate was fabricated from aluminum alloy 2024 and was hard anodized after machining. The remainder of the enclosure consisted of a 16 inch length of 24 inch outside diameter by 0.500 inch wall carbon steel pipe and an 18 inch diameter by 30 inch Pyrex bell jar; these items were separated by a 0.5 inch thick aluminum plate provided with a hole to allow for the difference in diameters, as shown in Figure 3. The inside of the carbon steel pipe was coated with machine oil during periods of exposure to the atmosphere; the oil was removed with ethyl alcohol during the final assembly of the vacuum system. Because the bell jar and the pipe were not concentric, the atmospheric load caused severe deflections of the separating plate, and supporting columns were provided to prevent deflections large enough to break the vacuum seal.

The vacuum pumping system was composed basically of a 3 inch oil diffusion pump backed by an 80 CFM mechanical pump. Supporting equipment included a 3 inch chilled-water type baffle, a 4 inch chevron type baffle that was supplied with refrigerant-12 by a small compressor unit, and a 4 inch gate valve located between the diffusion pump and the vacuum vessel. This combination of pumping equipment achieved an ultimate system pressure of 5×10^{-6} torr and was capable of maintaining a pressure 1×10^{-5}

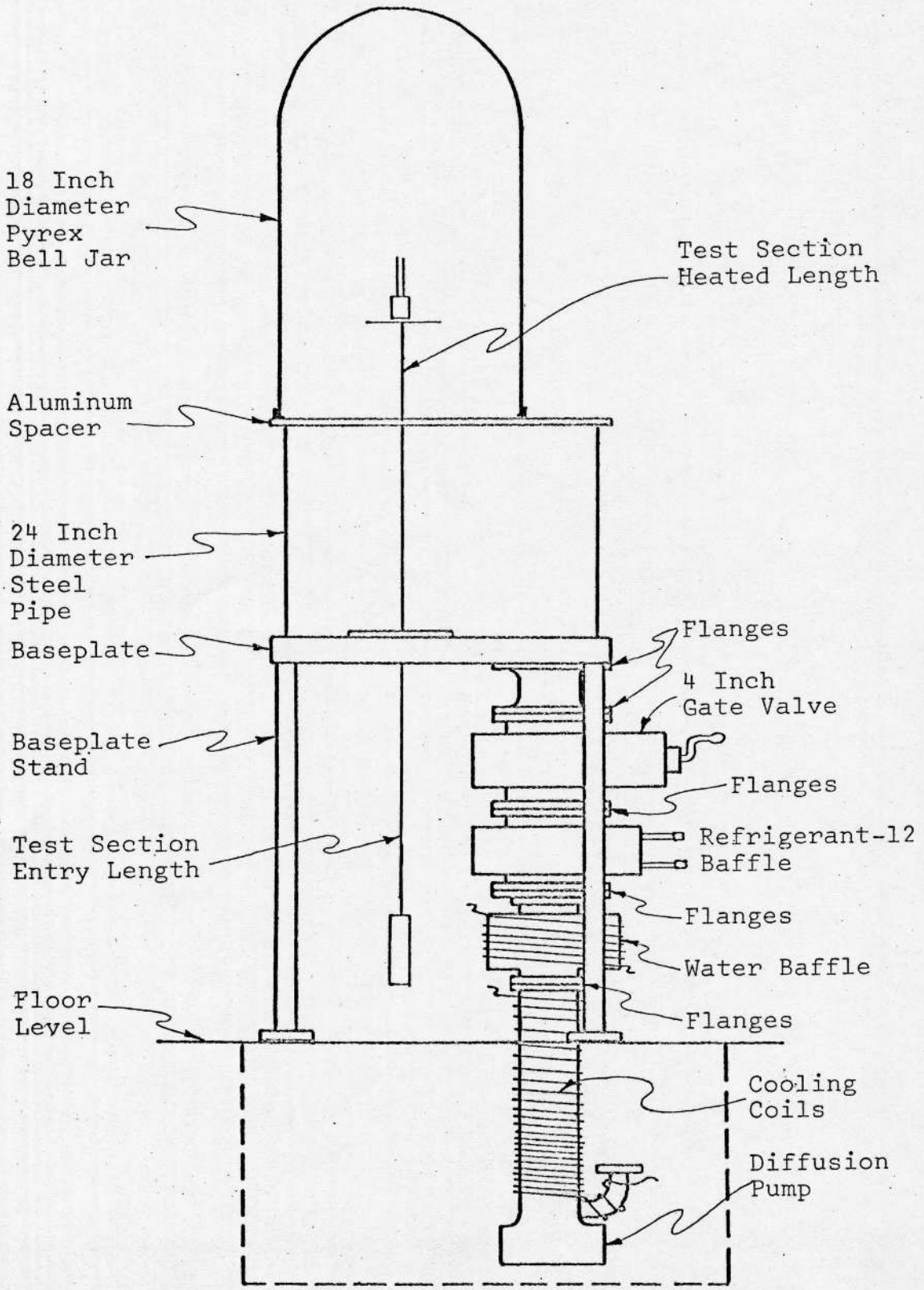

Figure 3. Vacuum System

torr during the process of data acquisition. System pressure levels were measured with Pirani gauges in the range from 2 torr to 1×10^{-3} torr and with a cold-cathode discharge gauge in the region below 1×10^{-3} torr.

The various seals used on the vacuum system took several forms. A standard neoprene bell jar gasket was used on the bell jar, and the 24 inch diameter pipe was sealed at both ends with neoprene Parker Gask-O-Seals. The pumping system was assembled with either groove type O-rings or O-rings with retaining rings as required. Most of the feedthroughs were provided with O-rings by the manufacturer; those that were equipped with pipe threads were sealed with Teflon tape. The rubber O-ring in the exit gas feedthrough was replaced with one made of copper because of the extreme temperatures at that location, and the flange that separated the hydrodynamic entry length from the heated portion of the test section was equipped with a Parker V-seal made of Teflon coated Inconel because that region was subjected to both high and low extremes of temperature.

Some difficulty was encountered in the initial evacuation of the vacuum system due to leakage through the 48 wire thermocouple feedthroughs supplied by Aremco Products, Inc. Each of these devices that was tested was found to leak either through the silicone rubber vacuum

seal or through the space between the teflon insulation and the copper wires. Leakage was also found at the ceramic insulator in the power feedthrough devices manufactured by Nanmac Corporation; the exit gas feedthrough, obtained from the same source, required repair with epoxy cement after operation at a temperature below zero degrees Fahrenheit. The vacuum system was not entirely troublefree during operation of the test section at high temperatures; the positioning feet on the upper mixer were lubricated with a solution of molybdenum disulfide in mineral oil, and the mineral oil evaporated at a temperature of about 600 degrees Fahrenheit causing a temporary excursion of the system pressure. This situation could be alleviated by having the appropriate parts commercially coated with molybdenum disulfide; it should be mentioned that graphite is not a suitable lubricant when used in vacuum applications. The lubricating properties of graphite are due to the presence of adsorbed water; this water is lost during exposure to low pressures.

Power System

The heating power for the test section was provided by a 3 KVA transformer that was driven by a Sorensen Model 2501 line voltage stabilizer and a variable auto transformer (see Figure 4). Because a

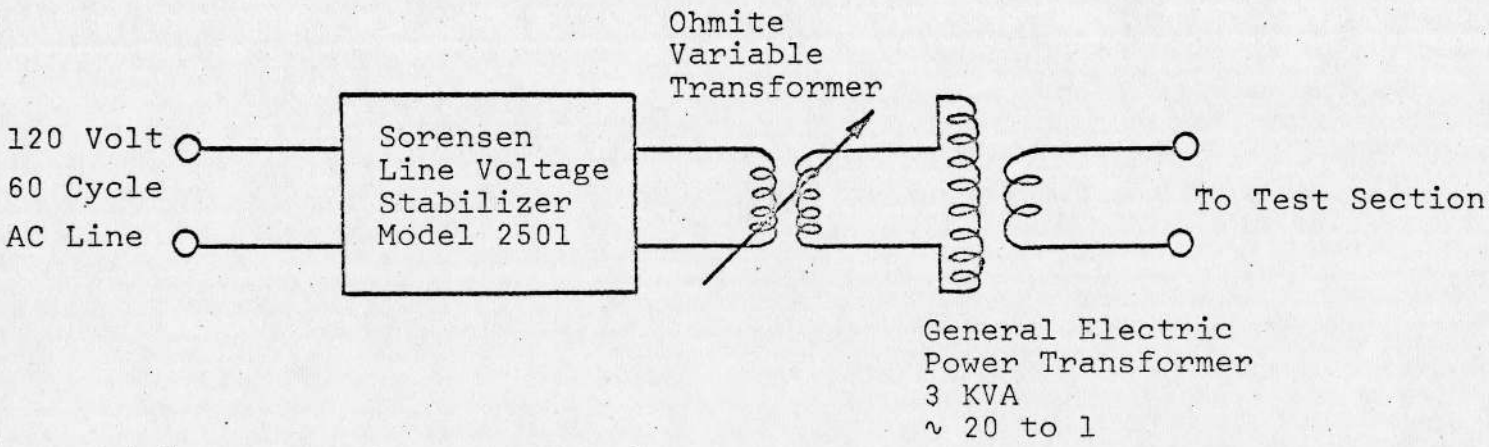

Figure 4. Alternating Current Power Supply

minute misalignment of the thermocouple wires welded to the test section would cause large errors in the temperature signal with direct current heating (Davenport, Magee, and Leppert, 1962), only alternating current was used for the test section power.

The schematic diagram for the power system is shown in Figure 5. Connection of the power supply to the test assembly was accomplished by means of welding cable; one side of the power supply was connected to the vacuum system baseplate and to an earth ground. The ungrounded side of the power supply was passed through the baseplate by means of three 200 ampere vacuum feedthroughs. A bus bar of 3/8 x 1 inch copper bar was constructed inside the vacuum chamber and each of the bolted joints in the bus bar was coated with a colloidal suspension of graphite in water in order to insure good electrical contact. The final connection between the bus bar and the mixer-electrode assembly was made with strands of 2/0 gauge cable from which the insulation had been removed.

A wire strand was attached to the upper mixer-electrode assembly for use as a voltage tap; the connection to the outside of the vacuum system was identical to that employed for the test section thermocouples. Another wire attached to the lower flange on the outside of the vacuum system was provided for overall

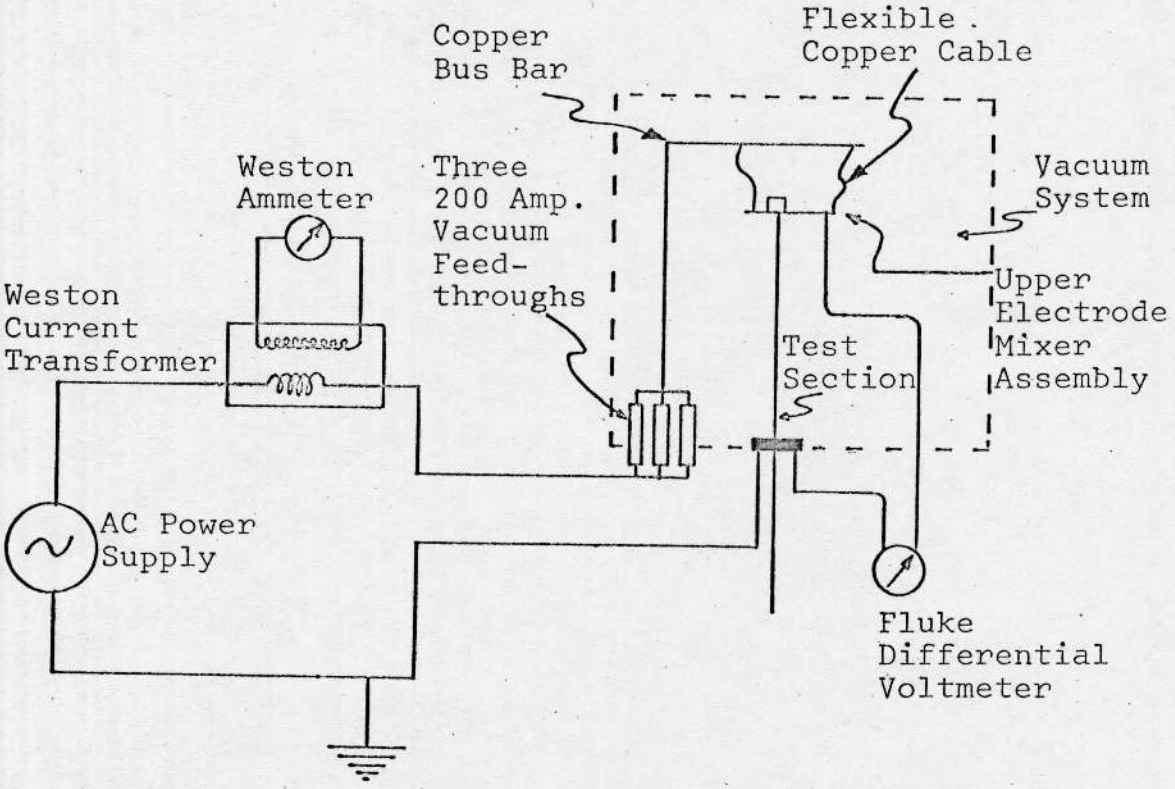

Figure 5. Diagram of Electrical System

voltage drop measurements, and the thermocouple wiring scheme was such that the test section thermocouple wires could be used for local voltage drop measurements. The possibility of a short to ground through the gas exhaust line was removed by the installation of a glass section in the exhaust line; the double glass-to-metal seal assembly was manufactured by the Vacumen Corporation and was rated at 100 psi and 800 degrees Fahrenheit.

Temperature Measuring System

Temperature measurements on the test section wall were made by means of 0.005 inch diameter Chromel-Alumel wires spot welded to the tube; the axial locations are shown in Table I. Thermocouples were also attached to the test section at each pressure tap location to provide an indication of the wall temperature depression due to the presence of the pressure tap.

In order to provide a degree of flexibility in the choice of future types of thermocouple wire, the feed-through devices that passed the thermocouple wires across the border of the vacuum system were wired with copper. This scheme required a reference cold junction located inside the vacuum system; some technique was also necessary in order to provide an ice reference for the thermocouples. A copper box was installed inside the vacuum

system to serve as an isothermal region for thermocouple wire connections. The small test section thermocouple wires were attached to 0.032 inch diameter Chromel and Alumel wires that could be shaped and directed more easily; the larger wires were in turn conducted through Teflon sleeving into the copper box. The connection to the copper-wired vacuum feedthrough was achieved inside the copper box by means of miniature, gold plated plugs and sockets. The connecting cables and instrument wires were also of copper.

In order to compensate for the fact that the reference junction in the circuit described above was not at ice temperature, a Chromel-Alumel junction was formed and immersed in an ice bath. The Chromel and Alumel wires from this junction were conducted through the baseplate into the vacuum system and connected to copper wires inside the copper isothermal box. These copper wires were then returned to the outside of the vacuum system and the circuit to the measuring instrument was completed. Because the Chromel and Alumel wires from the test assembly thermocouples and the Chromel and Alumel wires from the ice reference junction underwent a transition to copper wire at the same temperature, there was no net effect on the measuring circuit due to the presence of the copper wires. An identical scheme was used for thermocouples that were located outside the vacuum system; the isothermal box

for this circuit was constructed of wood and lined with copper.

A schematic diagram of the entire thermocouple circuit is shown in Figure 6. The thermocouples associated with the experiment were divided into three groups, the thermocouples on the test section wall, the thermocouples inside the vacuum system but not on the test section wall, and the thermocouples outside the vacuum system. Each of these groups was controlled by a multipoint switch, and each group was connected with an independent ice junction. The three switch banks were mechanically linked so that only one temperature at a time could be measured; except for this fact the three circuits were independent. The test section wall thermocouple wires were provided with taps to a bank of sockets to facilitate voltage measurements at various points on the test section. The thermocouples that were located inside the vacuum system but not on the test section wall were used to measure both hardware temperatures and gas temperatures at various points. For example, the upper and lower test section electrodes were provided with thermocouples at different radial positions to allow the evaluation of the conduction heat transfer, and the exit mixer was provided with thermocouples to allow the determination of the exit bulk temperature. Also, since some of the materials used

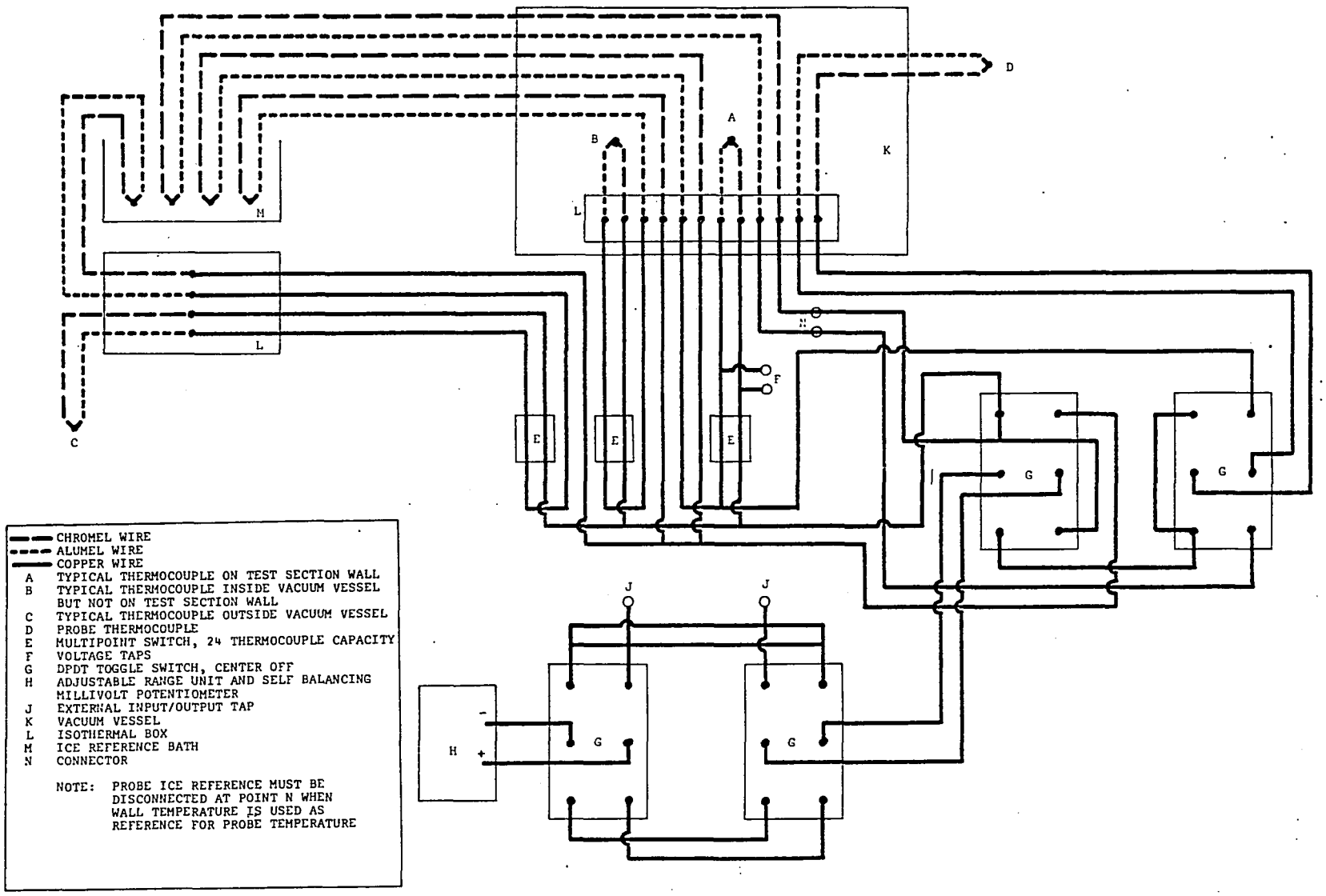

Figure 6. Thermocouple Circuit

in the fabrication of the test assembly had definite temperature limitations, thermocouples were provided in appropriate locations to provide an indication of possible overheating.

During some of the heat loss calibration runs, a Chromel-Alumel thermocouple probe was inserted into the test section and placed opposite a wall thermocouple by equalizing the above ground potentials exhibited by the wall thermocouple wire and a wire attached to the probe. The thermocouple circuit was arranged to allow a choice of measurements; it was possible to measure the probe temperature referenced to ice, the wall temperature referenced to ice, or the probe temperature referenced to the wall temperature. The probe wires were connected to copper wires inside the vacuum system isothermal box, and the probe circuit was equipped with an individual ice junction. Subsequent to the location of the probe opposite a particular test section wall thermocouple, probe temperature measurements in the vicinity of the thermocouple were obtained by moving the exposed end of the probe through distances which could be measured with a machinist's scale.

The instrument used to measure the output of the thermocouples was a Honeywell "Electronik 18", millivolt indicating potentiometer equipped with an adjustable range unit. A switching circuit provided a means of

checking the calibration of the instrument with a Leeds and Northrup Model 8686 millivolt potentiometer; it was possible either to measure the thermocouple signal with the Leeds and Northrup potentiometer or to supply a calibration signal from the Leeds and Northrup potentiometer to the Honeywell instrument.

Flow System

The test gas was supplied to the test section by a series of devices that were used to set the flow conditions and to measure the mass flow rate of gas passing through the apparatus. A compressor and pressure tank assembly with a capacity sufficient for all of the air runs reported in this work was available, but the air supplied by this equipment was too moist for any situation that involved liquid nitrogen precooling. A high pressure manifold was constructed to allow the simultaneous use of four standard gas cylinders; both the air and the helium used in pre-cooled runs were supplied in this manner. The cylinder pressure was lowered to about 20 psi by a series of three regulators; the final control of the operating pressure was achieved by means of a Honeywell Model 802H1 precision manual loading regulator.

The flow rate of the gas through the system was measured upstream from the test section by one of two

Brooks Rotameters that had been individually calibrated by the factory to an accuracy of one percent with air flow. When possible, the flow rate was measured downstream from the test section by a wet test meter. A heat exchanger supplied with chilled water was installed between the test section and the wet test meter to cool the gas to ambient conditions prior to its passage through the meter. The main flow control valve was also located in this part of the system to allow the operation of the test section at a variety of pressures while the wet test meter operated at essentially atmospheric conditions. A precooling coil of copper tubing was located on the upstream side of the entry mixer; this coil was immersed in a 50 liter Dewar flask which could be supplied with liquid nitrogen.

A manifold connected to a Heise Bourdon tube gauge and a mercury manometer permitted the measurement of the pressure at a point adjacent to each flow meter as well as the gauge pressure at the first pressure tap on the test section. The temperature at each meter and at the inlet mixer was obtained by means of thermocouple probes mounted in the flow stream. A diagram of the flow system is shown in Figure 7; although the system was also designed to accomodate a Foxboro differential pressure cell and a Meriam laminar flow element, only those instruments actually used are shown in the diagram.

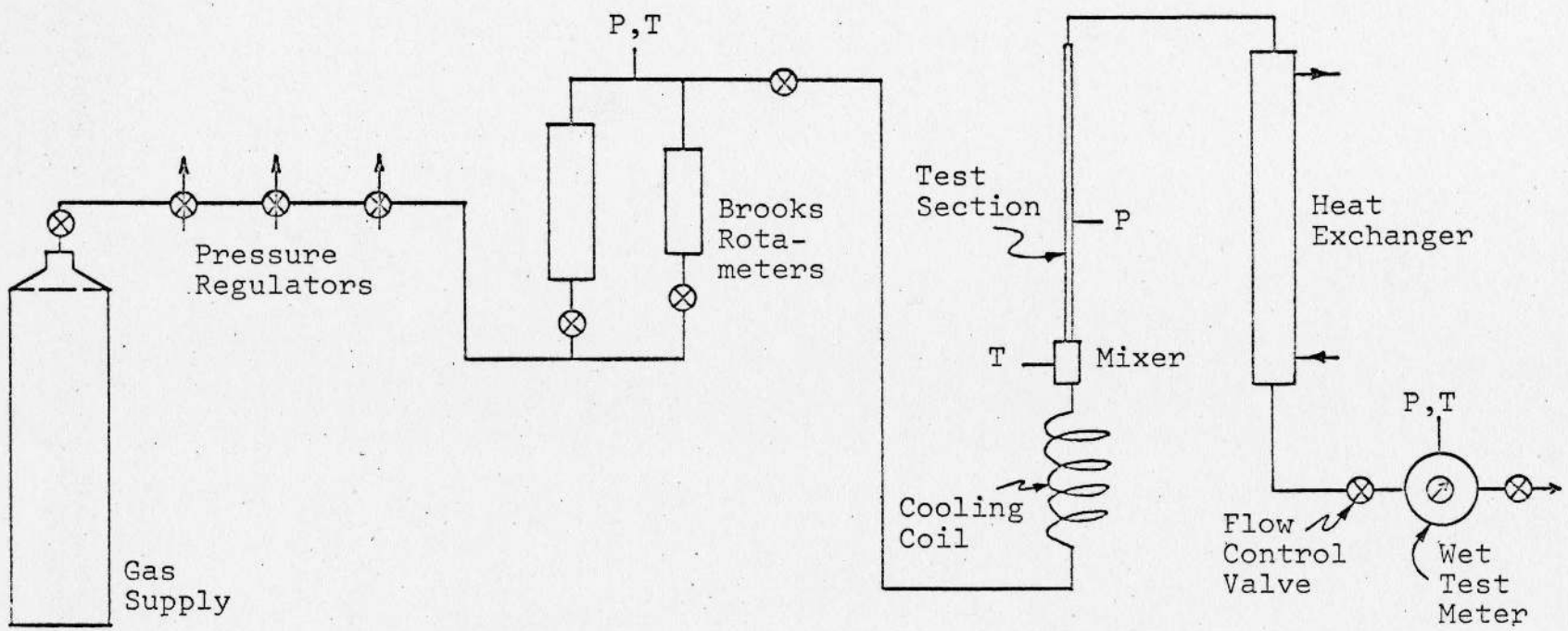

P--Pressure Tap
T--Thermocouple Well

Figure 7. Flow System

Pressure Drop Measuring System

The pressure drops between the test section pressure taps were measured by a selection of manometers having different ranges and sensitivities. Because the technique used to calculate the friction factors employed two adjacent pressure drops, i.e., three pressure taps, an attempt was made to pair the manometers and measure adjacent pressure drops simultaneously. The manometers, all manufactured by the Meriam Instrument Company, consisted of a pair of 60 inch vertical water manometers and a pair of 60 inch inclined water manometers with ten inch range. In addition, a Meriam Model 34FB2 micromanometer was available for the measurement of very small pressure drops, and a Heise Bourdon tube gauge was provided for pressure level measurements.

The connection of a particular set of pressure taps to a particular manometer was accomplished by means of a manifold designed to accomodate ten pressure taps and five pairs of instruments as shown in Figure 8. The manifold employed Whitey OKS2 valves, and the connections to the pressure taps were made with 0.125 inch outside diameter tubing except for the 0.0625 inch outside diameter tubing used in the vacuum feedthroughs.

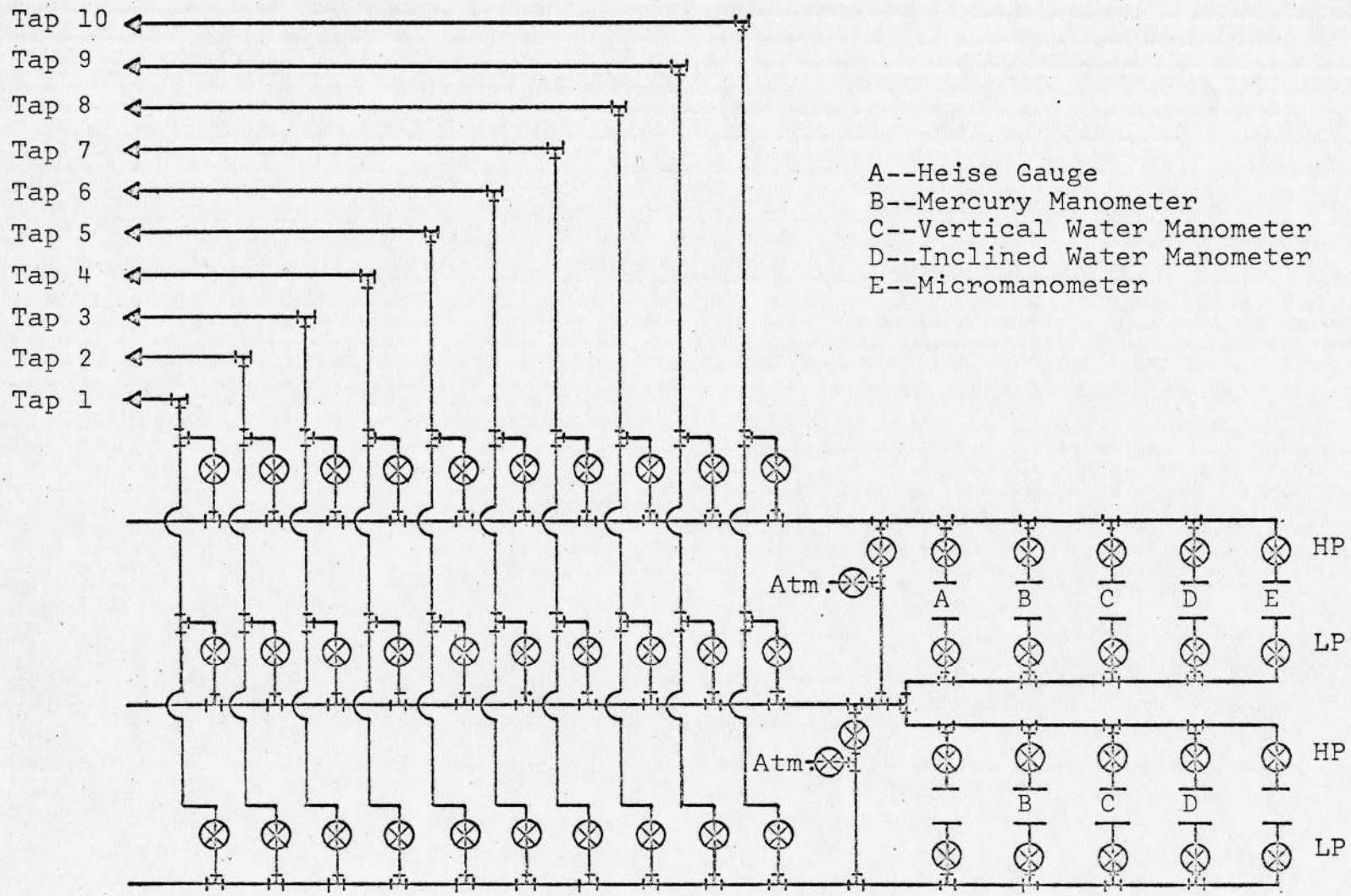

Figure 8. Pressure Tap System

Precooling System

The precooling of the test gas with liquid nitrogen was achieved by passing the gas through a copper coil that was inside a cylindrical Dewar flask; the gas passed directly from the coil into the entry mixer and then into the hydrodynamic entry length of the test section. The liquid nitrogen was obtained in two 50 liter transport Dewar flasks which could be pressurized by a five psi air supply. Both of the transport flasks were used simultaneously; one provided flow directly into the precooling flask through a solenoid valve, while the other provided a slower but continuous flow through a shielding coil surrounding the hydrodynamic entry length. The shielding coil was constructed from a length of 1-1/2 inch copper pipe that had been wrapped with 0.25 inch diameter copper tubing; the pitch of the coil was approximately one inch, and the coil was soldered to the pipe. The length of the coil was approximately equal to the length of the hydrodynamic entry portion of the test section, and the device was supported by means of an adapter bolted to the test section vacuum flange.

The shielding coil was employed to decrease the energy transfer to the gas in the hydrodynamic entry length; assurance was thereby provided that the measured entry mixer temperature was approximately equal to the

temperature of the gas at the start of heating. During the heated flow runs with precooling, the thermocouples attached to the hydrodynamic entry length revealed that the temperature in the entry length did not vary appreciably from the inlet mixer temperature except in the vicinity of the test section flange. The energy transfer by conduction through the test section flange was accounted for in the data reduction technique.

CHAPTER IV

EXPERIMENTAL PROCEDURES

Instruments

The acquisition of data from the test assembly required the use of a wide variety of measuring instruments. A concerted effort was made to obtain the best equipment that was available and to assure that the various instruments were performing at their optimum level during the duration of the experiment.

Measurements of the power dissipated by the test section during heated flow runs were obtained from the AC voltage drop across the test section and the circuit current. The voltage was measured with a Fluke Model 883 AB differential voltmeter having an AC accuracy of $\pm$ (0.1 percent of reading + 25 microvolts); the current was measured with a Weston Model 370 ammeter having an accuracy of $\pm$ 0.25 percent of full scale and which had been factory calibrated with the Model 327 current transformer that was used. All of the test section voltages were measured with respect to ground potential due to the fact that some difficulty was encountered in the use of the Fluke meter for the measurement of the difference between two voltages both of which were above ground

potential. During early heat loss calibration runs a Weston Model 310 wattmeter with a matching Model 327 current transformer was used; the wattmeter had a rated accuracy of 0.25 percent of full scale.

The volumetric flow rate of the test gas was determined from a pair of Brooks Rotameters and, when possible, from a Precision wet test meter. The Rotameters were individually calibrated at the factory to an accuracy of $\pm$ 1 percent of full scale; the maximums of the ranges available during the course of the experiment were approximately 0.15, 0.5, and 2.5 standard cubic feet per minute of air at the usual operating pressure. The wet test meter had a rated accuracy of $\pm$ 1/2 percent and was calibrated to a maximum flow rate of one standard cubic foot per minute of air.

It was necessary to obtain measurements of both pressure levels and small pressure differences during the experiments, and a variety of instruments was available for this purpose. Pressure level measurements were made with 0 - 150 psi Heise gauges having a rated accuracy of 0.1 percent of full scale (0.15 psi). When the pressure was below 30 psig, a 60 inch Meriam well-type mercury manometer that had a scale divided in tenths of an inch was used. Identical manometers, filled with water and with mercury, were attached to the pressure tap manifold

for pressure drop measurements, but the mercury manometers were not required for pressure drop measurements during the course of this experiment. In addition, water filled, 60 inch Meriam inclined manometers were available for pressure drop measurements; these instruments had a range of ten inches and a smallest scale division of 0.01 inches. Extremely small pressure drops were measured on a Meriam Model 34FB2 micromanometer that had an accuracy of 0.001 inch of water.

The temperature measurements were obtained by using premium grade Chromel and Alumel wire supplied by the Hoskins Manufacturing Company and having a stated accuracy of $\pm$ 2 degrees Fahrenheit below 530°F. The Honeywell "Electronik 18" indicator used to measure the thermocouple output had an accuracy of 0.3 percent of span; the Honeywell adjustable range unit had an accuracy of 0.3 percent of span plus 0.1 percent of the maximum suppression. The Honeywell units were calibrated against a Leeds and Northrup Model 8686 millivolt potentiometer, a portable secondary standard with an accuracy of 0.03 percent of reading plus 3 microvolts. The accuracy figures quoted above implied an uncertainty of approximately 40 microvolts for the Honeywell system, but the results of the calibration procedure revealed that the Honeywell instruments did not deviate from the Leeds and

Northrup potentiometer by more than 15 microvolts over the millivolt range applicable to the experiment.

Adiabatic Runs

After the installation of the test section and prior to the beginning of the heated flow runs, a series of adiabatic flow runs was conducted to serve as a calibration of the pressure taps attached to the test section. Although the entire flow system had been checked for leaks with helium at 50 psi during the construction process, a leak check at the operating pressure of approximately 20 psi was established as the first step in a daily series of runs. The system was pressurized and a gauge was observed for a period of one hour or more; further leak checking with a soap solution was performed if there was a noticeable deviation of the gauge. During the interval required for the leak check, the ice reference junction was filled and the thermocouples were checked to ascertain that the reading was that of the ambient temperature in the room. After satisfactory completion of the leak check, the flow system was opened to the atmosphere and all manometers and pressure gauges that were to be used were zeroed. The system was again pressurized, the manometer zero points were checked, and flow was initiated. The zero points of the manometers

were checked at convenient intervals by isolating the manifold from the test section and opening the bypass valves. In the case of the adiabatic runs, the quantities of interest were the tap-to-tap pressure drops, the overall pressure drop, the inlet mixer temperature, the gauge pressure at pressure tap number one, the barometric pressure, and the appropriate information from the flowmeters in use. The response time for the pressure drop measuring system was of the order of 2-5 minutes, and it was dependent upon the magnitude of the pressure drop; the manometers were observed until the operator was convinced that a condition of equilibrium had been reached. Because pairs of identical instruments were used in the pressure drop measuring system, simultaneous indications of two adjacent pressure drops, involving three pressure taps, could be obtained. The usual technique allowed the measurement of all pressure drops for a given run with four manifold settings; for example, the pressure drops associated with taps numbered one, two, and three were measured first, followed by the pressure drops associated with taps numbered three, four, and five, and so on. At the end of each series of runs the zero point of the differential pressure manometers was again checked with the system at operating pressure and at atmospheric pressure to ascertain that no drift in the zero had occurred.

Before the beginning of the runs that employed helium as the test gas, the flow system was purged with a small mechanical vacuum pump in order to insure the presence of only one gas in the apparatus. This process consisted of lowering the pressure to approximately the boiling point of the water in the manometers and then refilling the lines with helium. This routine was repeated several times.

Adiabatic friction results are reported in Chapter 6.

Heat Loss Calibration Runs

The energy balance from which the energy transfer from the heated wall to the flow stream is determined requires the specification of the energy loss by radiation from the test section at each thermocouple location. In order to determine the radiation heat loss, several series of calibration runs were performed during which the test section was heated without gas flow. The technique involved the measurement of the temperature of the test section wall, the temperature of the surroundings, and the energy generation rate. Because it was not possible to ignore the heat transfer by conduction at points near the ends of the test section, appropriate temperatures on the electrodes were also measured.

Although the test section provided an almost entirely resistive load for the heating circuit, an attempt was made during the first series of heat loss runs to evaluate any deviation from unity power factor. A Weston Model 310 wattmeter with a matching current transformer was connected to the power circuit, and simultaneous measurements were recorded of the voltage, current, and wattage. Because the nature of the instrument scales did not permit the same degree of accuracy in the wattage as in the EI product, no specific value of the power factor was decided upon, but all of the measurements showed it to be quite close to unity.

The heat loss calibration runs also provided an opportunity for the measurement of the depression of the test section wall temperature due to the presence of the thermocouples and pressure taps. Each of these objects had the effect of a radiating fin that contributed to the transfer of energy from the test section to the surroundings (Hess, 1965), but the magnitude of the energy loss was much greater in the case of the pressure taps because of the larger size. The measurement of the temperature depression was accomplished by means of a probe constructed from 0.125 inch outside diameter by 2 inch long ceramic beads containing four longitudinal holes. All of the holes contained 0.010 inch diameter

Chromel and Alumel thermocouple wire; but two of them were fitted at the top with relatively stiff alignment bars made of 20 gauge Chromel and Alumel wire that served to position the probe within the test section and to insure electrical contact with the wall, see Figure 9. The 0.010 inch diameter wires protruding from the end of the probe were spot welded together to form a thermocouple junction at a location opposite to that of the point of contact between the alignment bars and the test section wall; the thermocouple wires and the alignment bars were electrically isolated. Thus, if one of the alignment bars was positioned at the same axial location on the test section as one of the wall thermocouples, then the probe thermocouple would measure the temperature near the center of the test section at this same axial location. The probe was inserted in the test section from the bottom and oriented opposite a wall thermocouple by equalizing the above ground potentials of one of the wall thermocouple wires and one of the alignment bars. Sufficient time was allowed for an equilibrium condition to be achieved, and the probe temperature, the wall temperature at the location of the probe, and the measured difference between the two were recorded. It was noticed that more careful attention to the use of thermocouple wire would be necessary in the future; several different sizes of

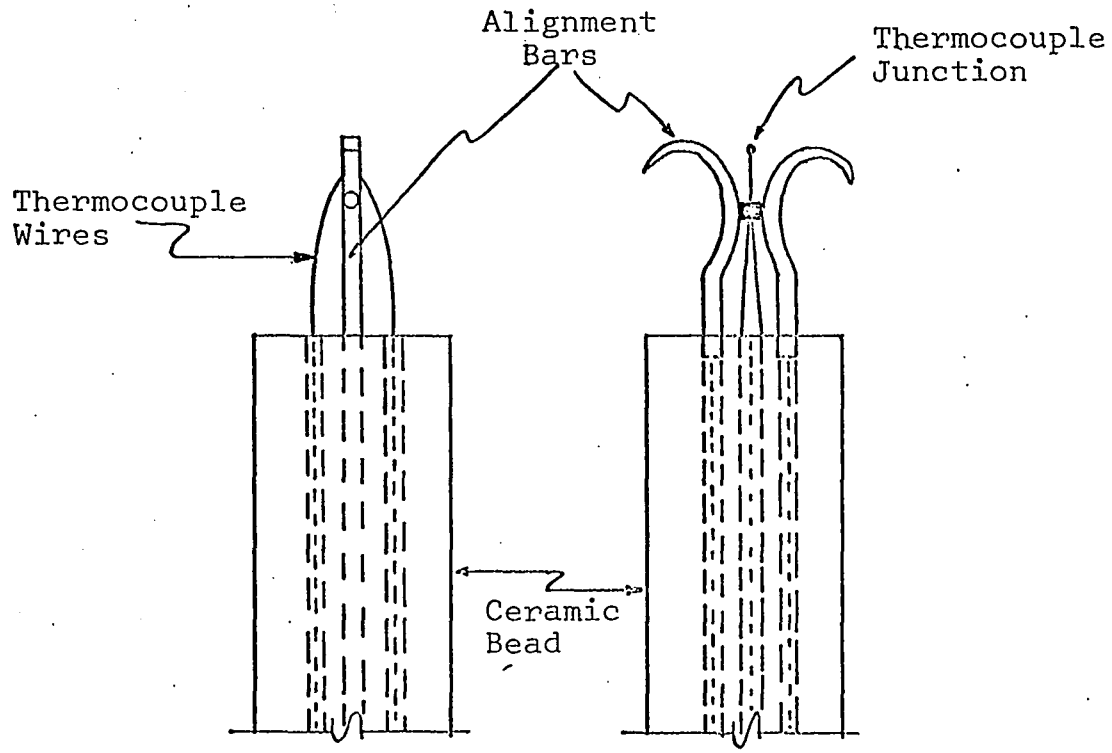

Figure 9. Heat Loss Probe Tip

Chromel and Alumel wire were used in the circuit, and the minute deviations of the various sizes from the standard calibration became important during the measurement of the small temperature differences between the probe and the wall. It is significant to note that the results of the probe technique were of little value near the ends of the test section where a steep temperature gradient existed; the energy transfer by conduction down the ceramic probe caused inaccurate probe temperature measurements. A graph of the wall temperature profile and the probe temperature profile is shown in Figure 10. On the basis of graphs such as this it was concluded that, although the pressure taps did cause a considerable depression of the wall temperature, the wall thermocouples at locations removed from pressure taps did give an accurate representation of the wall temperature; the probe temperature and the wall temperature were within 0.5 percent of one another in the range where readings were valid. The difference between the probe temperature and the wall temperature was possibly somewhat greater than the difference indicated by Figure 10 because of energy conduction along the probe. This possibility was suggested by the fact that the probe temperature was found to be lower than the wall temperature even for the moderate temperature gradient in the vicinity of $x/D = 20$.

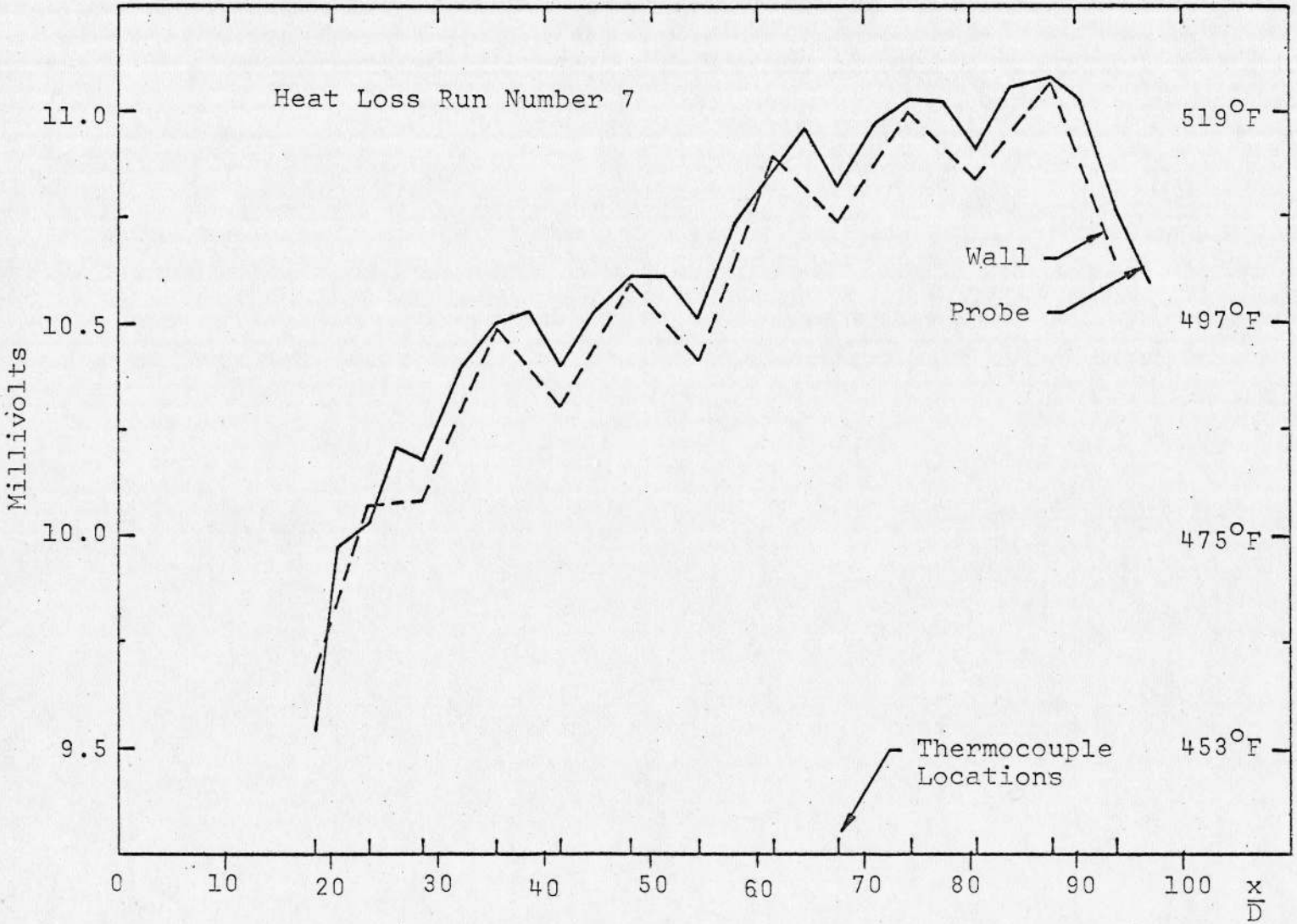

Figure 10. Temperature Profile Along Test Section

The temperature measurements made in close proximity to pressure taps were not used in the data reduction process.

During the course of the heat loss calibration runs, it was convenient to check the linearity of the test section voltage drop with the Fluke Model 883 AB voltmeter. The data reduction process for the flow runs employed the use of an energy generation rate per unit length of test section obtained by calculating the ratio of the total energy generation to the total expanded length of the test section; if the voltage drop was not linear, then this technique could lead to erroneous results for the wall heat flux. The linearity of the test section voltage is depicted in Figure 11 for one set of heat loss runs; it was concluded that reasonable accuracy could be expected from the data reduction technique described above. The dependence of the test section resistance on temperature was also examined during the calibration runs; the resistance was found to vary by no more than two percent over the entire range of the heat loss runs.

The sequence of the heat loss runs was adjusted to provide the best possible representation of the conditions during a set of flow runs. Because the test section oxidized and discolored when it was operated at temperatures above 1000°F, an attempt was made to provide some correspondence between the emittance of the

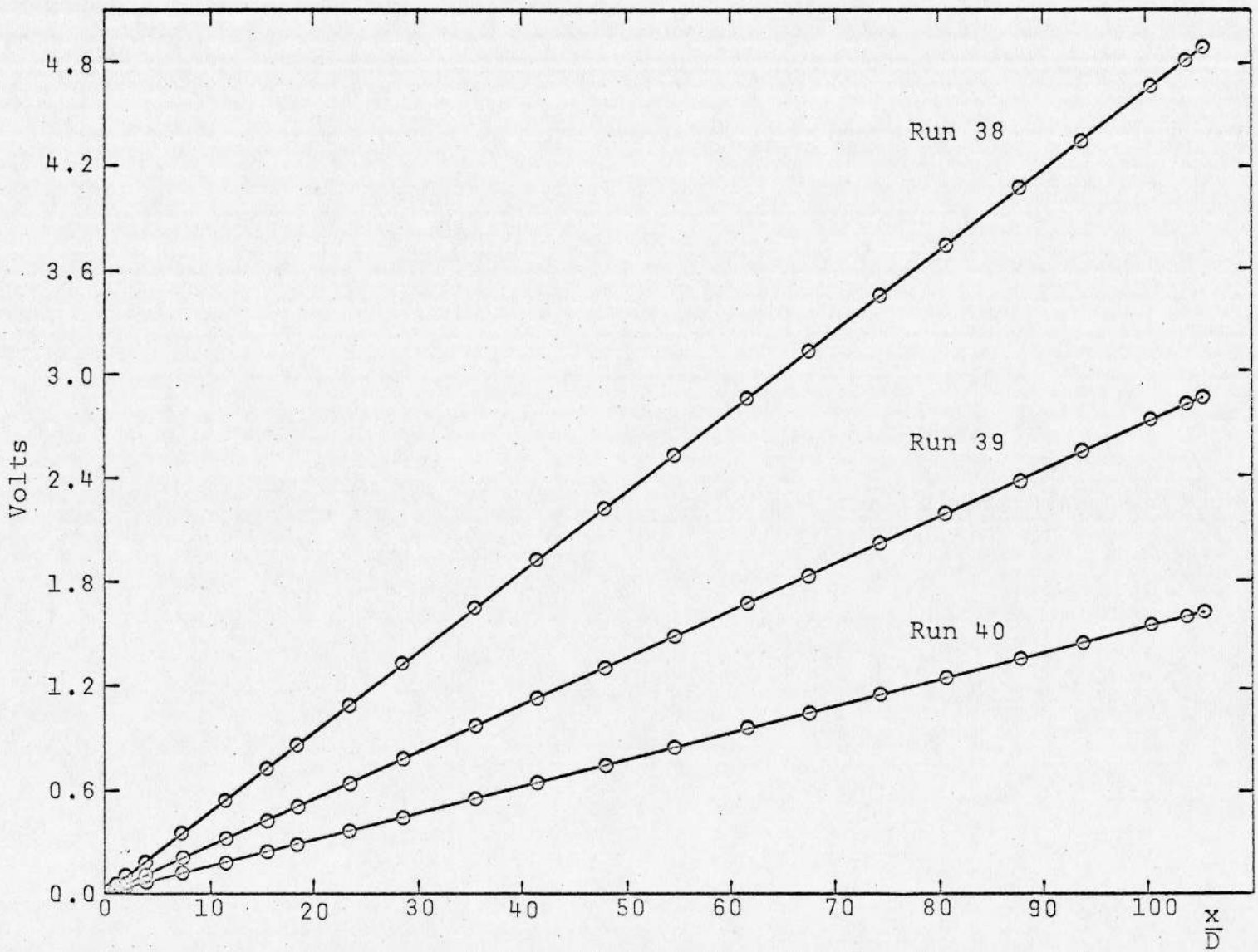

Figure 11. Above Ground Potential at Test Section Thermocouples

surface which occurred during the heat loss run and the emittance during the flow runs. For this reason, the heat loss runs that were conducted prior to a set of flow runs were taken at decreasing power levels, and heat loss runs that were conducted subsequent to a set of flow runs were taken at increasing power levels.

Heated Flow Runs

The procedure used at the beginning of each series of heated flow runs was identical to that employed for the adiabatic flow runs; the system was checked for leaks, the thermocouple circuits were checked, and the manometer zero points were checked. Flow was then established at a predetermined rate and an adiabatic flow run was usually conducted. The procedure then differed according to whether or not a heated, unprecooled run was desired. In the case of an unprecooled run, power was supplied to the test section and the necessary temperature, pressure drop, power, and flow rate information was recorded after a condition of equilibrium had been attained. This routine could then be repeated at higher power levels until some limiting point was approached.

A flow run that involved precooling was begun in precisely the manner described above for an unprecooled run. During the runs involving air, the flow was allowed to continue during the precooling process; helium flow

was stopped because of the high cost of helium. The transport flasks were slightly pressurized, and the liquid nitrogen was admitted to the precooling Dewar flask. The liquid nitrogen could flow into the flask either through a regulating valve and then through the entry length shielding coil, or through a solenoid valve directly. It was customary to use the solenoid valve method for an initial filling to the approximate desired operating level and then to attempt to match the rate of filling through the regulating valve (and the entry length shielding coil) with the continuous boil off from the precooling dewar. In this manner an attempt was made to maintain a continuous flow of liquid nitrogen through the shielding coil in order to keep the environment of the unheated hydrodynamic starting length at a constant temperature for the duration of a run. After the initial filling process, gas was again allowed to pass through the test section. The inlet mixer was monitored until a condition of equilibrium was reached, at which time the power was supplied to the test section. Following another period for the attainment of equilibrium, the flow run proceeded in a manner identical to that described for the unprecooled case. When the data had been accumulated, the power level was increased and the above process was repeated. After the run at the

highest intended power level, the power supply was turned off, the flow rate was decreased, and another series of runs began. The time required for an individual run at a particular flow rate and power setting was approximately ten to fifteen minutes; the acquisition of the pressure drop data was the controlling factor.

An attempt was made to conduct adiabatic flow runs using precooled air, but successful results could not be achieved. While operating the apparatus according to the procedure described for adiabatic runs and with liquid nitrogen in the precooling Dewar flask, extreme variations could be observed in the measurements of the test section wall temperature and the pressure drop; these variations were of the order of 20 percent and 100 percent respectively. The cause of the variations was attributed to condensation of the test gas in the precooling coil; the boiling point of liquid nitrogen at atmospheric pressure is below both the condensation point of oxygen and the boiling point of nitrogen at the test section internal pressure. The inlet mixer temperature was monitored with a strip chart recorder in an effort to maintain a steady value of about 200 degrees Rankine, but not enough precision was available in the liquid nitrogen level control system to maintain a constant mixer temperature above the boiling point of the liquid nitrogen.

The precooled air runs for which results are reported were conducted under circumstances which suggested the presence of condensation in the inlet mixer. The strip chart recorder indicated that the mixer temperature was stable at the boiling point of nitrogen; mixer temperature variations during the course of a run were no greater than three degrees Rankine. The oscillations in the wall temperature and the pressure drop were present to some degree during precooled and heated flow runs with air, but the effect diminished as the heating rate increased.

The fact that the variations in wall temperature and pressure drop did not manifest themselves during the runs with helium was taken as a confirmation that condensation was indeed the problem. During each of the helium runs, the inlet mixer temperature was approximately equal to the boiling point of nitrogen, and the maximum fluctuation during the process of data accumulation for a single run was about three degrees Rankine.

Data Reduction

The reduction of the experimental data was performed by means of a group of computer programs that is described in Appendix B. The data reduction process was, for the most part, composed of routine calculations,

but it was known from the outset that certain features might prove to be troublesome, and considerable attention was devoted to increased precision at these points. The following is a list of items that received particular emphasis.

1. The fin effect of the thermocouple wires was investigated during the heat loss calibration runs and the related thermocouple error was found to be less than five degrees Fahrenheit at wall temperatures of about 1000 degrees Fahrenheit.
2. The radial temperature difference between the outside and the inside of the test section wall was calculated for extreme cases and was found to be less than 0.3 degrees Fahrenheit.
3. Since heating of the gas causes an increase in the momentum of the flow, this acceleration was taken into account in the calculation of the friction factor.
4. Local gas properties were employed in the computation of local Nusselt numbers and local friction factors.
5. Thermal expansion of the test section in both the radial direction and the axial direction was

considered; expanded lengths and diameters were used in the appropriate calculations.

6. The conduction heat transfer through the test section wall in the axial direction was computed and included in the calculation of the energy transfer to the gas.
7. Due to the presence of the hydrodynamic entry length, it was not possible to measure the gas bulk temperature at the point where heating began; a copper shield cooled by liquid nitrogen was employed to minimize the temperature change in the entry length during precooled runs. A discussion of the wall temperature measurements for the hydrodynamic entry length is presented in Chapter III.
8. The energy transfer between the gas and the electrodes was taken into consideration by providing corrections in the heat loss program and in the enthalpy integration in the data reduction program.

CHAPTER V

ANALYSIS

The problem of transition from turbulent flow to laminar flow in a tube was examined from an analytical viewpoint in an attempt to predict the occurrence of the phenomenon. The situation was assumed to be that of steady, subsonic flow of a non-reacting gas in a smooth, circular tube of constant heat flux with a magnitude sufficient to cause significant property variations both radially and axially in the flow. No attempt was made to perform a thermal entry length solution in the classical sense; the primary goal was the determination of the effect of high heating rates on various parameters over the interval between a defined starting point and some axial location downstream from the starting point. The inlet condition, or starting point, was assumed to be that of flow with a uniform temperature profile and a fully developed adiabatic velocity profile, and the condition at an axial position was assumed to be that of a velocity profile which was based on the local conditions resulting from an assumed temperature profile.

The general approach to the analysis of the problem was that of an approximate, or integral,

technique rather than an assault on the governing differential equations, since the present state of turbulent analysis relies heavily on such artificial concepts as the eddy diffusivity and mixing length. The integral techniques have been used with good results in several situations; Kays (1966) has shown that the critical Reynolds number for transition from laminar flow to turbulent flow in a tube can be expressed in terms of a momentum thickness Reynolds number with the same numerical value as that obtained for transition of a boundary layer on a flat plate. The scheme discussed in the following paragraphs represents an attempt to apply the concept of a momentum thickness Reynolds number, Re_θ, to tube flow and to obtain a criterion for the transition from turbulent flow to laminar flow in terms of Re_θ. The utility of such a criterion is that it might permit prediction of turbulent to laminar transition in terms of local parameters; thus, for various geometries, velocity profiles, etc., a criterion for reverse transition would be available.

Definitions and Background

The concept of a momentum thickness was originally developed for flow over a flat plate, and its definition is based on a momentum balance for the flow

situation depicted in Figure 12. The definition of the momentum thickness is obtained by stating the equality

$$\rho_\infty u_\infty^2 \theta = \int_0^\infty \rho u(u_\infty - u)dy$$

where the term on the right hand side represents the change in momentum between the leading edge and the downstream point of interest; an extensive development of the definition is presented by Kays (1966). The salient features of the above definition are that the momentum thickness can be regarded as an area with unit depth and height θ oriented perpendicular to the flow direction and that the momentum thickness is related to the decrease in momentum brought about by the change in the velocity profile and the mass flow from the boundary layer into the free stream. The momentum thickness can be calculated from the definition if the velocity profile is known, and it can be related to the critical Reynolds number for transition from laminar flow to turbulent flow on a flat plate. The value for the critical Reynolds number

$$Re_{x,critical} = \frac{\rho u_\infty x}{\mu}$$

is considered to be between 200,000 and 500,000. If a value of 300,000 is selected, and if the momentum thickness predicted by the Blasius solution is substituted

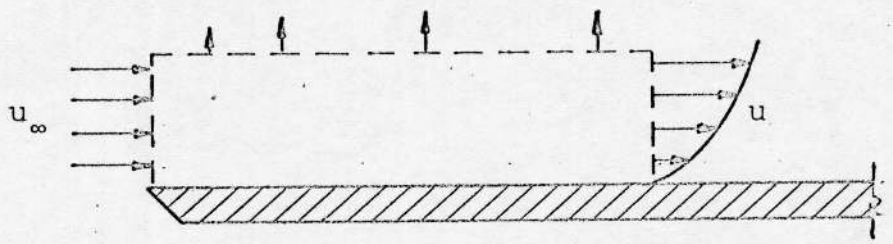

Figure 12. Control Volume for a Flat Plate.

for the length parameter x, then the result is a critical Reynolds number in terms of the momentum thickness,

$$Re_{\theta,\ critical} = \frac{\rho u_\infty \theta}{\mu} = 360$$

The momentum thickness is associated with the boundary layer integral equations, which were most helpful to Moretti and Kays (1965) in their prediction of turbulent to laminar transition for external flow, and it would be convenient if the momentum thickness concept could be applied to a circular tube. Kays (1966) suggests that, for laminar flow in a circular tube, a Reynolds number based on centerline velocity and momentum thickness has a value of 360 if the corresponding Reynolds number based on mean velocity and tube diameter has a value of 2000. The flat plate definition of momentum thickness,

$$\theta = \int_0^\infty \frac{\rho u}{\rho_\infty u_\infty} \left(1 - \frac{u}{u_\infty}\right) dy$$

can be applied directly to a tube by using the tube radius as the upper limit of integration, the centerline velocity as the free stream velocity, and the laminar velocity profile

$$u = u_{cl}\left(\frac{2y}{R} - \frac{y^2}{R^2}\right)$$

The definition of the momentum thickness becomes

$$\theta = \int_0^R \frac{u}{u_{cl}} \left(1 - \frac{u}{u_{cl}}\right) dy$$

for constant properties, and the resulting momentum thickness is

$$\theta = \frac{2R}{15}$$

which, when substituted into the accepted definition of critical Reynolds number yields

$$Re_{\theta,critical} \simeq 260$$

This figure is substantially different from the value of 360 suggested by Kays, and the result indicates some inconsistency in the direct application of the flat plate definition of momentum thickness to a circular tube.

It is instructive to return to the definition of momentum thickness which was obtained from a momentum balance on a control volume surrounding a flat plate. The same technique can be applied to a tube through the use of the control volume shown in Figure 13; this situation represents the development of the parabolic laminar profile from a uniform profile at the entrance to the tube. The momentum flux across sections AB and CD can be written as follows:

$$\text{momentum flux across AB} = \pi R^2 \bar{\rho}\bar{u}^2$$

$$\text{momentum flux across CD} = \int_0^R \rho(r)[u(r)]^2 \, 2\pi r dr$$

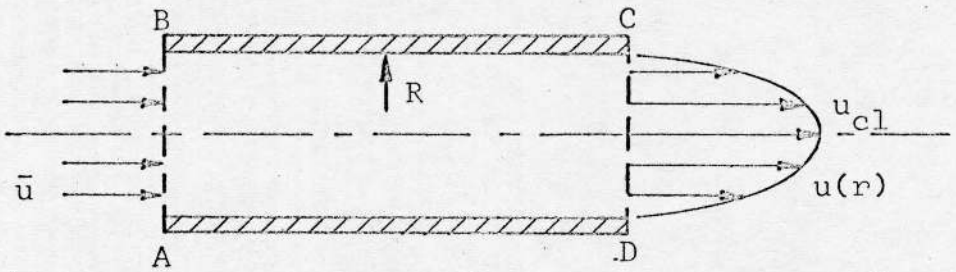

Figure 13. Control Volume for a Tube

The integral form of the momentum flux across CD may be evaluated by assuming the presence of the laminar velocity profile

$$u = 2\bar{u}[1-(\frac{r}{R})^2];$$

and, with the further assumption that the density is constant, the result is

$$\text{momentum flux across CD} = \frac{4}{3}\pi R^2\bar{\rho}\bar{u}^2$$

$$= \frac{4}{3}\,(\text{momentum flux across AB})$$

Thus, the momentum flux at the location of the fully developed profile is 1/3 greater than the momentum flux at the entrance to the tube; this result is in contrast to the momentum defect that results from a similar treatment of the boundary layer on a flat plate. It is possible to define a momentum thickness on the basis of this momentum difference by assuming that the added momentum lies in a ring of thickness θ adjacent to the wall and that the fluid in the ring travels at the mean velocity of the flow. The analogy to the flat plate momentum thickness definition then becomes

$$\bar{\rho}\bar{u}^2\pi[R^2-(R-\theta)^2] = \frac{1}{3}\pi R^2\bar{\rho}\bar{u}^2$$

which, for constant density, reduces to the quadratic equation

$$\theta^2-2R\theta+\frac{1}{3}R^2 = 0$$

after solving this equation and ignoring the choice of roots that would make the momentum thickness greater than the tube radius the result is

$$\theta = 0.1835R \approx 0.092D$$

The two pertinent Reynolds numbers can now be examined; the usual critical Reynolds number is

$$Re_D = \frac{\bar{u}D}{\nu} = \frac{u_{cl}D}{2\nu} = 2000$$

and the momentum thickness Reynolds number is

$$Re_\theta = \frac{u_{cl}\theta}{\nu} = \frac{u_{cl}D}{\nu}\,\frac{\theta}{D} = (4000)(0.092) = 368$$

This result agrees much more favorably with the suggestion made by Kays than does the result of the application of the flat plate definition of momentum thickness, and it provides a starting point for the consideration of the turbulent flow problem that is the subject of this study.

It is possible to apply the above technique to a turbulent velocity profile; the simple power profiles suggested by Nikuradse serve as an example. For a Reynolds number of 4000 the recommended radial velocity distribution is

$$\frac{u}{u_{cl}} = \left(\frac{y}{R}\right)^{1/6} ; \quad \frac{\bar{u}}{u_{cl}} = 0.791$$

The integral for the momentum flux across section CD in Figure 13 can be written in terms of the wall distance

parameter y as follows:

$$\text{momentum flux across CD} = 2\pi\rho\int_{o}^{R} [u(r)]^2\, r\,dr$$

$$= 2\pi\rho\int_{R}^{o} [u(y)]^2\, (R-y)(-dy)$$

Substitution of the velocity distribution and reversal of the limits of integration yields

$$\text{momentum flux across CD} = 2\pi\rho u_{cl}^2\int_{o}^{R}\left(\frac{y}{R}\right)^{1/3}(R-y)dy$$

$$= \frac{9}{14}\,\pi R^2\rho u_{cl}^2$$

which, expressed in terms of the bulk velocity, becomes

$$\text{momentum flux across CD} = 1.0274\pi R^2\rho\bar{u}^2$$

$$= 1.0274\ (\text{momentum flux across AB})$$

The corresponding result for the customary profile

$$\frac{u}{u_{cl}} = \left(\frac{y}{R}\right)^{1/7} \quad ; \quad \frac{\bar{u}}{u_{cl}} = 0.817$$

becomes

$$\text{momentum flux across CD} = 1.0196\pi R^2\rho\bar{u}^2$$

$$= 1.0196\ (\text{momentum flux across AB})$$

The outstanding feature of these results is the fact that, although the development of the turbulent profile requires an increase in momentum, the increase is smaller than the increase associated with the corresponding laminar profile.

Present Analysis

In the previous section it was demonstrated that the momentum thickness can be related to transition, in certain flow situations, through the use of an appropriate Reynolds number. An attempt was made to extend the various techniques to the transition from turbulent flow to laminar flow in a tube; momentum thickness Reynolds numbers were calculated by means of a computer program which performed operations based on a simplified model of the flow situation. The flow was examined at a single axial location; when changes in quantities such as momentum and temperature were required, it was assumed that the flow had originally posessed a uniform temperature profile and a fully-developed adiabatic velocity profile.

The first step in the procedure was the specification of the mass flow rate and the initial bulk temperature; a corresponding fully-developed velocity profile for constant fluid properties was then obtained. The local velocities for fully-developed turbulent flow were calculated for various values of the wall distance, y, between the tube wall and the centerline according to the universal velocity profile (law of the wall) suggested by Martinelli (Kays, 1966)

$$u^+ = y^+ \qquad (y^+ < 5)$$

$$u^+ = -3.05 + 5.00 \ln y^+ \qquad (5 < y^+ < 30)$$

$$u^+ = 5.5 + 2.5 \ln y^+ \qquad (y^+ > 30)$$

In the above expressions,

$$u^+ = u(g_c\tau_w/\rho)^{-0.5}$$

and

$$y^+ = y(g_c\tau_w/\rho)^{0.5}/\nu$$

The value of the wall shear stress, which was required for the calculation of u^+ and y^+, was obtained from the bulk entry Reynolds number and the Blasius friction factor relationship,

$$f = 0.079\ Re^{-0.25}$$

Subsequent to the calculation of the constant properties, law of the wall profile, an attempt was made to account for the effect of heating on the flow by means of the superposition of a temperature profile on the velocity profile. The temperature profile was assumed to be linear and to extend from some point in the stream, usually about $y^+ = 30$, to the wall; the temperature in the core of the flow was assumed to be equal to the bulk entry temperature. This technique allowed various wall-to-bulk temperature ratios to be specified, and a velocity profile for each temperature ratio was calculated using local fluid properties and the law of the wall relationship. A new value of the bulk temperature was calculated after each change in the wall-to-bulk temperature ratio according to the relationship

$$T_b = \frac{1}{Au_b} \int_A uTdA$$

where the local velocities were obtained from the profile computed for the preceeding value of the wall-to-bulk temperature ratio. The above expression is a convenient definition of the bulk temperature for use in the present investigation; a more appropriate definition would involve more explicit consideration of the dependence of the density on area. The wall shear stress for each of the variable properties velocity profiles was obtained from the Blasius relationship, but the overall results were quite sensitive to the choice of the Reynolds number; the bulk Reynolds number, the wall Reynolds number, and a Reynolds number based exclusively on wall properties were used during the course of the investigation. Different thicknesses, both constant and variable, were used for the specification of the temperature profile. As a check on the results, the mass flow rate was calculated by an integration routine from each computed velocity profile and the local values of the density.

Several different definitions were employed for the momentum thickness and the momentum thickness Reynolds number. The momentum thickness was calculated by using the flat plate definition, the circular tube definition based on a ring element, and simply the distance from the wall to the point where y^+ was equal to 30 or equal to 42. The momentum thickness Reynolds numbers were always

calculated using the bulk density, the centerline velocity, and the selected thickness, but the viscosity was adjusted to provide bulk Reynolds numbers or wall Reynolds numbers.

It was considered to be desirable that the thickness used in the calculation of the momentum thickness Reynolds number increase with an increase in the wall-to-bulk temperature ratio; this result would correspond to the thickening of a low velocity layer adjacent to the wall. Although the momentum thickness based on the momentum integral for tube flow was the most satisfying choice from a philosophical standpoint, the calculations revealed that it either failed to grow or decreased depending upon the choice of the Reynolds number used in the computation of the variable properties wall shear stress. The momentum change associated with the development of the profile is small, and it is apparently quite sensitive to the specification of the friction factor. The choice of definitions for momentum thickness and momentum thickness Reynolds numbers appeared to be subordinate to the choice of the Reynolds number used for the wall shear stress calculation.

Despite the simplicity of the model of the flow situation, some results were obtained which appear to reflect, at least qualitatively, the reaction of the flow

stream to high heating rates. The family of curves shown in Figure 14 is an example; in this case the momentum thickness Reynolds number

$$Re_\theta = \frac{\rho_b u_{cl} \theta}{\mu_w}$$

is displayed versus the wall-to-bulk temperature ratio. The wall Reynolds number was used to obtain the wall shear stress, and the definition of momentum thickness for a flat plate was used in the calculation of the momentum thickness Reynolds number. Each of the curves in Figure 14 represents a particular mass flow rate, and therefore a particular bulk entry Reynolds number. Since the calculations were based on turbulent flow velocity profiles, mass flow rates corresponding to laminar flow in the adiabatic case were not considered. For each curve, the momentum thickness Reynolds number was computed first for the case of a wall-to-bulk temperature ratio of unity; subsequent calculations for larger values of the wall-to-bulk temperature ratio resulted in lower values of the momentum thickness Reynolds number. Furthermore, the curves appear to have the proper relationship to one another, since, for a specified momentum thickness Reynolds number, a higher value of T_w/T_b is required for a large bulk entry Reynolds number (mass flow rate) than for a small bulk entry Reynolds number.

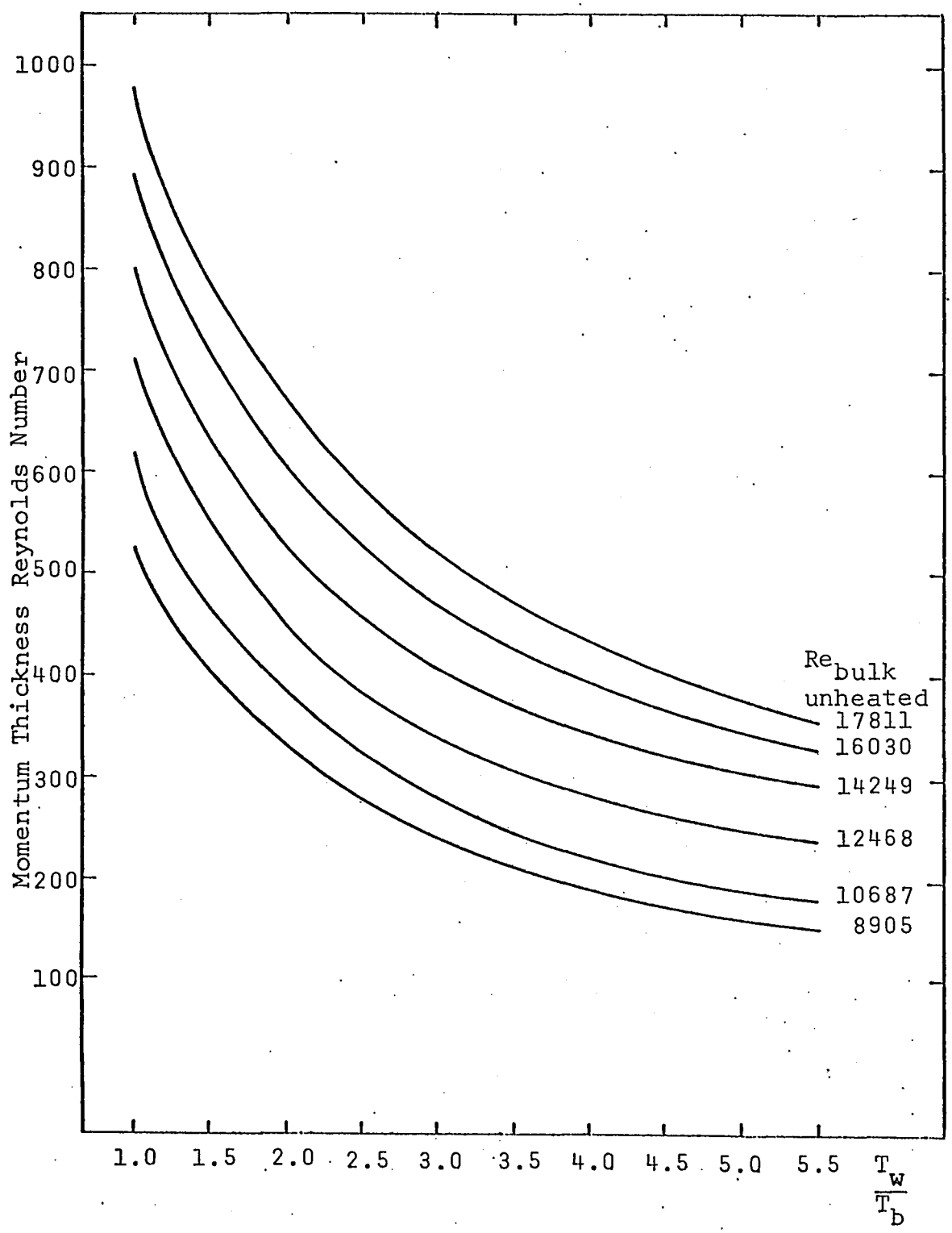

Figure 14. Variation of Momentum Thickness Reynolds Number with T_w/T_b for Various Bulk Entry Reynolds Numbers.

Throughout the calculations on which Figure 14 was based, a tube inside diameter of 0.230 inches was assumed, and the properties of air were used. The experimental results were used to attach further significance to Figure 14; additional discussion is provided in Chapter VI.

As a gas passes through a heated tube, the viscosity in the immediate vicinity of the wall increases and the local velocity is depressed below the value that would be predicted by a constant properties relationship such as the law of the wall. In order to satisfy the continuity equation under these circumstances, it is necessary for the velocity near the center of the tube to increase. The change in velocity near the tube wall, as predicted from the analysis described above, is depicted in Figure 15; examination of the velocity profiles indicates that the proper trends are present.

The intent of the analytical scheme described in the preceeding paragraphs was to provide an indication of the effect of high heating rates on a turbulent flow situation through the use of integral techniques. Since the basic technique was simply the application of successively higher wall-to-bulk temperature ratios to a turbulent profile at a particular location, no conclusions concerning the flow in an "entry length" may be drawn.

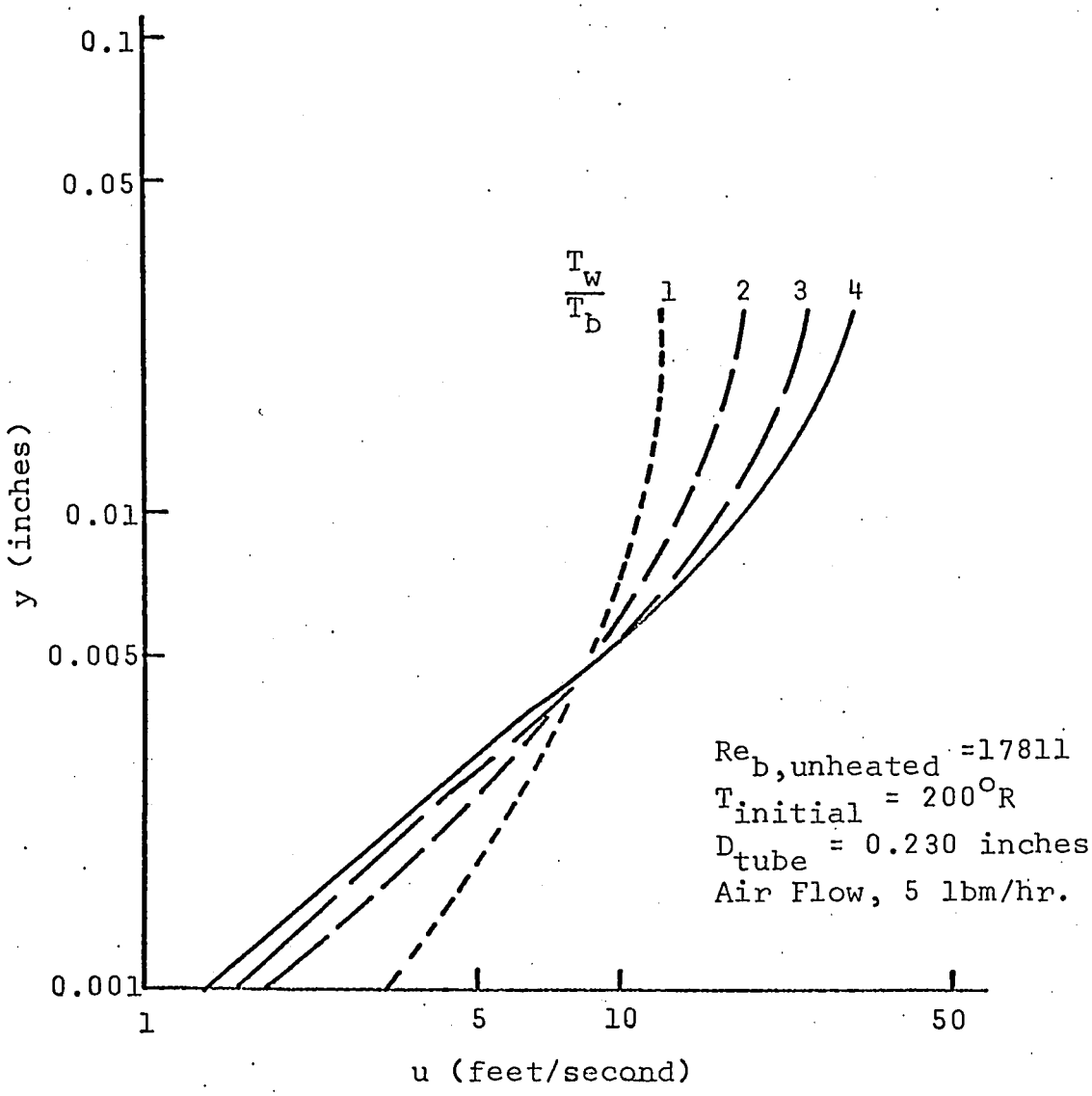

Figure 15. Velocity Profiles Near Wall

The primary virtue of the scheme is that it does demonstrate the applicability of the integral techniques, which are common tools in the analysis of external flows, to internal flow situations. In essence, the present analysis provides a starting point for future investigations employing more complex models of the flow.

CHAPTER VI

RESULTS AND DISCUSSION

The experimental results provided by the test facility encompassed a range of conditions broader than that which was specifically applicable to the study of the phenomenon of turbulent-to-laminar transition. Of particular interest to the work at hand were those runs that actually involved the transition effect, but, as mentioned previously, some data was obtained in domains reported by other investigators in order to establish a level of confidence for the test section and the data reduction techniques. The following discussion will concentrate first on the relatively well-established topics such as adiabatic flow and mildly heated flow without precooling; the results will then be used as a basis for the consideration of the situations involving reverse transition. Table II provides a summary of the information pertinent to the experimental runs involving heat transfer and friction data. These are explored in the following discussion. Runs not shown were heat loss or adiabatic friction factor runs. Subsequent to run number 57, accidental overheating of the test section caused the structural failure of pressure tap 8 and pressure tap 9;

Table II Summary of Heated Flow Runs

Run Number	Gas	Symbol	Conditions	T_{wall} Max °R	T_w/T_b Max	Bulk Inlet Reynolds
20	Air	○	Heating, No Precooling	999	1.35	17728
26	Air	◺	Heating and Precooling	1034	2.28	14249
28	Air	□	Heating and Precooling	970	2.46	16130
31	Air	◇	Heating and Precooling	1018/963	2.68	20685
32	Air	▱	Heating and Precooling	1269	3.08	19436
33	Air	◇	Heating and Precooling	1565	3.62	15712
35	Air	▽	Heating and Precooling	1031	2.09	10930
36	Air	◺	Heating and Precooling	1371	2.97	12016
37	Air	□	Heating and Precooling	1699	4.43	16944
41	Helium	◭	Heating and Precooling	674/778	1.91/1.99	7885/8511
42	Helium	◆	Heating and Precooling	874	2.12	8720
43	Helium	■	Heating and Precooling	1124	2.68	8795
44	Helium	●	Heating and Precooling	1392	3.30	9052
46	Helium	▰	Heating and Precooling	1084	2.21	4327
47	Helium	◆	Heating and Precooling	1489	2.59	4195
49	Helium	⬮	Heating and Precooling	1240	2.22	2580
52	Helium	⬮	Heating, No Precooling	1072	1.34	7445
54	Helium	◆	Heating, No Precooling	1086	1.32	4064
56	Helium	▰	Heating and Precooling	1057	2.04	1711
57	Helium	▰	Heating and Precooling	1506	2.39	1724
64	Air	⬡	Heating, No Precooling	1053	1.44	37543
66	Air	▢	Heating, No Precooling	1025	1.41	32389

Note: Maximum Mach Number = 0.15

no data are reported from these locations for runs with numbers larger than 57.

Both the raw data accumulated during the experimental runs and the reduced data obtained from the computer programs are recorded in the files of the Energy, Mass, and Momentum Transfer Laboratory of the University of Arizona.

The results of the analysis of the experimental uncertainties presented in Appendix C indicate that the Nusselt numbers and friction factors for the heated runs can be expected to be accurate to within 10 percent and 13 percent, respectively. The pressure drop measurements for the adiabatic runs were more stable than were those for the heated runs; the adiabatic friction factors can be expected to be accurate to within 10 percent. These limits apply to the figures and to the comments that follow, and they should be helpful in the evaluation of the experimental results.

Adiabatic Friction Factor Results

Adiabatic flow runs were conducted at convenient intervals during the course of the data acquisition as a means of checking the performance of the pressure taps and the associated pressure drop measuring system. The pressure gradients were calculated with Procedure FIT;

this technique employs two adjacent pressure drop measurements for the calculation of the pressure gradient at a particular location. Each computed friction factor, therefore, involves information obtained at pressure taps upstream and downstream from the stated location, and values are not produced for the first and last pressure taps.

The calculated friction factors were compared to the Blasius friction factor that would prevail at the bulk entry Reynolds number for each run; the results of this comparison are shown in Figure 16. From the data displayed in this manner, it was observed that pressure tap number five characteristically produced values more than five percent lower than those obtained from the other taps; the friction factors at pressure tap number five were considered suspect in the examination of subsequent data. The erroneous results at tap number five could have been caused by either a small burr on the inside of the tube as a result of the electrostatic drilling operation or a change in the cross sectional area of the tube caused by the brazing process.

In addition to the strictly adiabatic friction factors, Figure 16 also depicts the results of run 21, during which the air was precooled with liquid nitrogen prior to passing through the unheated test section.

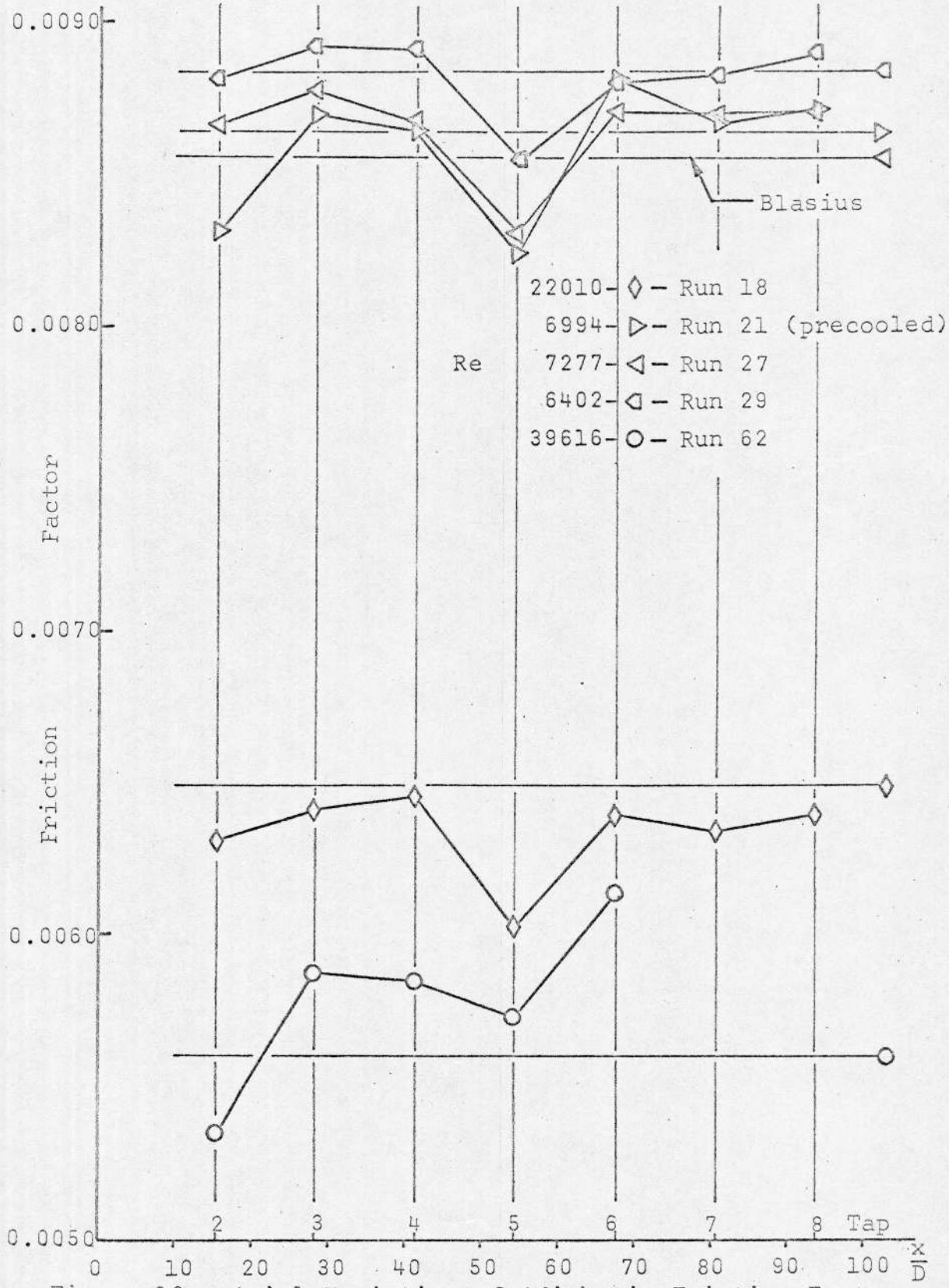

Figure 16. Axial Variation of Adiabatic Friction Factors

Although this condition was technically that of a heated flow run because of the energy transfer to the gas from the surroundings, the increase in the gas bulk temperature was observed to be less than 50 degrees Fahrenheit, so that the adiabatic flow computation technique at least provides an approximation to the precooled but unheated condition. Examination of Figure 16 shows that the results of run 21 exhibit the same trends and approximately the same degree of agreement with the Blasius prediction as do the results of the adiabatic runs.

Heated Flow Without Precooling

Several experimental runs involving heated flow without precooling were conducted in order to provide a correspondence with the findings of other investigators. Both air and helium were employed, and the range of Reynolds numbers was large enough to include the region of primary interest.

The conventional heat transfer parameters applicable to the downstream region of the tube ($x/D>40$) are displayed in Figure 17 along with the following correlation equation chosen to represent the data points:

$$Nu_b = 0.022\ Re_b^{0.8}\ Pr_b^{0.4}\ \left(\frac{T_w}{T_b}\right)^{-0.5}$$

The variation of the fluid properties is accounted for by means of the wall-to-bulk temperature ratio raised to

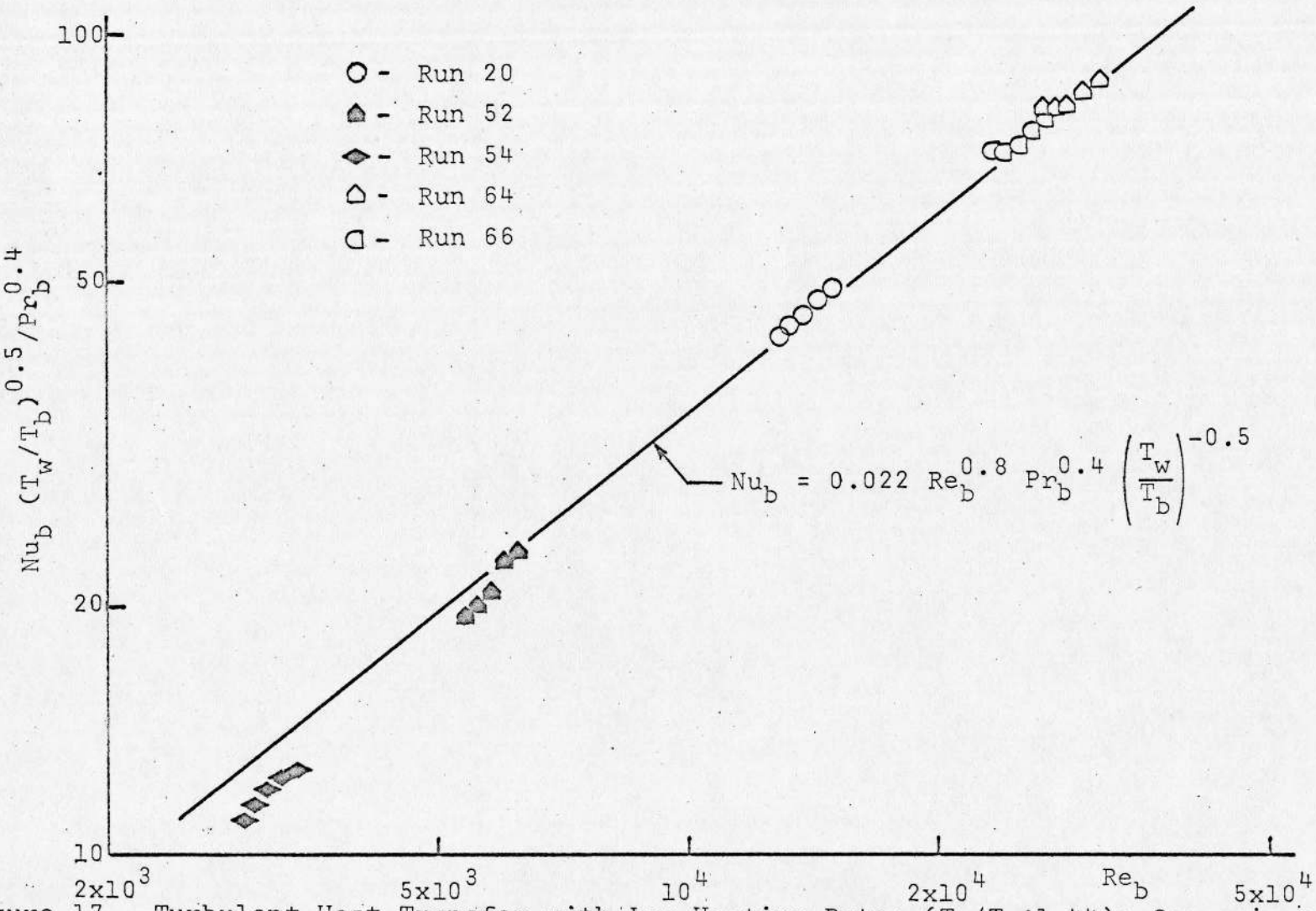

Figure 17. Turbulent Heat Transfer with Low Heating Rates (T_w/T_b<1.44): Comparison of Data to Accepted Correlation.

some power and by means of the coefficient which depends upon the location of the bulk of the data; it is significant to note that there is no generally accepted value for either the exponent or the coefficient. According to Kays (1966), the analytical treatment of Deissler and Eian suggests a value of -0.34 for the exponent, but Perkins and Worsoe-Schmidt (1965) found that a value of -0.7 was more suitable. Barnes (1960) suggested different values of the exponent for different gases, specifically -0.4 for air and -0.185 for helium in the range of Reynolds numbers from 10000 to 20000. The basis of the selection of -0.5 as the value of the exponent in Figure 17 was the fact that it appeared to provide a better fit to both the air and the helium data points than did the other values that were considered. There is considerable support for the value chosen; Humble, Lowdermilk, and Desmon (1951) and McCarthy and Wolf (1960) each recommend values of -0.55 for the exponent, while McEligot (1963) suggests a value of -0.5 for the exponent and a value of 0.021 for the coefficient. It should be noted that the value of the constant in the correlation expression must also be considered. Perkins and Worsoe-Schmidt (1965), for example, found that the constant had a value of 0.024 when the exponent -0.7 was used, while McEligot (1963) reported that a constant of 0.021 was

necessary to correlate his data when the exponent -0.5 was employed. It would appear that the relationship chosen for the present data most closely resembles the form suggested by McEligot.

Examination of Figure 17 indicates that the correlation equation suggested above agrees with the experimental data to within five percent except for the low Reynolds number range in which the flow is bordering on the transition region. This result suggests a possible dependence of the exponent of the wall-to-bulk temperature ratio on Reynolds number, a result also indicated by Barnes, but it is more probable that the correlation equation does not represent the data accurately in the low Reynolds number range. The maximum wall-to-bulk temperature ratio for the experimental runs represented in Figure 17 was less than 1.5; both McEligot (1963) and Reynolds (1968) have discussed heat transfer correlation for low Reynolds number flow at low heating rates. In comparison to the Dittus-Boelter correlation

$$N_u = 0.021\ Re^{0.8}\ Pr^{0.4}$$

for Reynolds numbers in the neighborhood of 3000, McEligot observed approximately the same trends as those shown by Figure 17 while Reynolds observed good agreement between the Dittus-Boelter relation and experimental data that had been corrected for the effect of variable

properties. It may also be observed that the agreement near a Reynolds number of 3000 in Figure 17 would be greatly improved by the use of 0.021 as the correlation coefficient.

The friction factor information provided by the runs for which the gas was heated but not precooled was also examined with respect to accepted empirical relationships; Figure 18 illustrates the comparison between the measured friction factors and the Blasius correlation for these runs. The maximum deviation from the Blasius line is about ten percent, but it should be pointed out that the results from pressure tap number five, previously found to be consistently erroneous, have not been included in the figure.

Heated Flow With Precooling

Friction factors in the laminar regime were obtained during two runs with bulk entry Reynolds numbers less than 2100, relatively high heating rates, and precooling. The results are shown in Figure 19 which employs the correlation relationship

$$f = \frac{16}{Re_b} \left(\frac{T_w}{T_b}\right)^{1.4}$$

to account for the variable properties effects; the maximum deviation from the laminar line is about ten percent. Although the analytical solution of

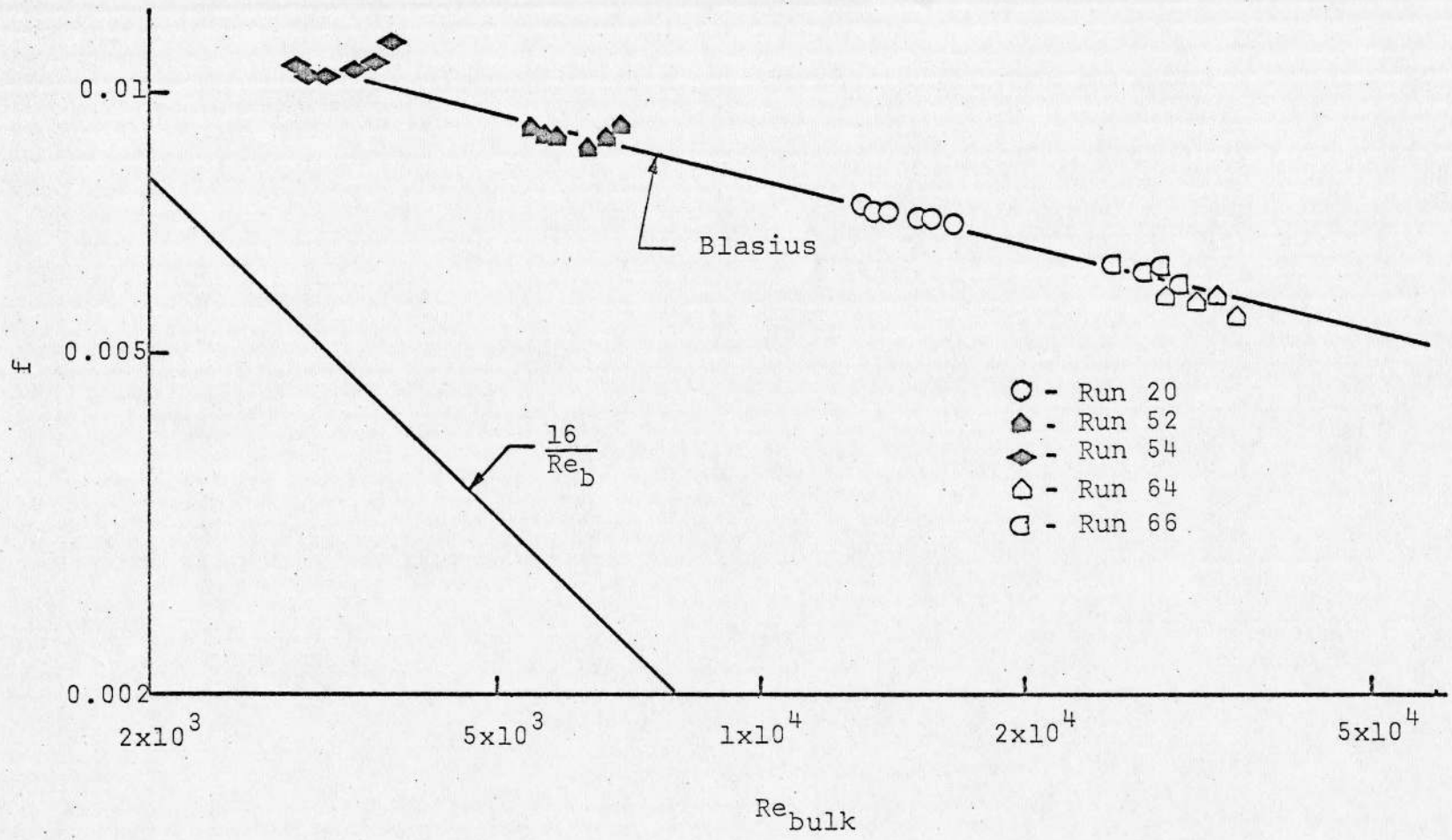

Figure 18. Turbulent Friction Factors with Low Heating Rates ($T_w/T_b<1.44$): Comparison of Data to Accepted Correlation.

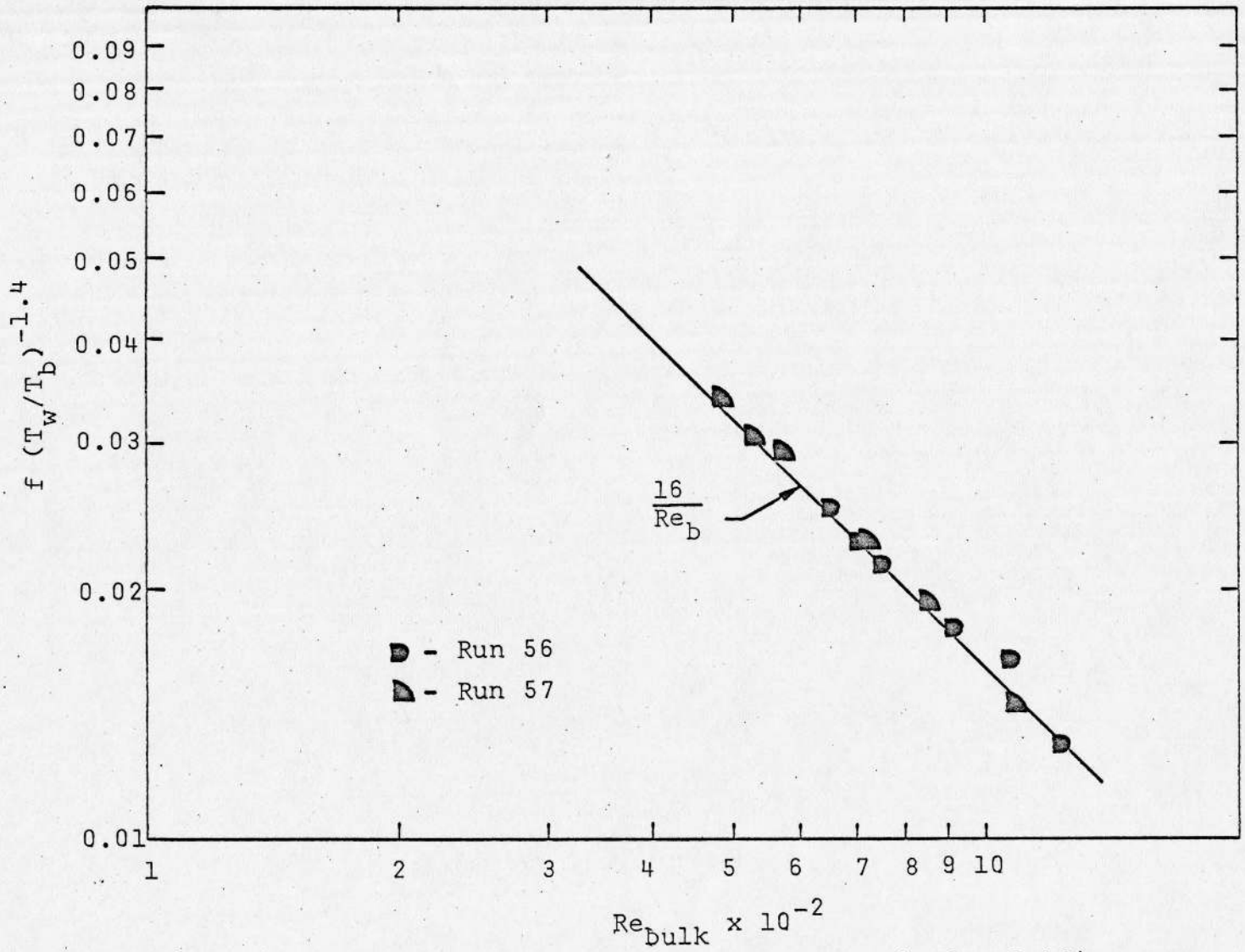

Figure 19. Laminar Friction Factors with Moderate Heating Rates ($T_w/T_b < 2.49$): Comparison of Data to Accepted Correlation.

Worsoe-Schmidt and Leppert (1965) suggested that the value of the exponent of the wall-to-bulk temperature ratio should be unity, the experimental results of other investigations suggest a value of about 1.4. For example, Bankston, Sibbitt, and Skoglund (1966) used a value of 1.41, and Davenport and Leppert (1965) recommended a value of 1.35.

The heat transfer results for the laminar flow runs with relatively high heating rates and precooling are shown in Figure 20; the coordinates are the bulk Nusselt number and the Graetz solution length parameter $(x/D)/Re\ Pr$. The solid line represents the analytical thermal entry length solution for laminar flow with constant fluid properties and constant wall heat flux in a circular tube (Kays 1966). Examination of Figure 20 reveals good agreement between the analytical prediction and the experimental results; except for data points which were obtained near the ends of the test section, the deviation of the experimental results from the prediction is no greater than ten percent.

The discussion to this point has been devoted to quantities which have been treated in detail by other investigators. The material presented in Figures 16, 17, 18, 19, and 20 does, however, provide an indication that the apparatus, the procedure and the data reduction

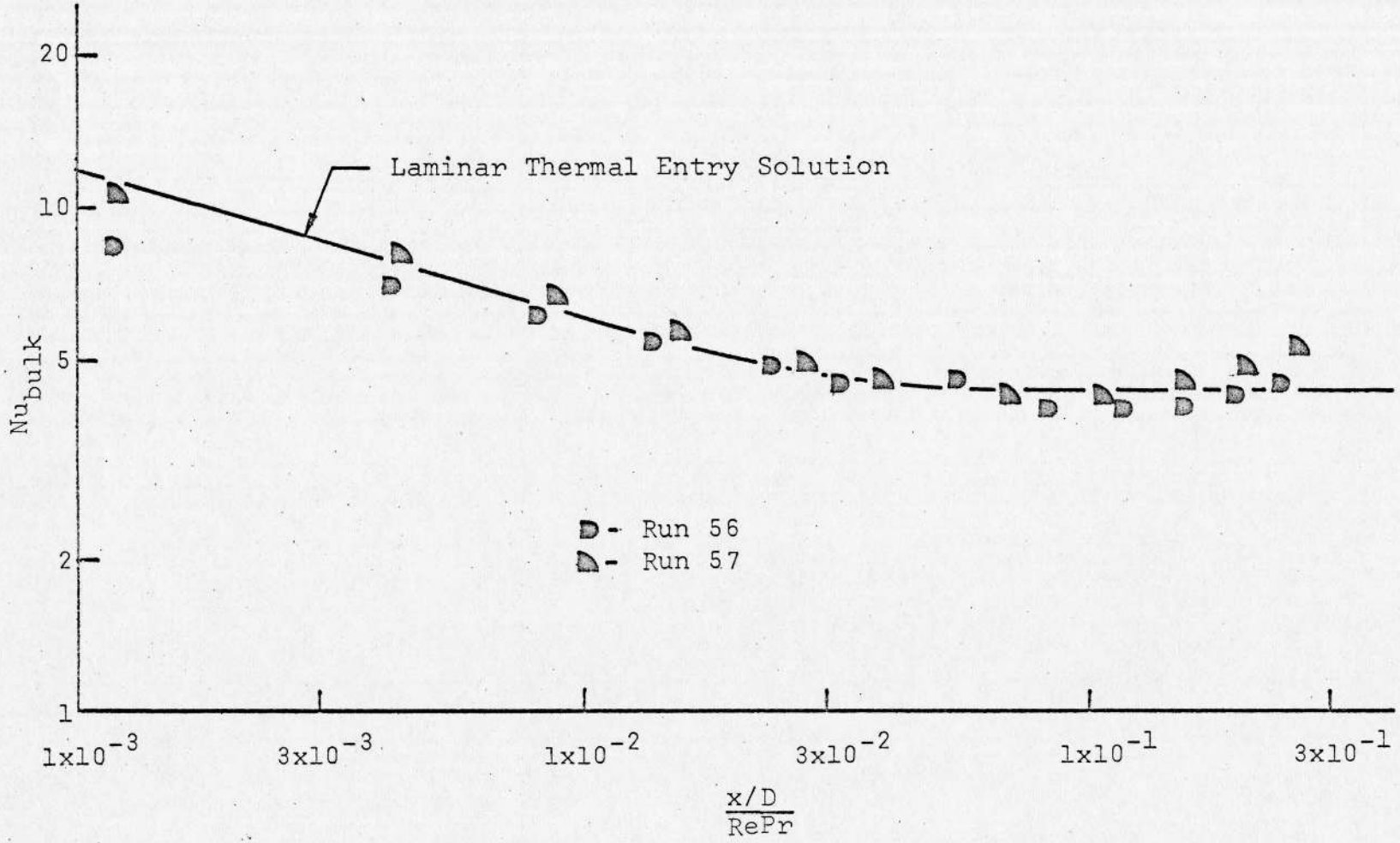

Figure 20. Comparison of Laminar Heat Transfer Data to the Laminar Thermal Entry Solution for Constant Properties, Runs 56, 57.

process combine to yield results that compare favorably with generally accepted criteria. In general, the deviations from accepted correlation parameters lie within the predicted uncertainty intervals for the experiment. Since the comparisons have been made over a relatively wide range of Reynolds numbers which contains the region of primary interest, it is reasonable to assume that reliable information can be obtained for the transition region by employing the same techniques.

Transition Results

Several techniques were employed for the graphical demonstration of the phenomenon of turbulent-to-laminar transition. After demonstrating the reliability of the various experimental and numerical procedures, graphs of the bulk Nusselt number versus the Graetz solution length parameter $\frac{x/D}{RePr}$ were constructed as shown in Figures 21 through 25. The solid line on these figures represents the analytical constant properties thermal entry length solution for laminar flow in a circular tube; a turbulent flow situation should yield a downstream value which is dependent on Reynolds number and which is considerably higher than the laminar downstream value.

Figures 21 and 23 show that this is indeed the case for runs 20 and 51 through 54 during which no pre-cooling was used and during which the wall-to-bulk

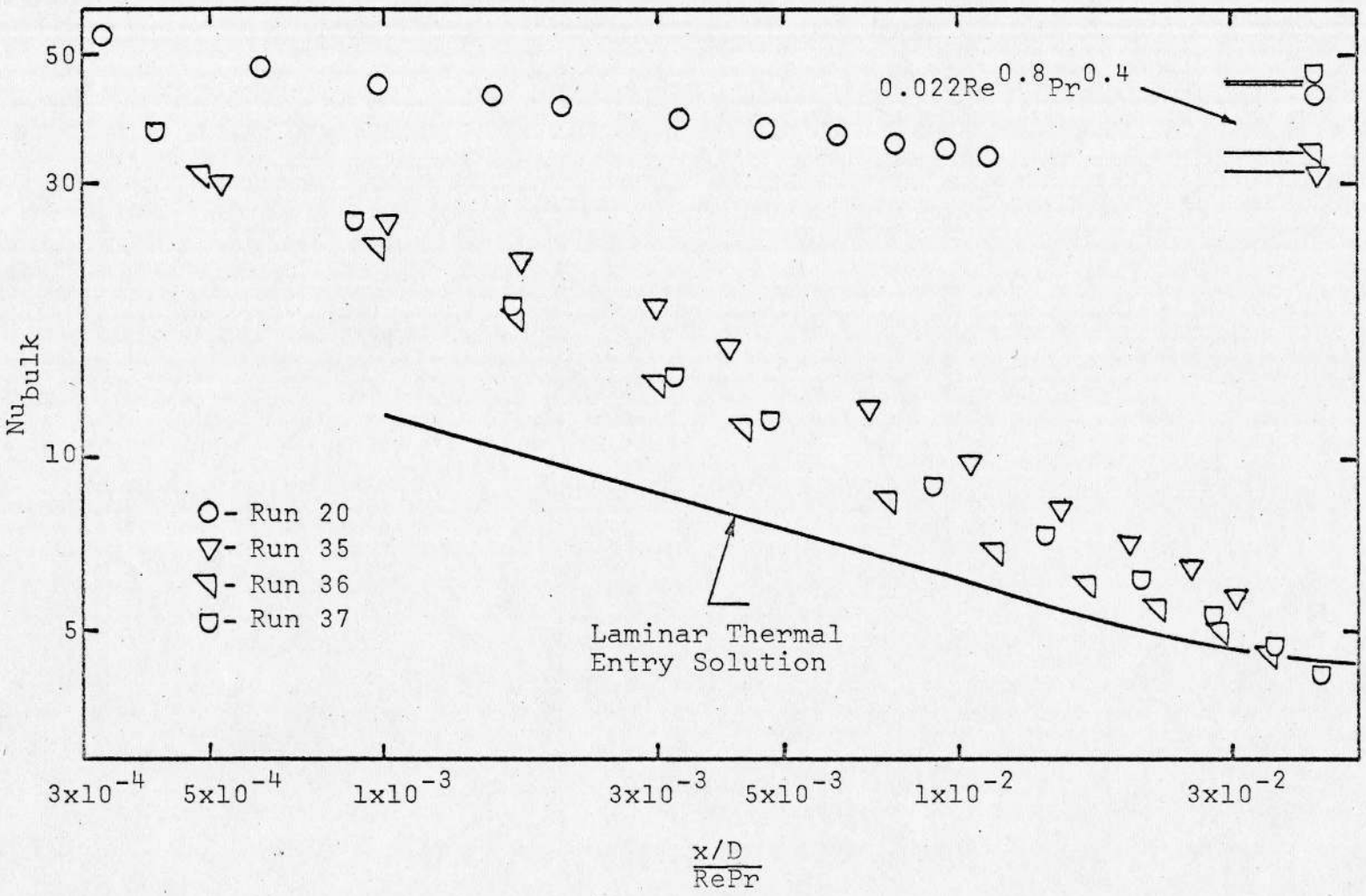

Figure 21. Comparison of Heat Transfer Data to the Laminar Thermal Entry Solution for Constant Properties, Runs 20, 35, 36, 37.

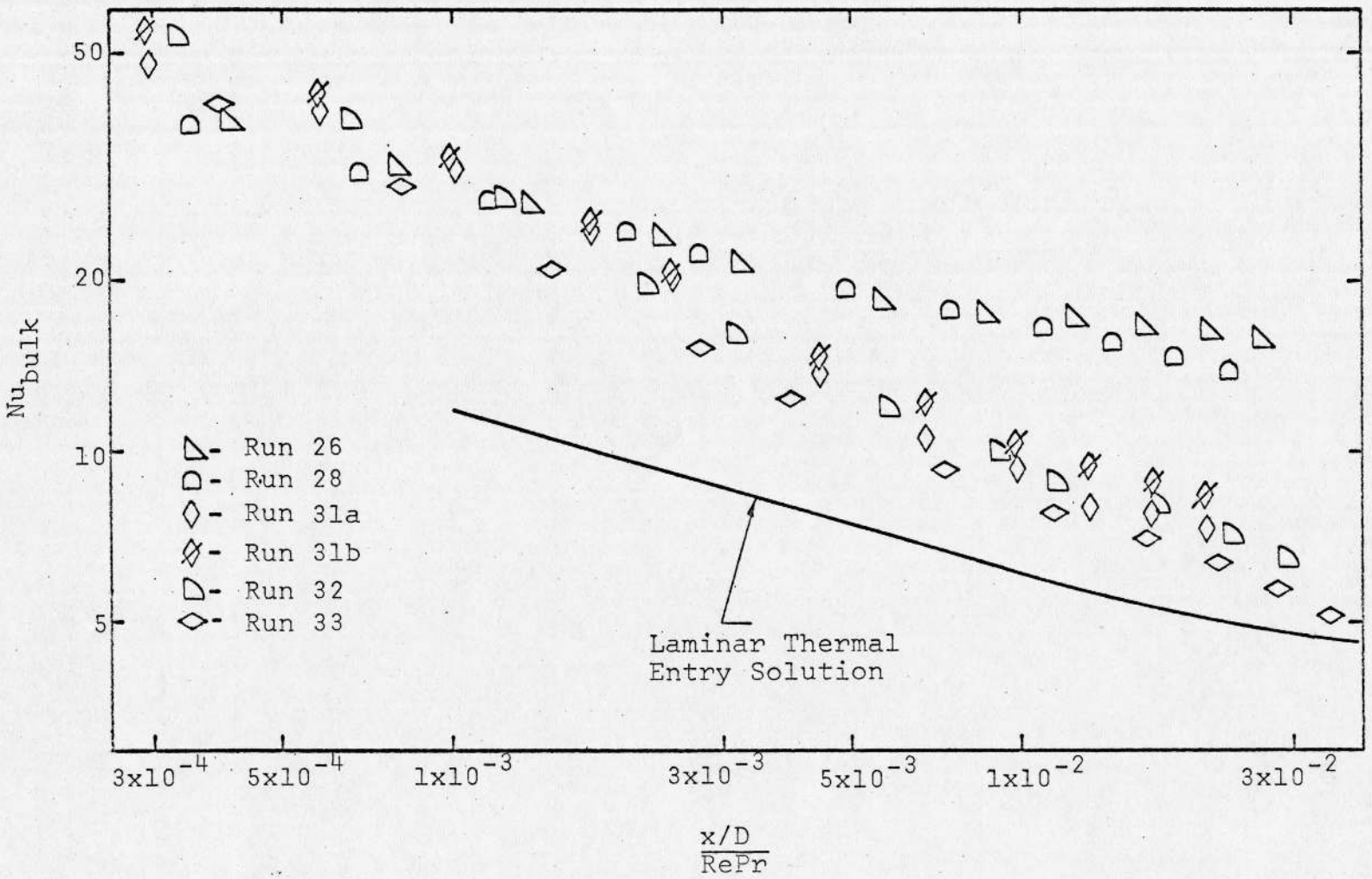

Figure 22. Comparison of Heat Transfer Data to the Laminar Thermal Entry Solution for Constant Properties, Runs 26, 28, 31a, 31b, 32, 33.

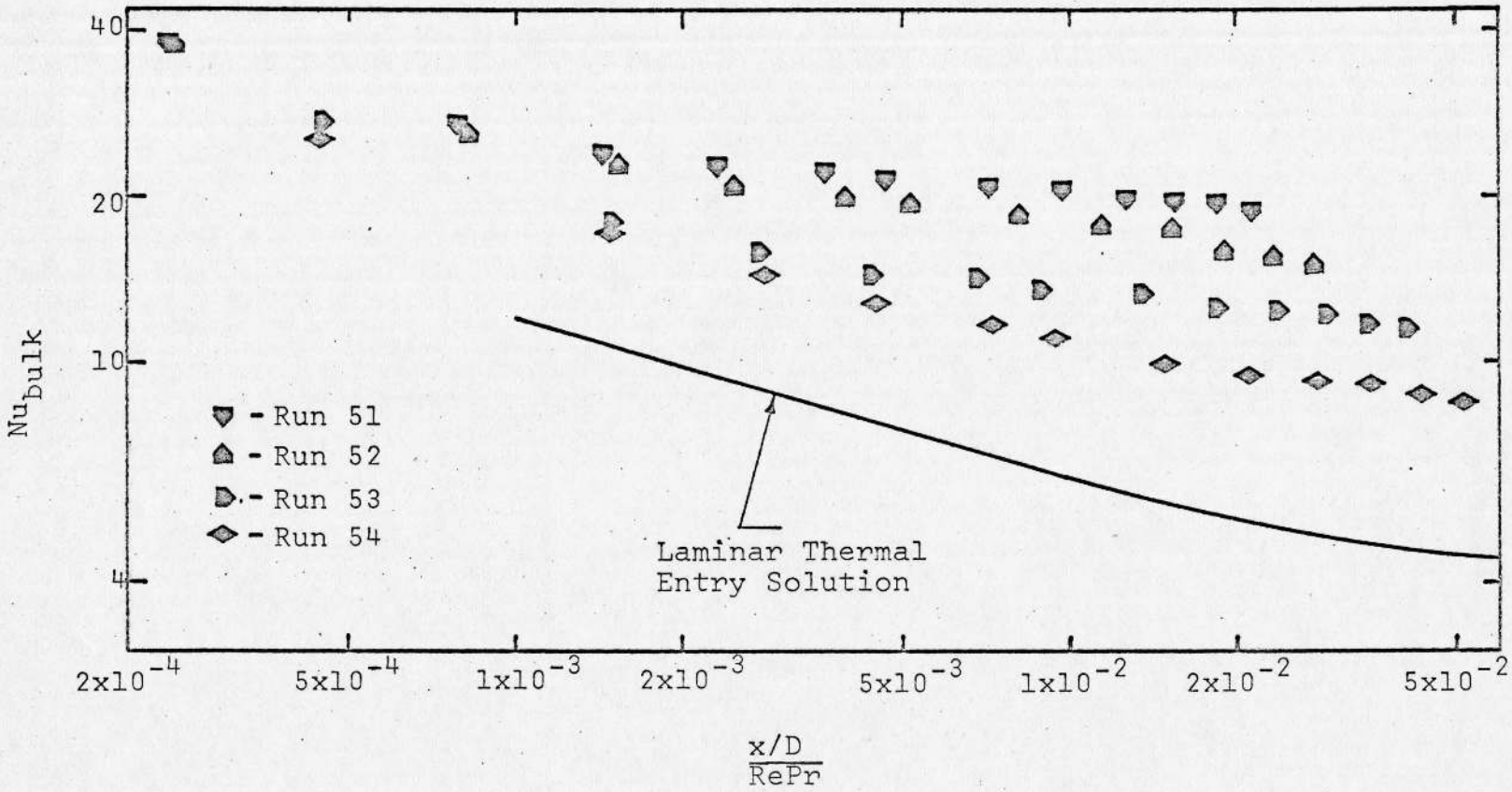

Figure 23. Comparison of Heat Transfer Data to the Laminar Thermal Entry Solution for Constant Properties, Runs 51, 52, 53, 54.

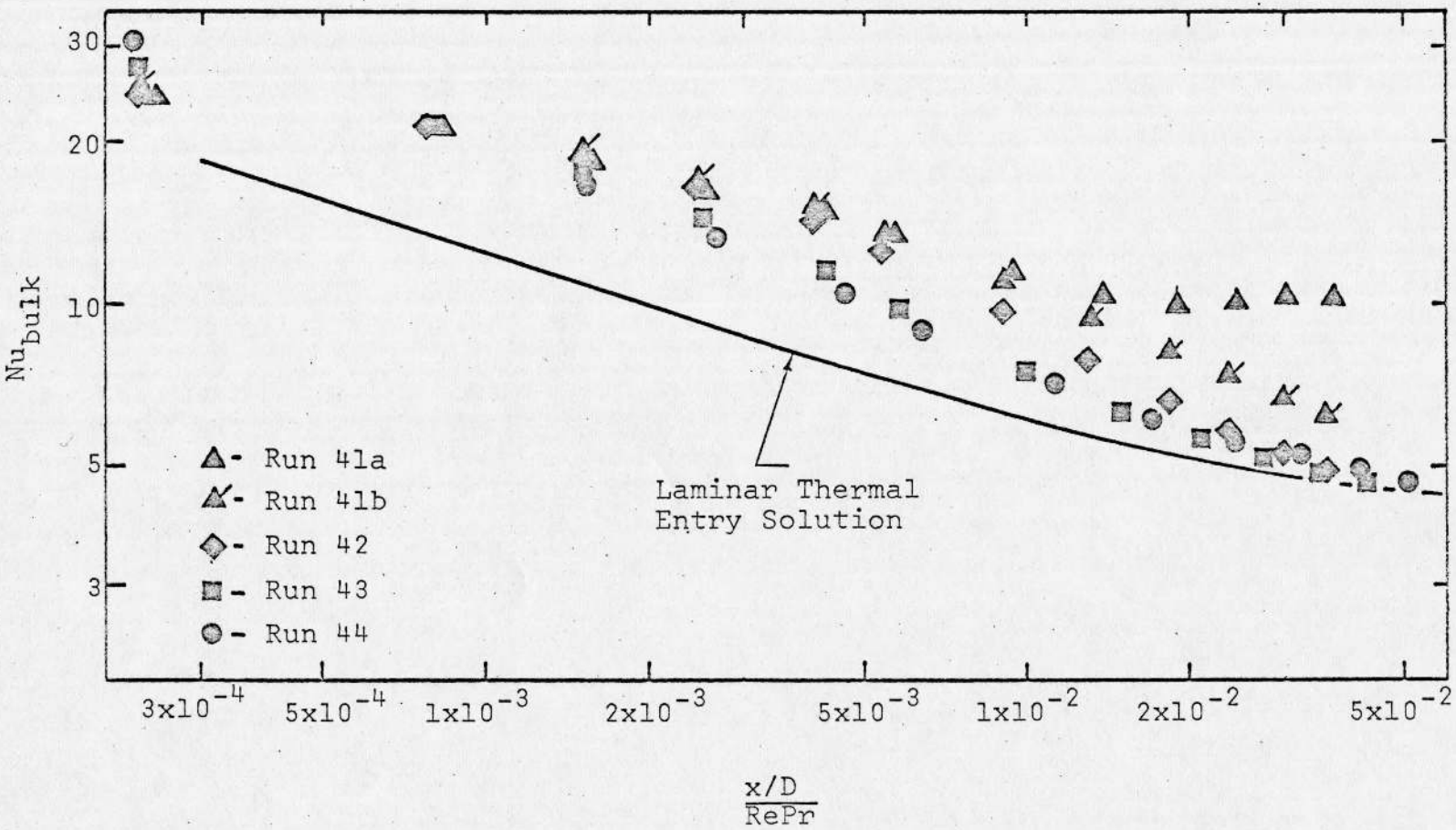

Figure 24. Comparison of Heat Transfer Data to the Laminar Thermal Entry Solution for Constant Properties, Runs 41a, 41b, 42, 43, 44

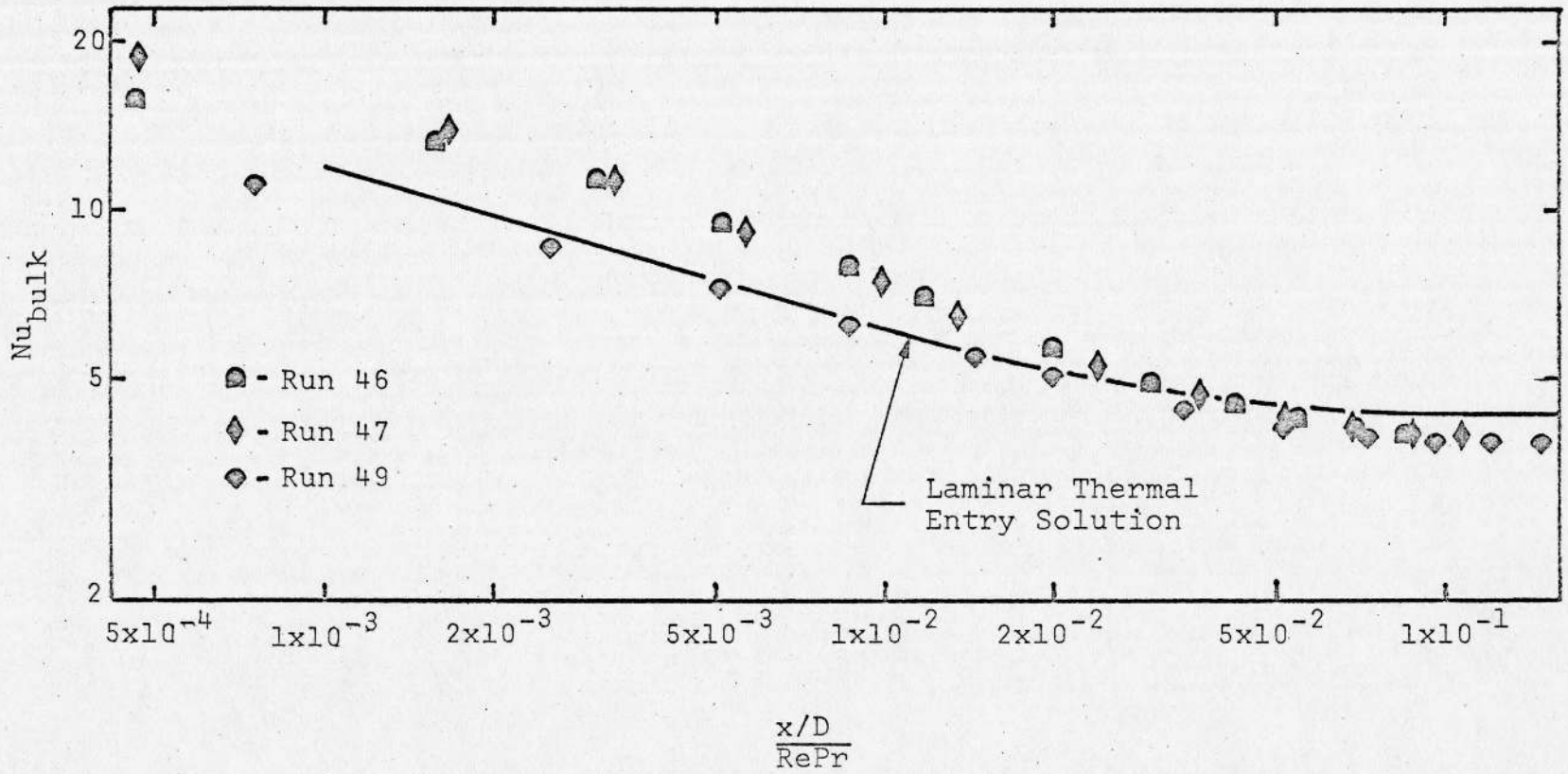

Figure 25. Comparison of Heat Transfer Data to the Laminar Thermal Entry Solution for Constant Properties, Runs 46, 47, 49.

temperature ratio never exceeded 1.35. The results for these runs are typical of turbulent flow, and they provide a dramatic contrast to the runs conducted at higher heating rates. For wall-to-bulk temperature ratios in excess of two, a marked depression of the Nusselt number below the characteristic turbulent value occurs; in several cases values of the Nusselt number that would be expected for laminar flow are attained in the downstream region of the tube. A careful examination of the figures indicates that the degree of depression of the Nusselt number is dependent on both the wall-to-bulk temperature ratio and the bulk entry Reynolds number. For example, Figure 22 shows that a wall-to-bulk temperature ratio of 2.28 caused a substantially reduced, but nevertheless turbulent, downstream Nusselt number for a flow situation with a bulk entry Reynolds number of 14249 (run 26), while a wall-to-bulk temperature ratio of 3.62 was sufficient to cause very nearly laminar values for a bulk entry Reynolds number of 15712 (run 33). From these indications, it would appear that both the peak wall-to-bulk temperature ratio and the bulk entry Reynolds number are potentially valuable as parameters that could be used to predict the occurrence of turbulent to laminar transition. The peak temperature ratio and the bulk entry Reynolds number should be more appropriate than the

local values of temperature ratio and Reynolds number for the development of a prediction that will be applicable to the design of future equipment.

Of particular interest in Figure 24 is the apparent double valued character of run 41. This result occurred by virtue of a change in the wall temperatures during the run; the power and flow rate control settings were the same for both sets of points. Because the situation occurred on the first run of the series in which helium was used, the apparent instability could be attributed to inadequate equilibrium time for the apparatus. However, after a delay in the data acquisition process necessary for the repair of a sudden malfunction of the pressure drop measuring system (the author's adviser blew an inclined manometer), oscillations of the wall temperature were again observed for the same power setting and flow rate used in run 41. This result suggests that the conditions of run 41 represent a possible borderline value that can be employed in the prediction of the turbulent to laminar transition phenomenon.

Further evidence of the occurrence of turbulent to laminar transition was obtained from an examination of the variable fluid properties heat transfer correlation equation

$$Nu_b = 0.022\ Re^{0.8}\ Pr^{0.4}\left(\frac{T_w}{T_b}\right)^{-0.5}$$

for the downstream region of the tube. Figures 26 and 27 are graphical representations of this relationship for values of x/d greater than 40. This equation should represent turbulent flow data reasonably well for Reynolds numbers in excess of 3000, and the results depicted in Figure 17 show that this is indeed the case for moderate heating rates. For some of the runs, however, the results show values of the heat transfer parameter more than 50 percent lower than those predicted by the correlation equation, and it is significant to note that the percentage deviation increases as the value of x/d increases, i.e. the deviation increases as the bulk Reynolds number decreases. The same runs cited previously again serve as good examples; at the moderate heating rates of run 26 the data points agree with the correlation, but a pronounced and continuously increasing difference between the data and the correlation can be observed for run 33.

It is possible that a higher numerical value of the exponent of the wall-to-bulk temperature ratio in the correlation equation, say $(T_w/T_b)^{-0.7}$, would provide better agreement for the runs represented in Figure 26 by points that lie parallel to, but below, the correlation line. However, these runs possessed bulk inlet Reynolds numbers of 4000 or less, so that a high degree of accuracy cannot be expected from the turbulent

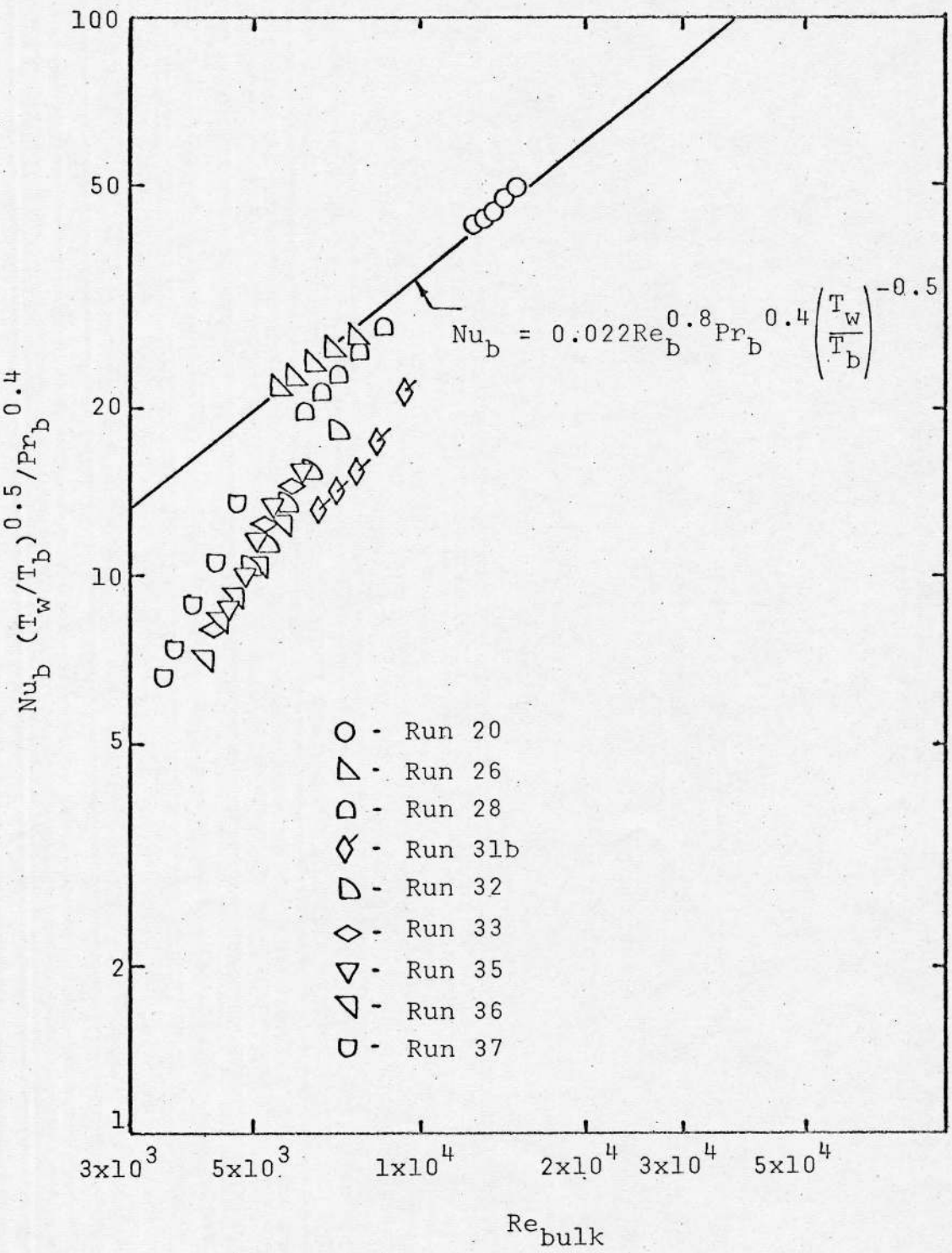

Figure 26. Heat Transfer Data in the Turbulent Low Reynolds Number Region for Air with $1.35<(T_w/T_b)_{max}<4.43$: Comparison to the Accepted Turbulent Correlation

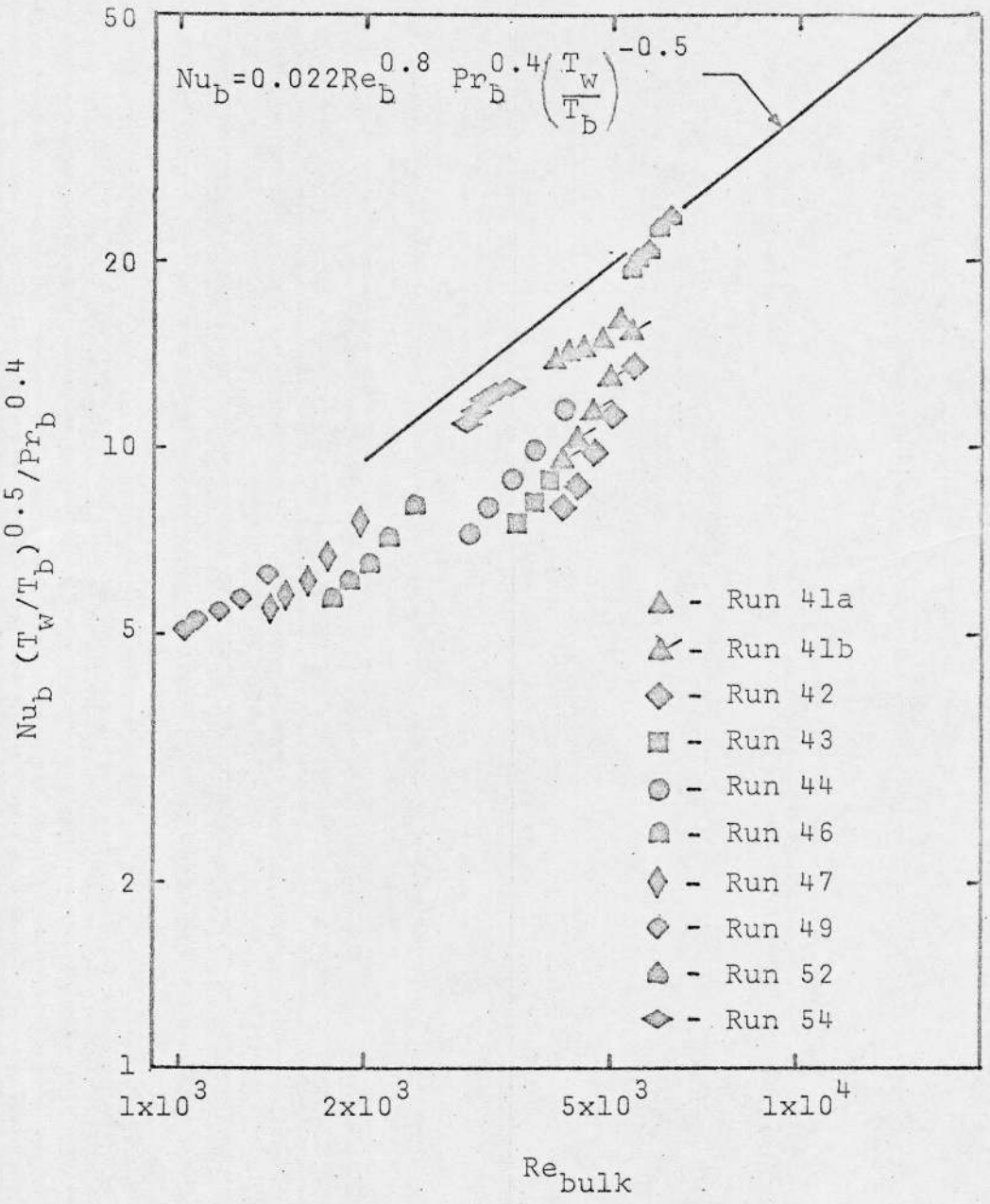

Figure 27. Heat Transfer Data in the Turbulent Low Reynolds Number Region for Helium with $1.32 < (T_w/T_b)_{max} < 3.30$: Comparison to the Accepted Turbulent Correlation

correlations, and the larger exponent might cause a deviation from the correlation for the high Reynolds number, low heating rate runs.

Another source of information concerning the transition from turbulent flow to laminar flow was provided by the friction factor data. The results of experimental runs involving laminar flow with moderate heating and turbulent flow with mild heating were presented in Figures 18 and 19; it was demonstrated that the friction factors for these conditions conformed quite well to accepted correlation equations. The friction factors obtained in circumstances for which turbulent to laminar transition was probable are displayed in Figures 28 and 29 with the more conventional results described above as reference values, but the distinction between the coordinates must be carefully noted. Each of the figures displays data for one run with mildly heated turbulent flow, one run with moderately heated laminar flow, and four runs for which turbulent to laminar transition was suspected. It should be emphasized, however, that Figure 28 employs a correlation of the type used by Perkins and Worsoe-Schmidt (1965) for turbulent flow,

$$f = \frac{.079}{Re_w} \left(\frac{T_w}{T_b}\right)^{-0.6}$$

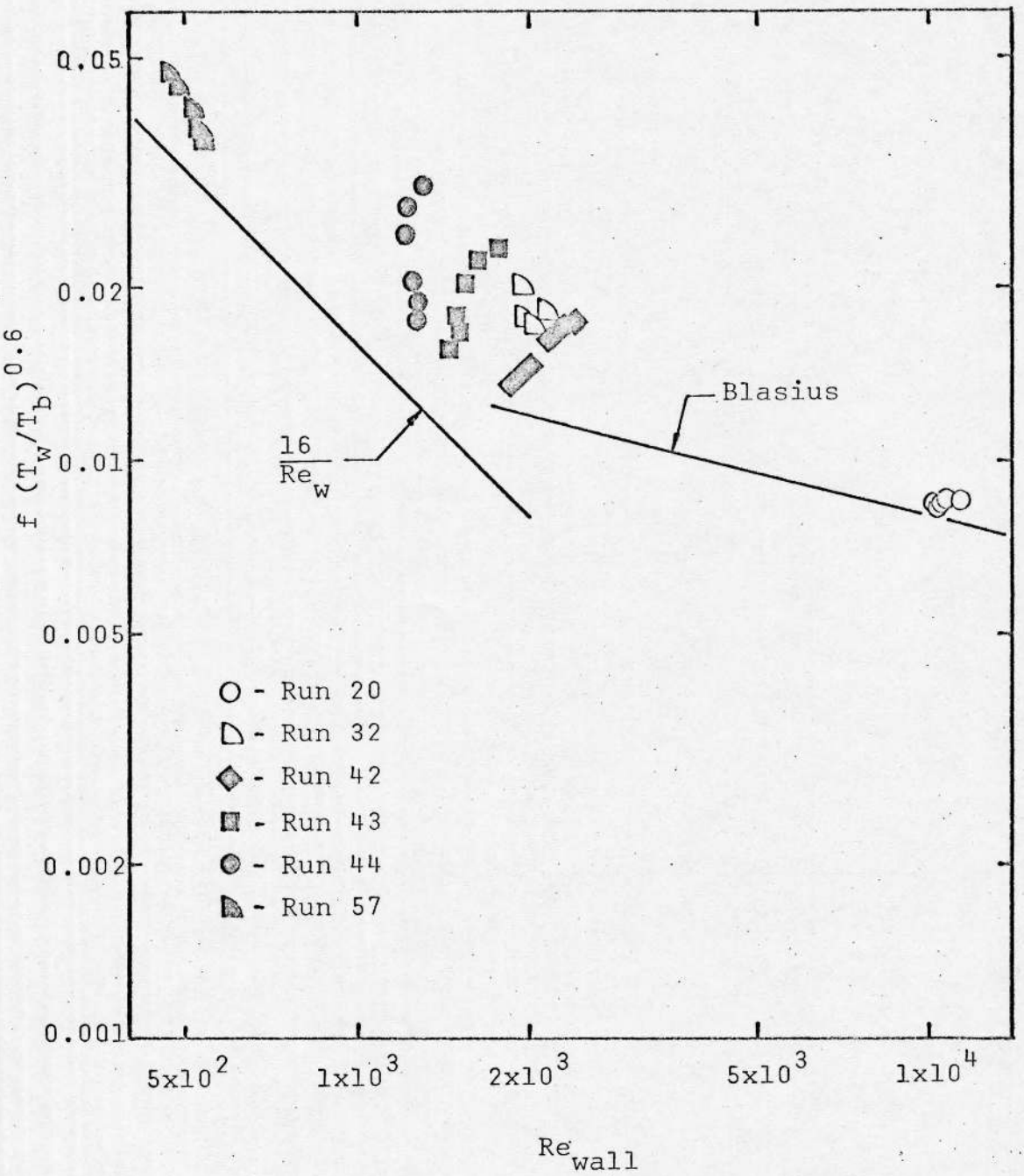

Figure 28. Correlation of Friction Factor Data with the Turbulent Variable Property Parameters of Perkins and Worsoe-Schmidt (1965).

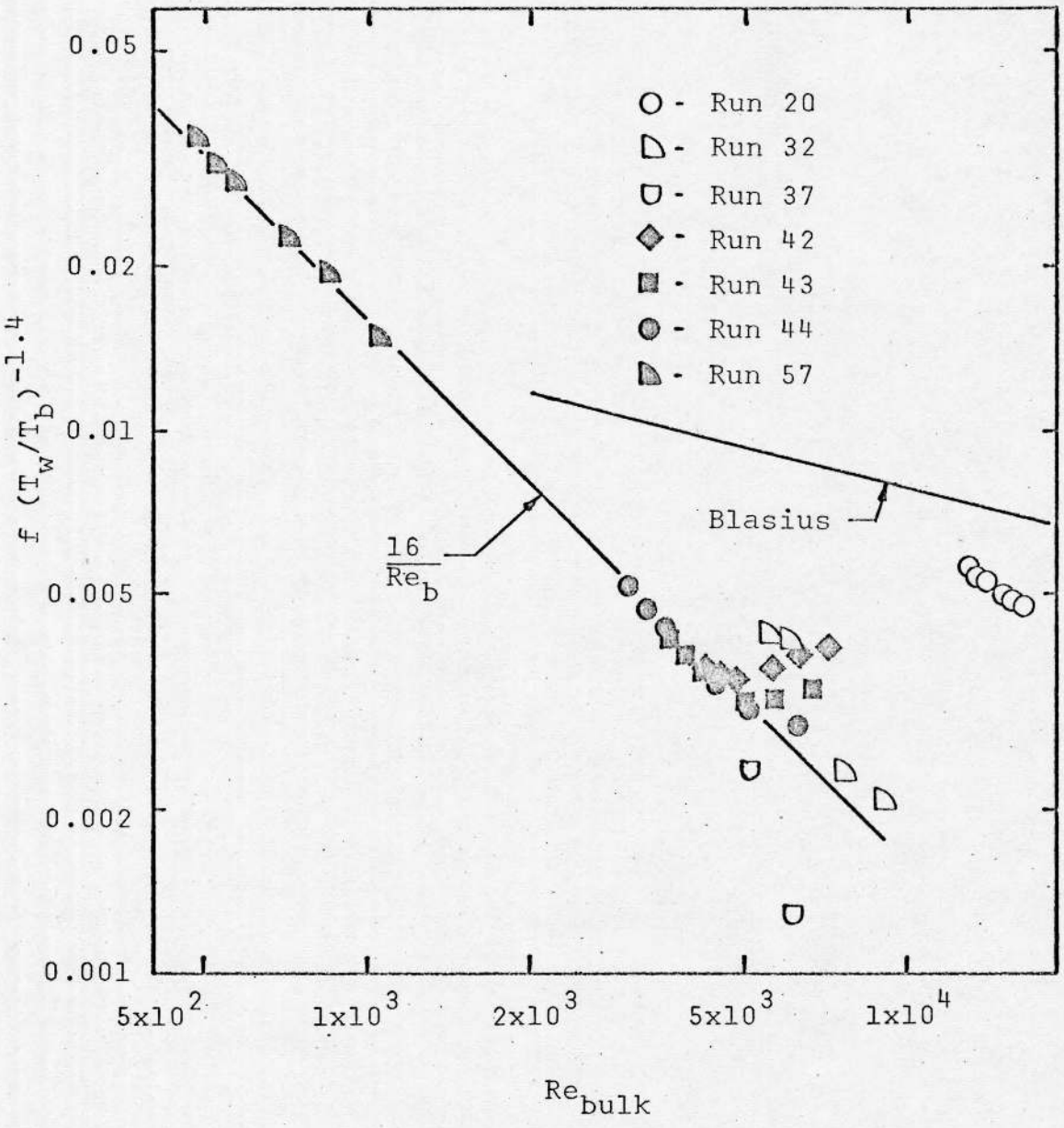

Figure 29. Correlation of Friction Factor Data with the Laminar Variable Property Parameters.

while Figure 29 depicts the correlation suggested by the discussion of Figure 19 for laminar flow,

$$f = \frac{16}{Re_b} \left(\frac{T_w}{T_b}\right)^{1.4}$$

Examination of Figure 28 reveals that the turbulent flow correlation provides acceptable agreement with the experimental data for the case of turbulent flow with mild heating, but the comparison for the laminar and transition runs is poor. Figure 29, on the other hand, shows excellent agreement between the laminar flow data and the laminar flow correlation; in this case the turbulent results are displaced. It is interesting to note that the data points representative of runs for which turbulent to laminar transition was suspected exhibit a tendency to approach the laminar line in Figure 29 as the value of x/D increases. This result indicates that the laminar correlation would predict acceptable friction factors for tubes that were long enough to allow a complete turbulent to laminar transition.

It has been mentioned, in connection with the laminar friction factor results of Figure 19, that some disagreement exists with respect to the appropriate numerical value of the exponent of the wall-to-bulk temperature ratio in the laminar flow friction factor correlation. Davenport and Leppert (1964) and Bankston,

Sibbitt, and Skoglund (1966) recommend values of the exponent of about 1.4 on the basis of experimental results, while the analytical investigation of Worsoe-Schmidt and Leppert (1965) suggests a value of unity for the exponent. It should be noted, with respect to Figures 19 and 29, that the use of 1.4 as the exponent provided better agreement with the present experimental results than did the use of unity as the exponent.

For purposes of comparison and discussion, each of the heated flow runs was classified according to the type of flow that was found to be present. The primary basis of the classification scheme was the series of graphs using the Graetz solution length parameter, Figures 21 through 25; it was decided that these graphs provided the best representation of the turbulent to laminar transition phenomenon. The results of the classification of the runs were compared to the graphs of the heat transfer parameter and the friction factor to insure consistency. Table III presents pertinent information for the flow runs in addition to the designation of the existing flow condition; it should be noted that the phrase "turbulent to transition" designates an initially turbulent flow situation that exhibits a marked deviation from the turbulent prediction

Table III Classification of Flow Regimes for Runs, Based on Friction and Heat Transfer Data

Run Number	Gas	Symbol	Bulk Inlet Reynolds	Bulk Exit Reynolds	Classification
20	Air		17728	12940	Fully Turbulent
26	Air		14249	5569	Turbulent to Transition
28	Air		16130	6208	Turbulent to Transition
31	Air		20685	6630	Turbulent to Transition
32	Air		19436	4958	Turbulent to Transition
33	Air		15712	4231	Turbulent to Transition
35	Air		10930	4558	Turbulent to Transition
36	Air		12016	4193	Turbulent to Laminar
37	Air		16944	3458	Turbulent to Laminar
41	Helium		7885/8511	4049/4170	Turbulent to Transition
42	Helium		8720	4160	Turbulent to Laminar
43	Helium		8795	3527	Turbulent to Laminar
44	Helium		9052	2968	Turbulent to Laminar
46	Helium		4327	1768	Turbulent to Laminar
47	Helium		4195	1403	Turbulent to Laminar
49	Helium		2580	1014	Fully Laminar
52	Helium		7445	5411	Fully Turbulent
54	Helium		4064	2918	Fully Turbulent
56	Helium		1711	612	Fully Laminar
57	Helium		1724	459	Fully Laminar
64	Air		37543	26903	Fully Turbulent
66	Air		32389	23348	Fully Turbulent

over the length of the tube, while the phrase "turbulent to laminar" represents runs for which laminar Nusselt numbers and friction factors actually occur in the downstream region of the tube.

It is important to note that several of the runs (36, 37, 42, 43, 44) exhibit a transition to laminar flow even though the Reynolds number, based on bulk properties, did not reach a value of 2200. For example, run 37 had an inlet bulk Reynolds number of 16944 and an exit bulk Reynolds number of 3458. However, the T_w/T_b reached in this run was 4.43 and this was sufficient to cause laminar like heat transfer and friction results in the downstream region.

Several investigators have suggested techniques through which conditions leading to a turbulent to laminar transition might be recognized, and a comparison between those schemes and the present work will be performed in the following discussion. McEligot, Ormand, and Perkins (1966), subsequent to classifying the experimental runs as laminar, transitional, or turbulent, displayed the results on a graph of the wall-to-bulk temperature ratio versus the modified wall Reynolds number and placed approximate borderlines between the regimes. Figure 30 shows downstream data points for typical runs from the present investigation compared to these

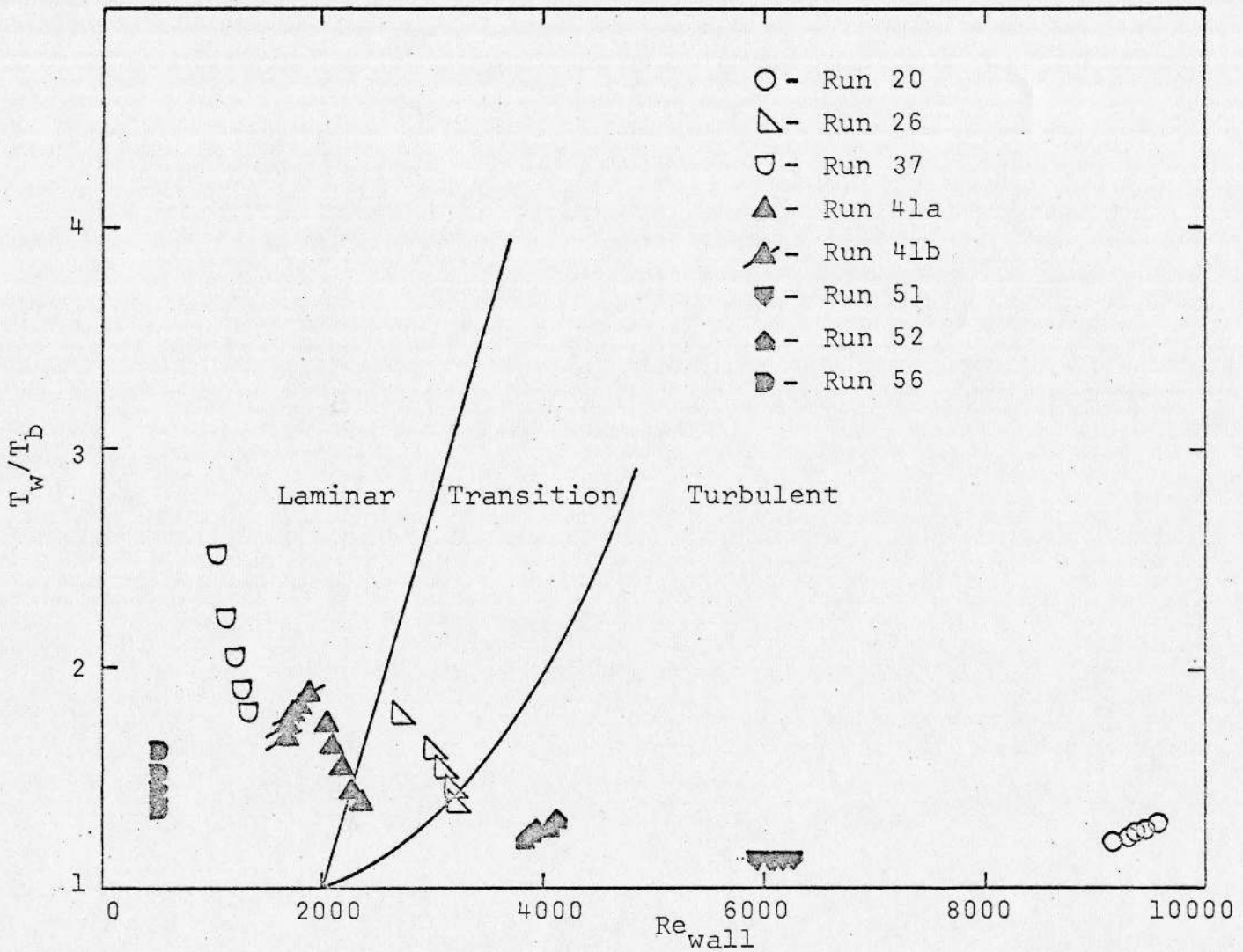

Figure 30. Comparison of Data to the Flow Regime Classification of McEligot, Ormand, and Perkins (1966).

borderlines; it can be observed that the data previously shown on various figures describing completely laminar or completely turbulent runs lie well within the appropriate regime, while the runs for which turbulent to laminar transition can be inferred on the basis of Figures 21 through 25 are described by points in the laminar or transition regions. The double-valued run is again of singular interest; Figure 24 suggests that a downstream Nusselt number should be equal to the laminar prediction for one branch and should be between the laminar prediction and the constant properties turbulent prediction for the other branch. This suggestion is substantiated by the location of the data points with respect to the regime boundaries in Figure 30; note that the wall-to-bulk temperature ratio decreases as x/D increases in the downstream region of the tube.

A similar scheme was employed by Bankston, Sibbitt, and Skoglund (1966) to classify the flow regimes. Instead of the modified wall Reynolds number, however, the parameter

$$Re_b \left(\frac{T_b}{T_w}\right)^2$$

was used; the experimental downstream data points for the present investigation are shown with respect to this quantity in Figure 31. Since the wall Reynolds number

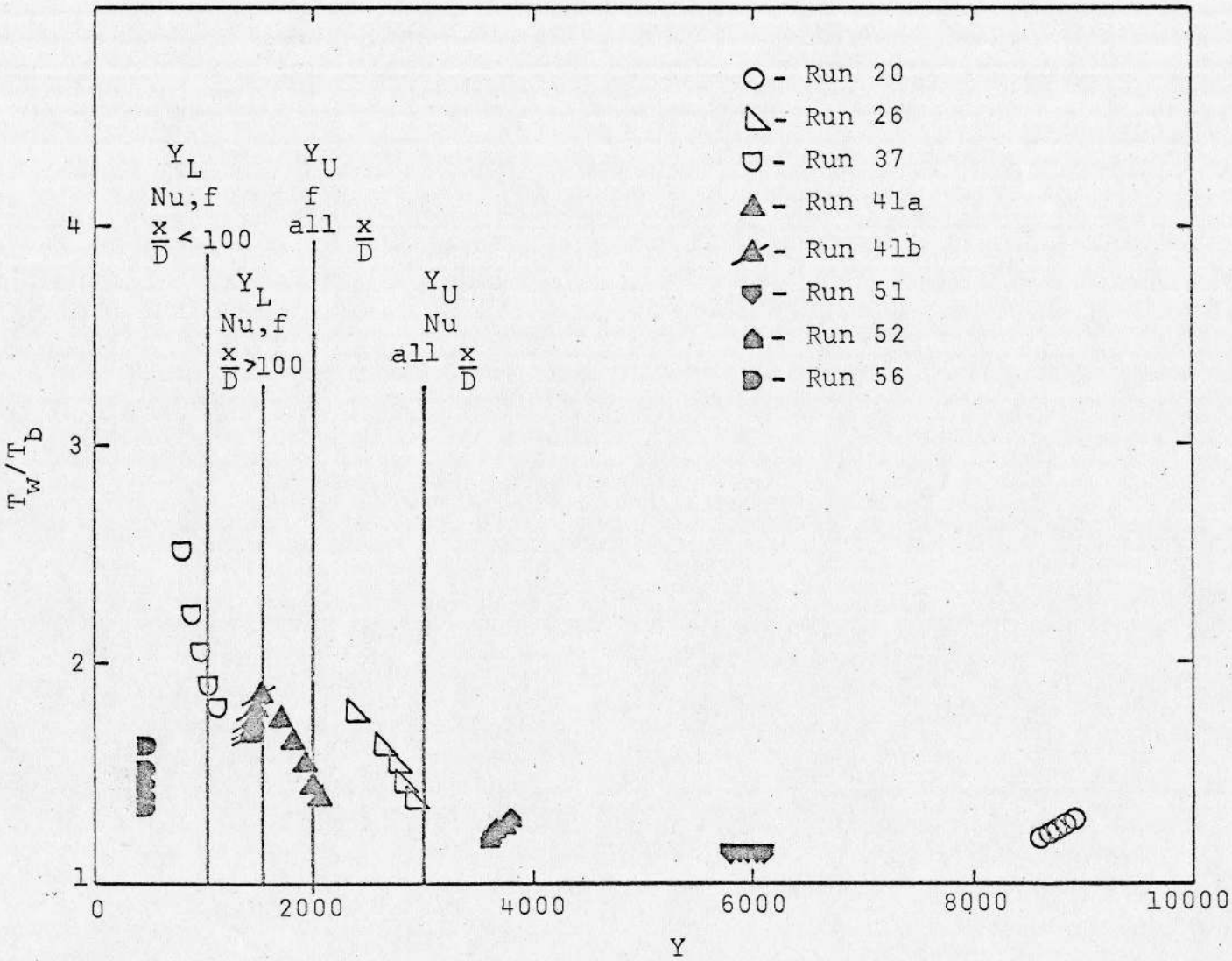

Figure 31. Comparison of Data to the Flow Regime Classification of Bankston, Sibbitt, and Skoglund (1966).

$$Re_w = \frac{\rho_b D u_b}{\mu_w} \left(\frac{T_b}{T_w}\right)$$

and since the viscosity for a gas can be approximately represented by the relationship

$$\frac{\mu_w}{\mu_b} = \left(\frac{T_w}{T_b}\right)^{0.7}$$

it follows that

$$Re_w = \frac{\rho_b D u_b}{\mu_b} \left(\frac{T_b}{T_w}\right)^{1.7} = Re_b \left(\frac{T_b}{T_w}\right)^{1.7}$$

Thus the parameter employed by the authors of the work cited above and the parameter employed by McEligot, Ormand, and Perkins differ only slightly.

Bankston, Sibbitt, and Skoglund (1966) selected different sets of regime boundaries for values of x/D less than 100 and greater than 100 and for Nusselt numbers and friction factors; the various boundary lines are shown in Figure 31. Although the data points representing the present work conform reasonably well to the boundaries shown, it appears that the values

Y = 1500, for a lower limit, and

Y = 3000, for an upper limit,

provide the regime boundaries most consistent with the previous classification of the runs shown in Figure 30.

Another parameter used in the description of the turbulent to laminar transition process was the quantity

defined by Moretti and Kays (1965) for external boundary layer flows subjected to strong accelerations,

$$K = \frac{\nu}{u_\infty^2} \frac{du_\infty}{dx}$$

In the work cited, it was found that the onset of transition was marked by large increases in the value of K, and it was suggested that laminar results would be obtained if the value of K exceeded 3.0×10^{-6}. For the experimental runs associated with the present work, local values of the parameter K were obtained by using the bulk velocity and the bulk kinematic viscosity and by using Procedure FIT (described in Appendix B) to calculate the derivative. The results are shown for several typical runs in Figure 32; a more thorough treatment of a larger group of runs and a discussion of the axial distance required for complete transition will follow. It can be observed from Figure 32 that the value of K exhibits little change with axial distance along the tube; no sudden increase is apparent. The disparity between Figure 32 and the results of Moretti and Kays can be explained in terms of the velocity required by the definition of K; the bulk velocity for tube flow is not subject to arbitrary change, but the free stream velocity in the external flow experiment cited above was deliberately increased by a variation of the duct geometry. It should be noted with

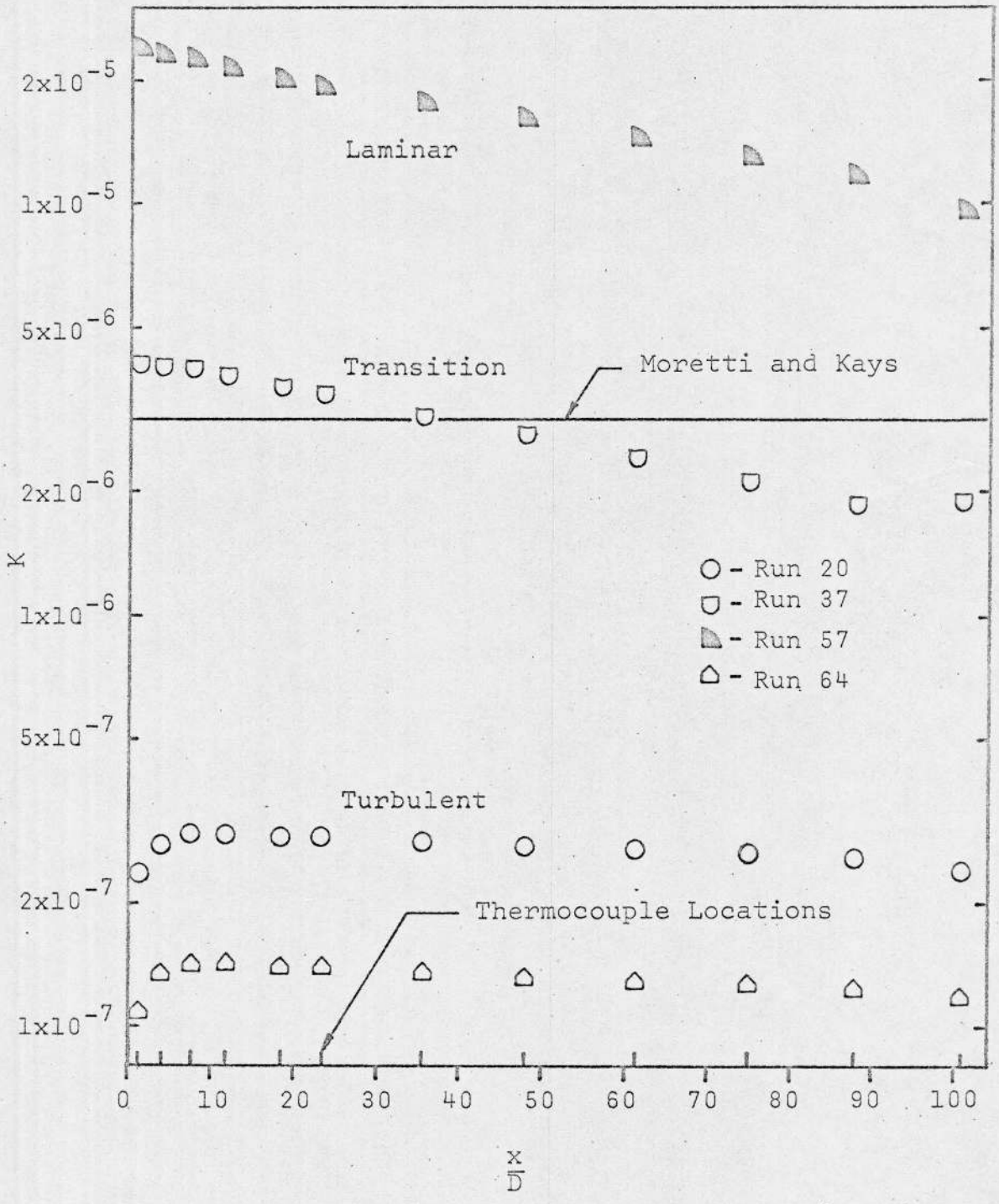

Figure 32. The Acceleration Parameter $K = \frac{\nu}{u_b^2}\frac{du_b}{dx}$ versus Distance along the Tube for Selected Runs.

respect to Figure 32, however, that the completely laminar run exhibits a larger value than the critical value of K suggested by Moretti and Kays while the completely turbulent runs have significantly lower values. It is of particular interest to note that the data points from run number 37, which has previously been classified as a run in which laminar results were observed within the 100 diameter tube length, exhibit a value quite close to the critical value predicted by Moretti and Kays. In particular, the value of K for run number 37 ranges from 4.1×10^{-6} near the beginning of the heated length to 1.8×10^{-6} near the end; the critical value of K suggested by Moretti and Kays (3×10^{-6}) lies within this range. In connection with the determination of the appropriate critical value, it is significant to note that Back and Seban (1967) found that a value of K equal to 2×10^{-6} for the external flow form of the parameter was in better agreement with their data than was the value obtained by Moretti and Kays; this result is in good agreement with the evaluation of K for the downstream region of the tube in the present investigation. The above results indicate that the external flow acceleration parameter described by Moretti and Kays

$$K = \frac{\nu}{u_\infty^2} \frac{du_\infty}{dx}$$

can be adapted to tube flow through the substitution of the bulk velocity for the free stream velocity, and the resulting parameter

$$K_\phi = \frac{\nu}{u_b^2} \frac{du_b}{dx}$$

should be useful in the prediction of turbulent to laminar transition for tube flow. Also, the critical value of the parameter that describes the onset of laminar flow in a tube is approximately equal to the numerical values suggested by Moretti and Kays and by Back and Seban for external flow.

An effort was made to translate the external flow acceleration parameter into terms pertinent to tube flow. Using the bulk velocity, the quantity becomes

$$K_\phi = \frac{\nu}{u_b^2} \frac{du_b}{dx}$$

and from the continuity equation for a constant area duct,

$$\frac{du_b}{dx} = - \frac{u_b}{\rho} \frac{d\rho}{dx}$$

From the perfect gas equation of state,

$$\frac{d\rho}{dx} = - \frac{p}{RT^2} \frac{dT}{dx} + \frac{1}{RT} \frac{dp}{dx}$$

but, for a typical run for which transition is expected, the second term on the right hand side can be neglected, so that

$$K_\phi = \frac{\nu}{u_b^2} \quad \frac{u_b}{\rho} \quad \frac{p}{RT^2} \quad \frac{dT}{dx}$$

Now, the relationship, provided by an energy balance,

$$q''\pi D dx = \dot{m} c_p \quad \frac{dT}{dx} dx$$

can be used to provide an expression for dT/dx so that

$$K_\phi = \frac{\mu}{\rho u_b T} \quad \frac{q''\pi D}{\dot{m} c_p}$$

or, in terms of the mass flux G,

$$K_\phi = \frac{4}{G^2 D} \quad \frac{\mu}{T} \quad \frac{q''}{c_p}$$

The quantity K_ϕ is shown in Figure 33 in the same representation employed for the external flow parameter. The general features and the trends of the graph are the same as those described for the external flow parameter, but K_ϕ is composed of quantities that are more readily available from the specification of a design problem for a tube flow situation than are the quantities that comprise K, Re_w, or T_w/T_b. Thus, a classification of experimental runs on the basis of K_ϕ should prove more helpful to the designer of a device, such as a

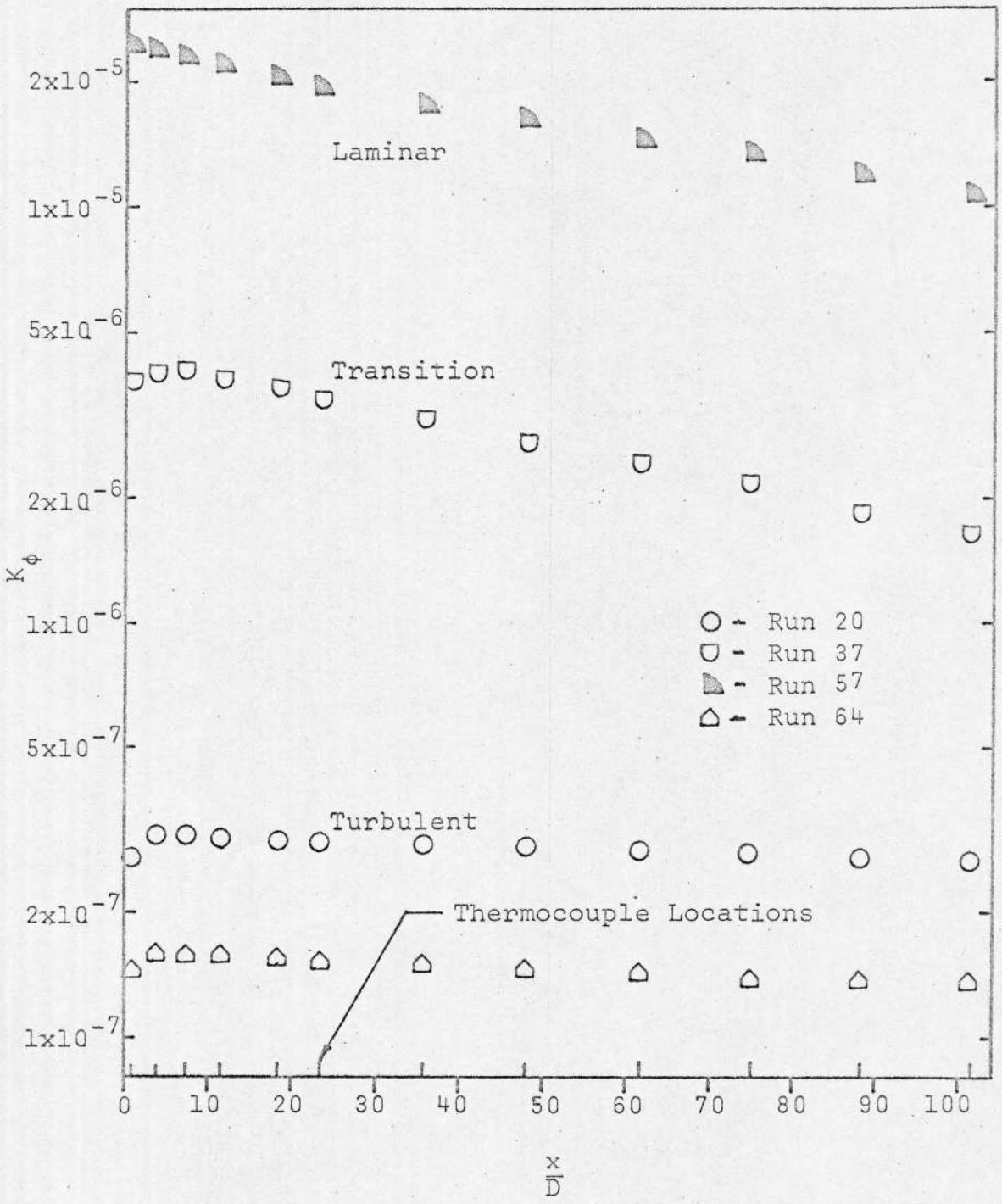

Figure 33. The Acceleration Parameter $K_\phi = \frac{4 \mu q''}{G^2 D T c_p}$ versus Distance along the Tube for Selected Runs.

reactor coolant channel tube, than would a classification based on any of the previously mentioned parameters. The fact that K is approximately constant along the tube can be explained by examining the terms appearing in K_ϕ. For the present experiment, q", G^2, and D were constant along the tube. Since μ increases approximately as $(T)^{0.7}$ and c_p is almost constant with temperature the μ/T term does not exhibit much change along the tube and therefore K is essentially constant with x.

Figure 34 is a representation of the various values of K_ϕ for a wide range of experimental runs; because K_ϕ exhibits only slight variations with axial distance along the tube, single values typical of the downstream region of the tube were selected for each run. It can be observed that the runs involving turbulent flow with mild heating exhibit values of K_ϕ in the neighborhood of 10^{-7}, while the completely laminar runs have values in the vicinity of 10^{-5}. It is also interesting to note that a number of points are grouped together near the value

$$K_\phi = 1.5 \times 10^{-6}$$

and that these are precisely the runs for which a significant departure from the turbulent prediction can be observed in the graphs involving the Graetz solution length parameter, Figures 21 through 25. Whether or not

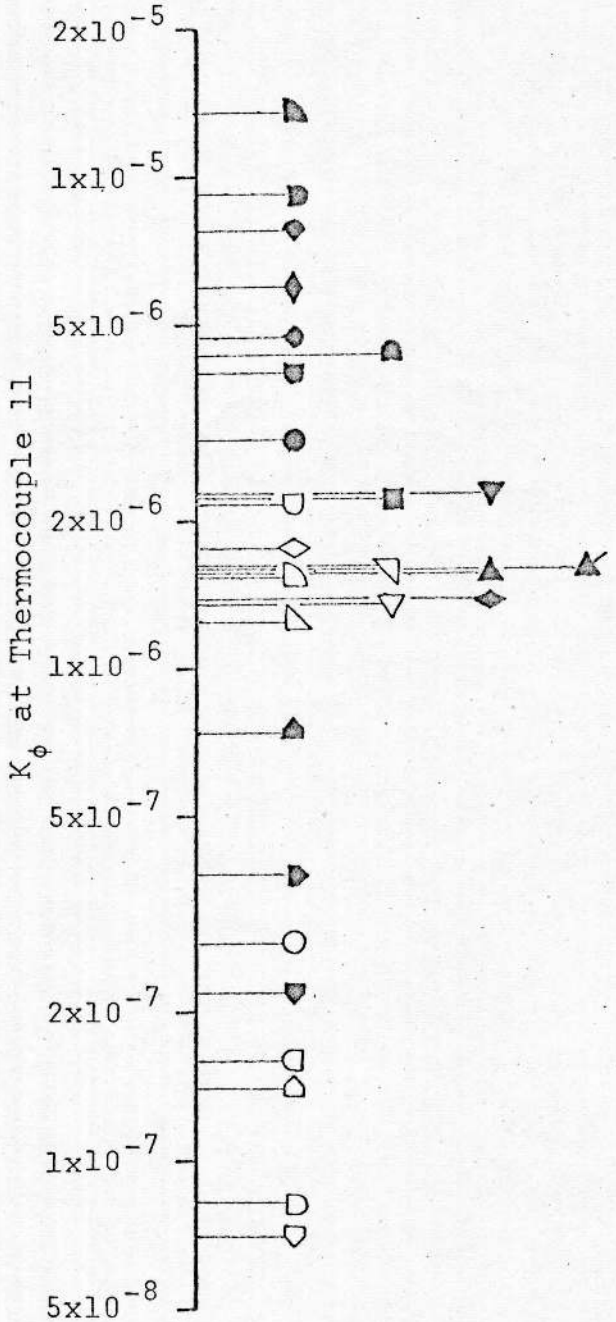

Run	Re_b Entry	(T_w/T_b) max
57	2068	2.49
56	2052	2.06
49	2580	2.22
47	4195	2.59
55	2024	1.76
46	4327	2.21
48	2632	1.78
44	9052	3.30
43	8795	2.68
45	4404	1.69
37	16944	4.43
26	14249	2.28
32	19436	3.08
33	15712	3.62
35	10930	2.09
36	12016	2.97
41a	7885	1.91
41b	8511	1.99
54	4064	1.32
52	7445	1.34
53	4070	1.08
20	17728	1.35
51	7691	1.10
66	32389	1.41
64	37543	1.44
65	32955	1.21
63	39613	1.23

Figure 34. A Tabulation of a Downstream K_ϕ for the Experimental Runs.

fully laminar flow actually prevails at x/D ≈ 100 for runs in which $K_\phi = 1.5 \times 10^{-6}$ is difficult to ascertain from Figure 34, but it can be concluded that the conventional turbulent flow correlation equations, whether for constant properties or variable properties, will not yield acceptable results when applied to situations for which a turbulent inlet Reynolds number occurs but K_ϕ exceeds 1.5×10^{-6}. Under these circumstances the flow exhibits the effects of transition, but the transition process is not necessarily complete at the values of x/D available in the present study.

The value of 1.5×10^{-6} is smaller than the value of 3.0×10^{-6} suggested by Moretti and Kays (1965) for external flow but compares favorably with the recent results of Back and Seban (1967) in which a value of 2×10^{-6} is suggested.

The axial distance required for a complete transition from turbulent flow to laminar flow was also examined on the basis of the experimental data presented in the preceding material. It was regarded as a foregone conclusion that, for a sufficiently long tube and continuous heating, the flow would eventually become laminar because of the increase in viscosity; the effect of high heating rates is to reduce the distance required

for the transition process to occur. It was assumed that a relationship that would predict the onset of laminar flow would have the form

$$\left(\frac{x}{D}\right)_{\text{critical}} = a \left(Re_{b,\ \text{inlet}}\right)^{b} \left(\frac{T_w}{T_b}\right)_{\text{max}}^{-c}$$

where the constants a, b, and c could be evaluated from the experimental data. The values for $Re_{b,\ inlet}$ and $(T_w/T_b)_{max}$ were readily available from the calculations, and the value of x/D required for agreement with the laminar heat transfer correlation was obtained by extrapolation of the appropriate experimental curves on the graphs involving the Graetz solution length parameter, Figures 21 through 25. The value of the exponent b was obtained from a log-log graph of $(x/D)_{critical}$ versus $Re_{b,\ inlet}$ for a fixed value of $(T_w/T_b)_{max}$; the value of the exponent c was obtained from log-log graph of $(x/D)_{critical}$ versus $(T_w/T_b)_{max}$ for a fixed value of $Re_{b,\ inlet}$, and the value of the coefficient a was then determined by solving the proposed relationship for a, using the data of several experimental runs and averaging the results. It was found that the resulting expression provided reasonably good agreement with the experimental results for precooled gas runs, but the agreement was poor for situations in which the gas was at ambient

temperature at the start of heating. Since the rate of change of the viscosity with temperature for air and for helium at temperatures below 200°R is greater than the rate of change at higher temperatures, a correction for the entering temperature was introduced and the solution for the coefficient a was repeated. The resulting expression,

$$\left(\frac{x}{D}\right)_{critical} = (2 \times 10^{-8})(T_{inlet})(Re_{b,inlet})^2 \left(\frac{T_w}{T_b}\right)^{-1}_{max}$$

was found to yield reasonable estimates of the axial location at which the experimentally measured Nusselt numbers attained the values predicted by the constant properties laminar flow solution for runs both with and without precooling. For several runs, the length of the test section was not sufficient for the complete attainment of the laminar flow solution, and in these cases the predicted critical value of x/D was greater than the maximum value of x/D for the test section. It should be noted that, in the above expression, the inlet temperature is expressed in degrees Rankine.

It should be mentioned that the above relationship for predicting the axial location of the existence of laminar flow was obtained from the experimentally determined heat transfer parameters, and the possibility exists that the friction factors have a greater degree of

sensitivity to heating rate than do the Nusselt numbers. In other words, the friction factors for a situation involving turbulent to laminar transition might be predictable by a laminar correlation for values of x/D lower than the critical value suggested by the relationship above. The data of Perkins and Worsoe-Schmidt (1965) and of Figure 29 suggest that this is indeed the case; the friction factors appear to agree with the laminar correlation equations for values of x/D smaller than those predicted as required for the heat transfer to be in agreement with a laminar correlation.

Comparison of Experiment and Analysis

Among the results of the analytical work described in Chapter V was a set of curves (Figure 14) that depicts the change in a defined momentum thickness Reynolds number for various values of the wall-to-bulk temperature ratio and bulk entry Reynolds number. Although they have the proper shape and the proper relationship to one another, these curves do not allow a specific judgement to be made concerning the location of the turbulent to laminar transition. It was possible, however, to add to the significance of the analytical curves with the assistance of the results of the experimental runs summarized in Table III. Figure 35 is a display of the results of the

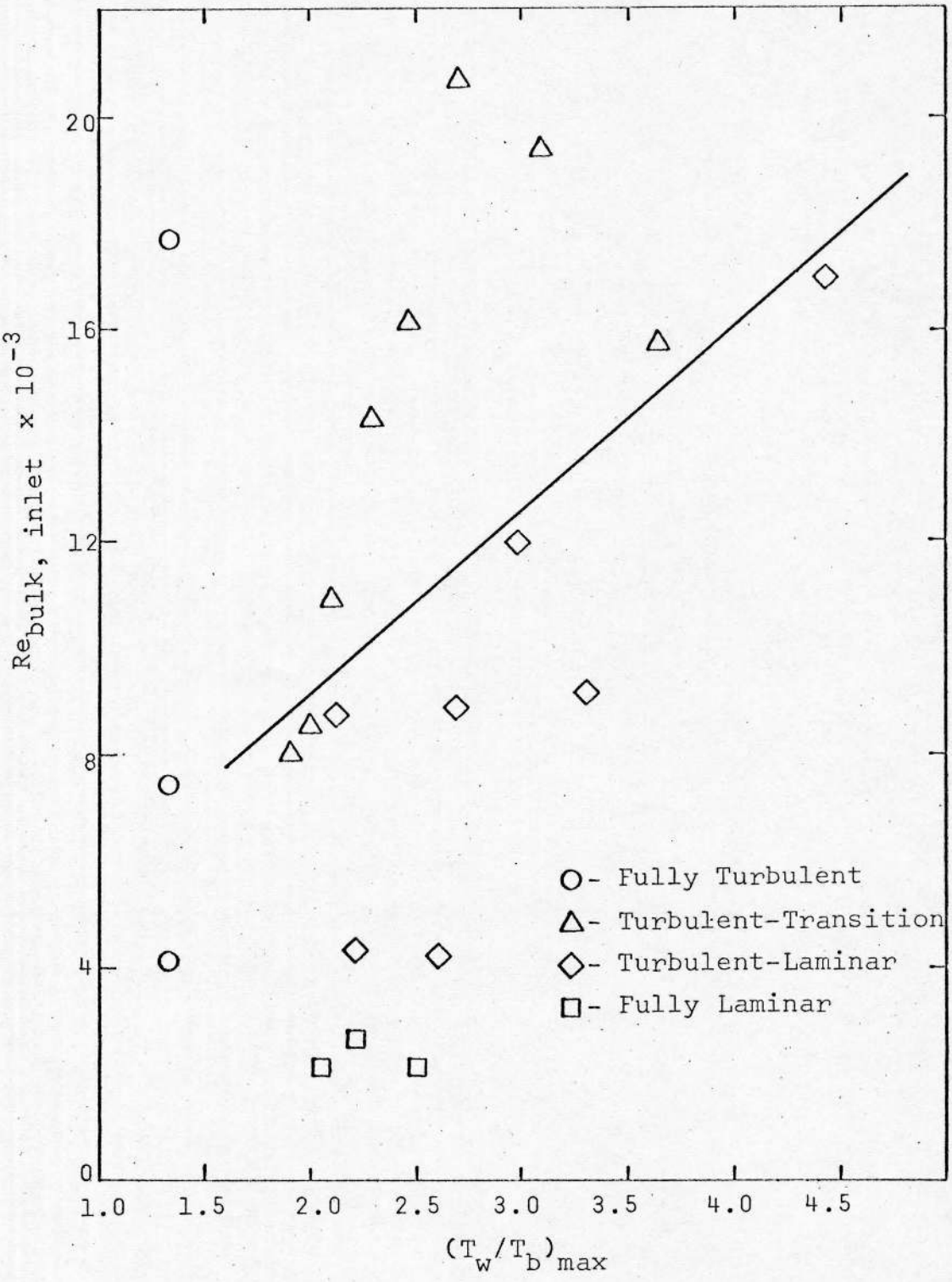

Figure 35. Correlation of Data, with the Bulk Inlet Reynolds Number versus $(T_w/T_b)_{max}$, According to Flow Regime.

classification scheme for the experimental runs set on convenient coordinates; the diagonal line represents a borderline between flow conditions. For the purposes of this discussion, it is assumed that points located above the line represent flow runs which did not completely attain values of the Nusselt number and friction factor characteristic of laminar flow within the 100 diameter tube length; the points below the line depict flow runs for which the Nusselt number and friction factor could be predicted reasonably well by laminar correlations in the downstream region. The diagonal line, therefore, represents a means for determining the value of the wall-to-bulk temperature ratio for which complete turbulent to laminar transition can be expected within 100 diameters for a given bulk entry Reynolds number.

Figure 36 is basically a duplicate of Figure 14; the values of the bulk inlet Reynolds numbers correspond to specified mass flow rates. In Figure 36, however, positions are marked on each curve that indicate the point, located from the diagonal line in Figure 35, subsequent to which the laminar correlations can be expected to hold. The average location of the transition points could be represented by a value of the momentum thickness Reynolds number of 375. This is in general agreement with the numerical value suggested by Kays

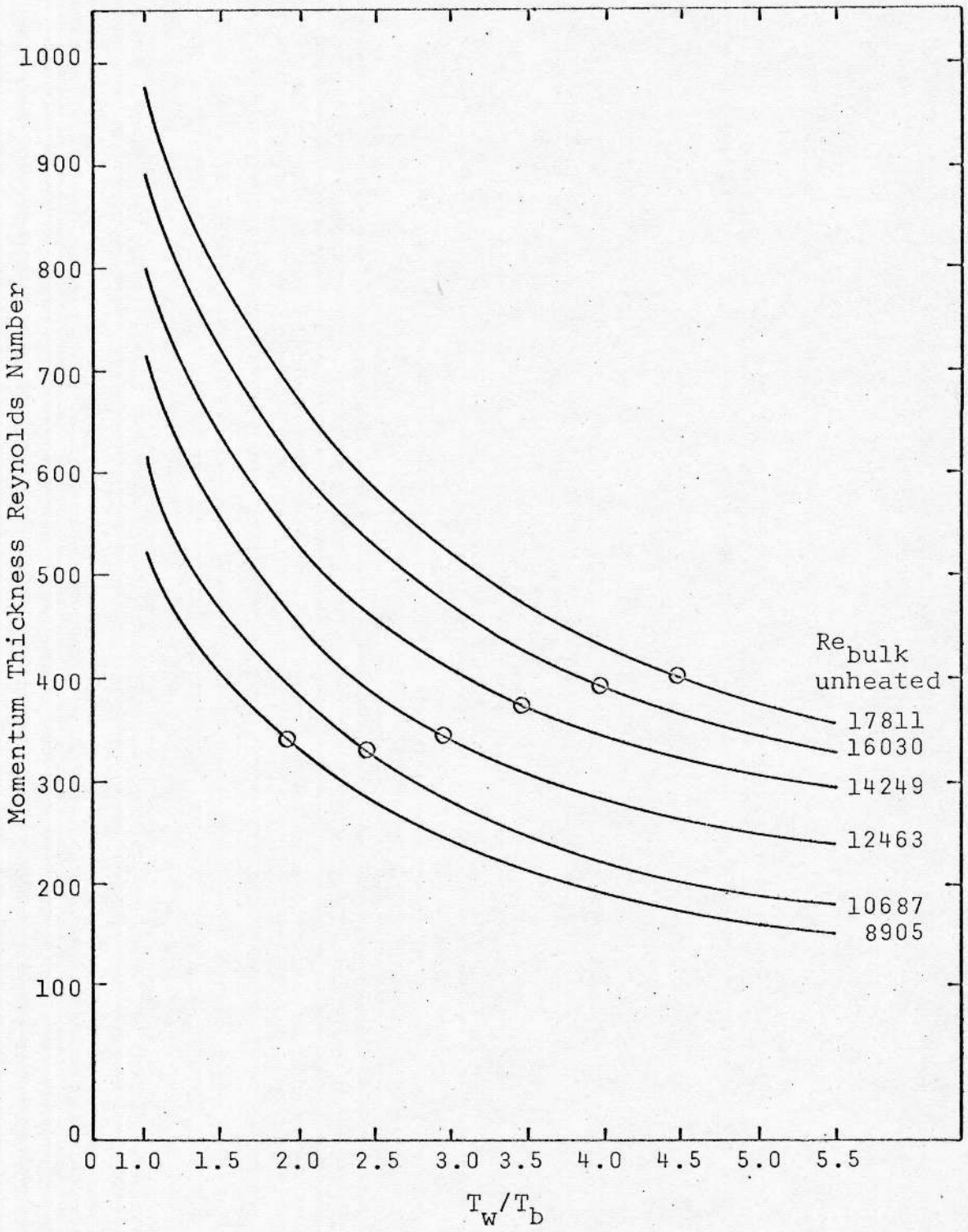

Figure 36. The Momentum Thickness Reynolds Number as a Function of $(T_w/T_b)_{max}$ and Bulk Reynolds Number for Complete Transition from Turbulent to Laminar Flow in a Tube of 100 Diameters Length.

for tube flow and constant properties, although it is important to note that the definition of the Reynolds number differs from that used by Kays in that the wall viscosity was used instead of the bulk viscosity and the flat plate momentum thickness was used instead of the circular tube momentum thickness.

CHAPTER VII

CONCLUSIONS AND RECOMMENDATIONS

The following conclusions, pertinent to the flow of a gas through a circular tube with a constant heat flux boundary condition, may be drawn from the results of this investigation:

1. Any initially turbulent flow will ultimately exhibit all of the properties of laminar flow provided that the tube is sufficiently long; the effect of high heating rates on an initially turbulent flow is a reduction of the tube length required for the initiation of the turbulent to laminar transition. Further, high heating rates may cause laminar values of heat transfer coefficients and friction factors even though the bulk Reynolds number lies well above 2200.

2. If the value of

$$K = \frac{4}{G^2 D} \frac{\mu}{T} \frac{q''}{c_p} \approx 1.5 \times 10^{-6},$$

based on bulk properties, is exceeded for an initially turbulent flow situation, then the turbulent flow correlations no longer provide acceptable predictions of the Nusselt number and the friction factor.

3. The Nusselt numbers and friction factors at locations downstream from the point

$$\left(\frac{x}{D}\right)_{critical} \approx 2 \times 10^{-8} \, (T_{inlet})(Re_{b,inlet})^2 \left(\frac{T_w}{T_b}\right)^{-1}_{max}$$

for bulk inlet temperatures in degrees Rankine, may be obtained from the laminar correlation equations even though the flow is initially turbulent.

4. The borderlines between the various flow regimes previously suggested by McEligot, Ormand, and Perkins (1966) and Bankston, Sibbitt, and Skoglund (1966) are in reasonable agreement with the present data.

The recommendations for future work on the problem considered in this investigation fall into two categories; both the effectiveness of the analysis and the precision of the experimental work could be improved. Ignoring the obvious benefits that would result from an exact solution to the problem of heated flow in the turbulent and transition regions, it is possible that the several attempts at approximate solutions presented in this work could be extended, or combined, to provide an accurate prediction of the turbulent to laminar transition phenomenon. The momentum thickness concept described in the present analysis has several attractive features, but it is possible that the whole approach suffers from the over-simplification of the velocity and temperature profiles.

A logical further step would be the use of a velocity profile more suited to the specific problem than the law of the wall profile; a more sophisticated temperature profile, perhaps involving two or three regions, would also be appropriate. The treatment is at present excessively dependent upon the specification of a friction factor, and it would be necessary to overcome this weakness in conjunction with the selection of the new velocity and temperature profiles. It is possible that another definition of momentum thickness, such as that suggested by Preston (1958), would provide better analytical results. Still another contribution would be the addition of another dimension to account for the axial changes in the various quantities.

The experimental portion of this study, despite the expenditure of considerable effort in behalf of accuracy, nevertheless provides another source of future work. The results presented here would benefit from the acquisition of more experimental data over a wider range of variables, but a more fruitful approach would be the quest of an increase in the precision of the results. In some cases improvements in technology might be required; the friction factor results could be vastly improved by a better technique for pressure tap construction (see Appendix D). However, more careful attention to

procedural detail would also improve the results; an example would be an even more elaborate scheme for the calibration of the thermocouples and the determination of the radiant energy loss from the tube. An immediate step in this direction might be the development of a technique for calculating the energy transfer from the surroundings to the gas during experimental runs with low heating rates in which the wall temperatures are less than the ambient temperature. There is also room for improvement in the data reduction process; the computer routines could be adapted to provide such benefits as better calculation of derivatives and better determination of electrode, pressure tap, and thermocouple wire heat losses.

The presentation of the experimental results provides another area in which further efforts would be desirable. It is possible that more practical results could be obtained through various manipulations of the data; it would, for example, be helpful if a better technique could be devised for the classification of laminar, transitional, and turbulent flow runs. A further examination of the possibility of a gas-dependent or Reynolds number-dependent exponent for the wall to bulk temperature ratio in the heat transfer parameter would be interesting, as would a deeper study of the exponents involved in the friction factor correlations. Further

efforts also might provide a more desirable parameter for the prediction of the departure from the turbulent correlations, and other attempts to relate the internal flow and external flow parameters might prove fruitful. The most immediate need, however, is further examination of the critical value of x/D for the beginning of laminar flow. The determination of the quantity might be improved through the use of more extensive data, and it might be possible to discover whether or not the Nusselt numbers and friction factors do in fact exhibit different sensitivities to high heating rates.

APPENDIX A

GAS PROPERTIES USED IN DATA REDUCTION

The gas properties employed in the data reduction process were stored in the computer memory in tabular form. Because the effect of pressure on the property values is slight, and because only absolute pressures between 25 and 35 pounds per square inch were encountered in the present work, the tables were constructed using temperature as the only interpolation parameter. The primary source of air properties was NBS circular 564 (Hilsenrath, et. al., 1960). Table IV provides further information regarding the air properties. Although most of the air properties are virtually independent of pressure, the specific heat varies strongly with pressure at low temperatures. The difference in the specific heat is about 15 percent between pressures of one atmosphere and four atmospheres at 135 degrees Rankine; the value of the specific heat at 135 degrees Rankine selected for the present work was 0.288 Btu per pound mass per degree Rankine.

Several sources were consulted for appropriate helium properties; the values finally selected are reproduced in Table V. In most cases it was necessary

to obtain property values at low temperatures by a process of extrapolation combined with use of the values presented in a standard textbook (Eckert and Drake, 1959).

Table IV Information Regarding Air Properties

Property	Source	Pressure
Prandtl number	NBS 564	1 atmosphere
Enthalpy	NBS 564	4 atmospheres
Speed of sound	NBS 564	4 atmospheres
Viscosity	NBS 564	1 atmosphere
Thermal Conductivity	NBS 564	1 atmosphere
Specific Heat	NBS 564	4 atmospheres
Gas Constant	NBS 564	

Table V Helium Properties

Property	Enthalpy	Viscosity	Thermal Conductivity	Specific Heat	Acoustic Velocity	Prandtl Number
Symbol	H	μ	κ	c_p	c	Pr
Units	BTU/lbm	lbm/ft hr	BTU/hr ft°R	BTU/lbm°R	ft/sec	----
Source	Note 1	Note 2	Note 2	Note 1	Note 3	Definition
Pressure	20 psi			1 atm	25 psi	
100°R	126.57	0.01573	0.0320	1.242	1730	0.6106
200°R	253.14	0.02478	0.04784	1.242	2120	0.6434
300°R	379.71	0.03336	0.0621	1.242	2525	0.6672
400°R	506.28	0.04048	0.0753	1.242	2880	0.6676
500°R	631.85	0.04681	0.0871	1.242	3217	0.6675
600°R	755.96	0.05270	0.0980	1.242	3525	0.6679
700°R	880.07	0.05829	0.1084	1.242	3808	0.6678
800°R	1004.18	0.06350	0.1181	1.242	4071	0.6678
900°R	1128.29	0.06861	0.1276	1.242	4318	0.6678
1000°R	1252.40	0.07337	0.1365	1.242	4551	0.6676
1100°R	1376.51	0.07806	0.1453	1.242	4773	0.6672
1200°R	1500.62	0.08254	0.1535	1.242	4985	0.6678

Table V--Continued

1300°R	1624.73	0.08693	0.1617	1.242	5189	0.6676
1400°R	1748.84	0.09120	0.1696	1.242	5384	0.6678
1500°R	1872.95	0.09535	0.1773	1.242	5573	0.6679
1600°R	1997.06	0.09942	0.1849	1.242	5756	0.6678
1700°R	2121.19	0.10337	0.1923	1.242	5932	0.6676
1800°R	2245.30	0.10728	0.1996	1.242	6106	0.6676
1900°R	2369.41	0.11106	0.2065	1.242	6272	0.6679
2000°R	2493.52	0.11481	0.2136	1.242	6435	0.6676
2100°R	2617.63	0.11847	0.2204	1.242	6555	0.6676
2200°R	2741.74	0.12208	0.2271	1.242	6749	0.6676
2300°R	2865.85	0.12565	0.2337	1.242	6901	0.6678
2400°R	2989.96	0.12914	0.2402	1.242	7050	0.6676

Note 1. Wilson, 1960
Note 2. Svehla, 1962
Note 3. Franklin Institute, 1961

APPENDIX B

DATA REDUCTION

The reduction of the experimental data was performed on the IBM 7072 computing facility at the University of Arizona. Programs were written for use with strictly adiabatic flow data, for calculation of the radiation heat loss from the tube during the runs without gas flow, and for reduction of the data obtained during heated flow runs.

A special routine was employed for the calculation of the derivatives that occur in the computation of the conduction heat transfer and the friction factor. The technique, referred to hereafter as Procedure FIT, was developed, tested, and explained in detail by McEligot (1963); it was found to be superior to several other machine techniques including the use of least mean squares methods with second and third order polynomials and the use of a parabola applied to three data points. In essence, Procedure FIT places a parabola through three adjacent data points and determines the first and second derivatives at the center point, but the process also involves a transformation to a more suitable coordinate system and a change in the scale of the variables.

During the evaluation of Procedure FIT by McEligot, it was found that good results were obtained for first derivatives of curves with small curvature and second derivatives of curves with large curvature; the converse of either of these conditions led to poor predictions of the derivatives.

Adiabatic Friction Factor

Adiabatic pressure drop data were accumulated from the completed test assembly as a means of qualifying the construction of the pressure taps and the associated measuring system. Because the results could be compared to well established correlations, any defects, such as small burrs, in the fabrication of the pressure taps and some oversights in the experimental technique would be revealed. The computer program used with the adiabatic data employed the Blasius correlation

$$f = 0.079\ Re^{-0.25}$$

for comparison purposes, and two different schemes were used for the calculation of the pressure gradient. The first method simply formed the ratio of the pressure drop between two taps to the distance between those taps; the second method employed procedure FIT and took into consideration the pressure drops and distances associated with three adjacent taps. The three tap technique has

the advantages of providing some smoothing for small deviations in the pressure drop measurements and of yielding results at the location of a particular tap instead of results at a point between two taps.

Heat Loss Program

A computer program was written for the evaluation of the radiation heat loss from the test section. The measured energy generation rate and the wall thermocouple temperatures were supplied to the machine, and it was assumed that all of the energy which was generated was lost by radiation except at the first two test section thermocouples which were located near the lower flange.

The position of each thermocouple after expansion due to heating was calculated by using the relationship

$$\varepsilon = \frac{\delta l}{l} = \alpha t'$$

where ε is the unit thermal expansion, α is an expansion coefficient, and t' is the temperature rise above a reference temperature of 70 degrees Fahrenheit. If the expansion coefficient is a function of temperature, then the above expression can be written in the form

$$\Delta l = \int \alpha(t')t'dx = \int_{t'_1}^{t'_2} \alpha(t')t' \frac{dx}{dt'} dt'$$

The assumptions that the expansion coefficient is a linear function of temperature

$$\alpha = a + bt'$$

and that the temperature is a linear function of distance

$$t' = mx + t'_1$$

allow the above integration to be performed with the following result:

$$\Delta l = \frac{1}{m}\left[\frac{a(t')^2}{2} + \frac{b(t')^3}{3}\right]_{t'_1}^{t'_2}$$

This quantity was evaluated successively for each thermocouple, and the expansion was added to the thermocouple spacings that had been measured on the unheated test section. The expansion coefficient was expressed in terms of two linear functions of temperature for use above and below 530 degrees Rankine; these functions

$$\alpha = (7.26 \times 10^{-6}) + (0.0012 \times 10^{-6})(T-530)$$

for $T>530$

and

$$\alpha = (7.26 \times 10^{-6}) + (0.0035 \times 10^{-6})(T-530)$$

for $T<530$

were obtained from tabulated data supplied by the International Nickel Company. Measurements of the overall expanded length of the test section were obtained with a precision cathetometer during one set of heat loss runs, and the elongations calculated according to

the above routine were found to agree with the measured quantities to within ten percent. The locations of the pressure taps in the expanded condition were obtained by linear interpolation from the thermocouple locations.

An energy balance was conducted for a portion of the test section as shown in Figure 37. The quantities shown are representative of a heat loss calibration situation in which there is no flow; the result of the energy balance for steady state conditions was

$$q_{gen} = \frac{\partial q_{cond}}{\partial x} dx + q_{rad}$$

The conduction term was expressed in terms of a rate equation

$$q_{cond} = -kA_{cond} \frac{\partial T}{\partial x}$$

Assuming a constant thermal conductivity at the point of interest, the energy balance was expressed as

$$q_{gen} = -kA_{cond} \frac{d^2T}{dx^2} dx + q_{rad}$$

or

$$\frac{q_{gen}}{\Delta x} = -kA_{cond} \frac{d^2T}{dx^2} + \frac{q_{rad}}{\Delta x}$$

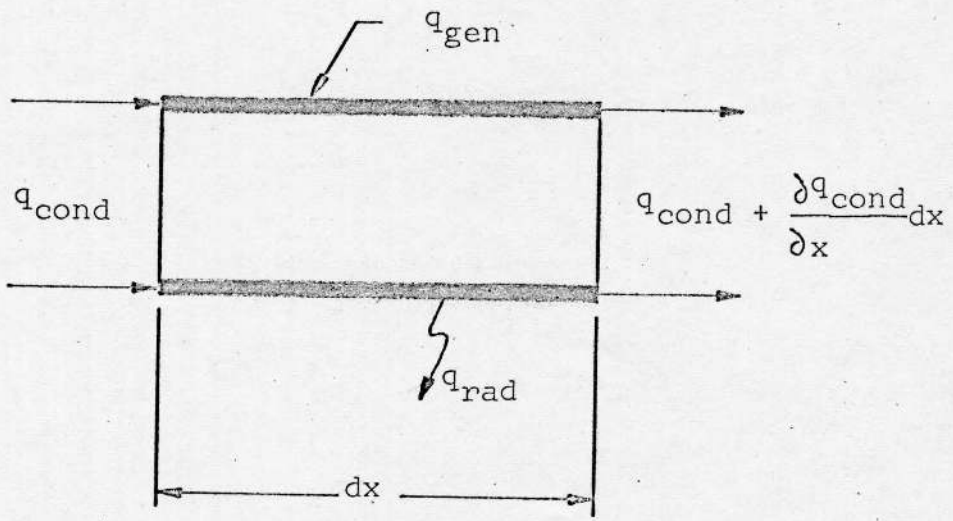

Figure 37. Element of Test Section

The local energy generation rate was obtained by evaluating the ratio of the product of the overall test section voltage drop and the heating circuit current to the overall expanded length of the test section. Since the local energy generation rate was used as the basis of the energy transfer to the gas at each thermocouple during the data reduction process, an examination of the linearity of the voltage drops along the test section was conducted in order to establish confidence in this technique. The energy transfer by conduction along the test section wall in an axial direction was obtained from the cross sectional area of the test section wall, the second derivative of temperature with respect to axial distance as calculated by Procedure FIT, and the thermal conductivity of Inconel obtained from tabulated data supplied by the International Nickel Company and expressed as a linear function of temperature (degrees Rankine)

$$k = 8.35 + (0.0055)(T-540)$$

The local radiation heat loss was then obtained from the energy balance as the difference between the generation and conduction terms.

A preliminary examination of the heat loss calculations indicated that the technique was not accurate in the region of the lower electrode. In that vicinity there was a considerable amount of conduction

heat transfer through the relatively massive test section flange, and in addition, the very nature of Procedure FIT caused it to yield inaccurate results at the end points of any sequence of values. The test section flange was equipped with several thermocouples spaced radially outward from the test section, and hand calculations showed that the radial energy conduction away from the test section was approximately equal to the energy generated by one inch of test section. In order to compensate for the conduction through the flange, the second derivatives at the first two thermocouples were set equal to zero, and the energy balance conduction terms for the first and second thermocouples were assigned values of 75 percent and 25 percent, respectively, of the energy generated by one inch of test section.

An additional step in the heat loss calculation was performed in order to make the values of the radiation heat loss more amenable to use in a situation involving gas flow. A set of three heat loss runs obtained at different power settings was considered, and a curve of the form

$$q'_{rad} = C_1 t' + C_2 (t')^2 + C_3 (t')^3$$

where $t' = T - 530°R$,

was fitted to the three values of the radiation heat loss available for each test section thermocouple. The set of

constants C_1, C_2, and C_3 was used by the data reduction program to evaluate the radiation heat loss at each thermocouple for the temperature attained in a flow situation. The values of the radiation constants for the first three thermocouples were different from the values characteristic of the other thermocouples on the test section; since the initial portion of the test section never attained a high temperature, no change in the radiation characteristics due to oxidation would be expected in that region. Furthermore, the values of the radiation constants are dependent on the energy transfer by conduction; the somewhat arbitrary assignment of values for the conduction at the first two thermocouples has been discussed previously.

Data Reduction Program

Another computer program was written for the purpose of obtaining conventional heat transfer and friction parameters from the experimentally measured quantities. In addition to Procedure FIT, the program contained a procedure for linear interpolation that could be used as required; the primary use of the interpolation routine was in locating specific values of the gas properties which were placed in the machine memory in tabular form. In addition to the array of gas properties, the program was supplied with the necessary

physical details of the test section and with the experimental data for each run. The output of each thermocouple in millivolts was converted to degrees Fahrenheit by means of NBS Bulletin 561, and the computer program performed a conversion of the input temperatures to the Rankine basis used throughout the calculations.

The data reduction program obtained the thermocouple and pressure tap locations for the heated condition, the local energy generation rate, and the axial heat transfer by conduction through the use of techniques identical to those used in the heat loss program. The radiation heat loss at each thermocouple was calculated from the previously described cubic equation using the constants supplied by the heat loss program. The energy transfer to the gas at each thermocouple was obtained from the local energy generation rate and the conduction and radiation losses by including the extra term in the energy balance for an element of the test section;

$$q'_{gas} = q'_{gen} - q'_{cond} - q'_{rad}$$

The relative magnitudes of the radiation heat loss and the energy transfer to the gas varied during the series of experimental runs; the comparative values of these quantities depended on the type of flow that existed in the tube. During runs that were characterized by a high flow rate and a low heating rate (run 20, run 64) the

heat loss did not exceed three percent of the heat transfer to the gas. Even with high heating rates, the heat loss remained smaller than ten percent of the heat transfer to the gas so long as the flow remained turbulent. However, for the case of laminar flow throughout the tube (run 57), the heat loss attained a value of 30 percent of the heat transfer to the gas. It is interesting to note that, for the transition from turbulent to laminar flow (run 37), the radiation heat loss was about three percent of the heat transfer to the gas near the beginning of the heated length, while in the downstream region the quantities were very nearly equal. The flow area at each thermocouple and pressure tap location was calculated by taking into consideration the radial expansion of the heated test section; this step was of particular importance in the friction factor determination which involved the fifth power of the test section diameter.

The bulk stagnation temperature at each thermocouple location was obtained from a trapezoidal integration of the stagnation enthalpy along the test section. The enthalpy at the temperature of the lower mixer was determined from the stored tables and corrected for the heat transfer by conduction through the test section flange. Thermocouples were provided on the flange so that the radial conduction heat transfer could be

calculated; for calculation purposes it was assumed that the flange was insulated on both faces, and the conduction equation in cylindrical coordinates was used. The heat transfer through the flange was normalized on the mass flow rate and added to the enthalpy of the gas at the inlet mixer temperature to obtain the enthalpy of the gas at the start of the heated length. For the flow runs with precooling, the energy transfer by conduction through the flange was approximately equal to the energy generated by 1/4 of an inch of the test section, or about one percent of the total energy generation. The relationship

$$h_i = h_o + \frac{1}{\dot{m}} \sum_{n=1}^{i} \left(\frac{q'_{gas,n} + q'_{gas,n-1}}{2} \right) (x_n - x_{n-1})$$

was applied for each thermocouple and the gas bulk stagnation temperature at each thermocouple was then obtained by linear interpolation from the enthalpy table. The bulk static temperature of the gas flow was calculated at each thermocouple location from the equation

$$c_{po} (T_{bo} - T_b) = \frac{u_b^2}{2g_c}$$

where $u_b = \frac{GRT_b}{P}$

The result of the implied substitution is a quadratic equation for T_b.

The results of the energy balance and trapezoidal integration described above were checked by a comparison of the predicted bulk stagnation temperature at the end of the test section with the temperature measured at the exit mixer; the agreement between the two values was on the order of five percent for runs during which the heat loss calculations could be considered reliable. There was, however, some doubt about the accuracy of the measured exit temperature since the two thermocouples located in the exit mixer did not produce identical readings. A higher level of confidence in the exit mixer temperature could be established by an examination of the mixer thermocouples; it is possible that the technique used for imbedding the thermocouples in the mixer did not allow a true representation of the temperature of the copper slug.

On the basis of a solution of the governing differential equation and the evidence obtained during the heat loss runs, it was assumed that the temperature on the inside of the test section wall was equal to the temperature measured on the outside of the wall. The heat transfer calculations required the density of the gas at each thermocouple, and this property was obtained from the perfect gas relationship

$$p = \rho RT$$

The local pressure needed in the above calculation was computed by linear interpolation from the overall test section pressure drop and the absolute pressure at the first pressure tap. The results of the calculations described above provided sufficient information for the computation of the various heat transfer parameters from the appropriate definitions.

That portion of the data reduction program that was devoted to friction factor calculations relied on previously obtained properties and conditions at the pressure tap locations, but the primary quantities considered were the measured pressure drops. The procedure employed pairs of pressure drops that involved three pressure taps, and the change in velocity of the gas was taken into account. The wall shear stress was defined as

$$\tau_w = - \frac{D}{4} \frac{d\phi}{dx}$$

where ϕ was the impulse function defined by

$$\phi = p + \frac{\rho u_b^2}{g_c}$$

In the definition of the impulse function, the latter term accounts, on a one dimensional basis, for the increase of momentum due to the acceleration caused by heating of the gas. Sets of pressure drops were considered individually; the impulse function was calculated, and the derivative was obtained from Procedure FIT. The Fanning friction

factor, which was defined in terms of the wall shear stress as

$$f = \frac{\tau_w}{\rho u_b^2/2g_c}$$

was then formed. The remainder of the friction factor portion of the program was devoted to the calculation of other quantities, such as Reynolds numbers, at the pressure tap locations.

The following is a list of the specific steps executed by the computer during the data reduction process; further details are included in the work of Spitler (1967).

1. Read gas properties.
2. Read tube data.
3. Read run data.
4. Convert temperatures to degrees Rankine.
5. Locate thermocouples in expanded position.
6. Locate pressure taps in expanded position.
7. Calculate the local energy generation.
8. Calculate the heat conduction at each thermocouple.
9. Calculate the heat loss by radiation at each thermocouple.
10. Calculate the heat transfer to the gas at each thermocouple.
11. Calculate pressure at each pressure tap and at each thermocouple.
12. Calculate stagnation enthalpy and gas bulk

stagnation temperature at each thermocouple.

13. Calculate flow area in expanded condition at each thermocouple.
14. Calculate wall temperature and expanded flow area at each pressure tap.
15. Calculate bulk static temperature at each thermocouple.
16. Calculate local heat transfer coefficient at each thermocouple.
17. Calculate bulk entry Reynolds number and bulk Reynolds number at each thermocouple.
18. Calculate bulk Nusselt number and Stanton number at each thermocouple.
19. Calculate bulk velocity and Mach number at each thermocouple.
20. Calculate heat flux to gas at each thermocouple.
21. Calculate wall Nusselt number and wall Reynolds number at each thermocouple.
22. Calculate wall-to-bulk temperature ratio and length/diameter ratio at each thermocouple.
23. Calculate bulk and wall heat transfer parameters at each thermocouple.
24. Calculate Graetz number and acceleration parameters at each thermocouple.
25. Calculate bulk velocity and Mach number at each pressure tap.

26. Calculate impulse function at each pressure tap.
27. Calculate wall shear at appropriate pressure taps.
28. Calculate friction factor at appropriate pressure taps.
29. Calculate bulk Reynolds number and Prandtl number at appropriate pressure taps.
30. Calculate wall-to-bulk temperature ratio and wall Reynolds number at appropriate pressure taps.
31. Print the output.

The following pages contain a reproduction of the output of the data reduction program for run number 32, which was chosen as a typical run.

DATABOOK NUMBER= 11 RUN NUMBER= 32
PAGE 1, GENERAL INFORMATION

AIR FLOW, C.COON APPARATUS,TEST SECT NO.1
TEST SECTION 0.250 IN.OD, 0.010 IN.WALL

TEST SECTION VOLTAGE= 4.969 AMPERAGE= 36.000
LOCAL ENERGY GENERATION RATE (BTU/HR IN)= 24.280
INLET MIXER TEMPERATURE (DEGR)= 149.3
MEASURED OUTLET MIXER TEMP (DEGR)= 664.7
CALCULATED OUTLET MIXER TEMP (DEGR)= 710.5

BAROMETRIC PRESSURE (PSI)= 13.350
MASS FLOW RATE (LBM/HR)= 3.984
BULK ENTRY REYNOLDS NUMBER= 19436.0

THERMOCOUPLE INFORMATION

TC	LOC COLD (IN)	LOC HOT (IN)	X/D
1	0.102	0.102	0.443
2	0.283	0.283	1.229
3	0.933	0.932	4.053
4	1.715	1.714	7.454
5	2.707	2.707	11.770
6	4.207	4.210	18.304
7	5.394	5.400	23.478
8	8.193	8.208	35.689
9	11.012	11.039	47.997
10	14.138	14.180	61.652
11	17.102	17.159	74.603
12	20.152	20.225	87.936
13	23.112	23.203	100.881
14	24.831	24.930	108.392

TC	2ND DERIV (DEG/INSQ)	Q COND (BTU/HRIN)	Q RAD (BTU/HRIN)	Q GAS (BTU/HRIN)
1	26.048	0.000	0.685668	23.595
2	137.400	-0.648	-0.240248	25.169
3	-43.559	0.221	0.008487	24.051
4	-23.713	0.129	0.187290	23.964
5	-17.157	0.099	0.635275	23.545
6	-14.380	0.090	1.092899	23.097
7	-13.488	0.088	1.480573	22.712
8	-6.503	0.045	2.285572	21.950
9	-2.537	0.018	2.964871	21.297
10	-1.080	0.008	3.313254	20.959
11	2.223	-0.017	3.808297	20.488
12	-2.277	0.017	4.635306	19.627
13	-71.149	0.553	5.148373	18.579
14	-1316.369	9.073	1.874432	13.333

TC	WALL TEMP (DEG R)	BULK STAG TEMP (DEG R)	BULK STATIC TEMP (DEG R)	ADIABATIC WALL TEMP (DEG R)
1	370.700	171.598	171.592	171.598
2	386.700	176.063	176.056	176.062
3	490.700	192.254	192.246	192.253
4	591.700	210.717	210.707	210.716
5	699.200	234.024	234.012	234.023
6	830.200	269.217	269.201	269.216
7	910.700	296.903	296.883	296.901
8	1026.700	361.261	361.231	361.258
9	1091.700	424.598	424.557	424.594
10	1140.030	493.472	493.416	493.466
11	1176.030	557.628	557.557	557.620
12	1233.700	621.519	621.432	621.509
13	1269.200	680.489	680.385	680.477
14	1016.367	709.016	708.902	709.003

TC	WALL/BULK TEMP RATIO	(TW/TB)**.5	MOD WALL REYNOLDS	WALL NUSSELT
1	2.160	1.470	3724.170	42.131
2	2.196	1.482	3535.297	40.833
3	2.552	1.598	2502.958	22.102
4	2.808	1.676	1968.684	14.612
5	2.980	1.729	1634.825	10.188
6	3.084	1.756	1401.052	7.187
7	3.068	1.751	1321.491	5.997
8	2.842	1.686	1314.752	4.865
9	2.571	1.604	1394.833	4.490
10	2.310	1.520	1508.330	4.411
11	2.109	1.452	1618.952	4.403
12	1.985	1.409	1666.997	4.111
13	1.865	1.366	1741.939	3.962
14	1.434	1.197	2624.192	6.448

TC	HEAT FLUX TO GAS (BTU/HRSF)	HEAT TRANS COEFF (BTU/HRSFDEG)	BULK NUSSELT NUMBER	BULK REYNOLDS NUMBER
1	4707.176	23.641971	88.703	16727.829
2	5020.692	23.835659	87.242	16270.182
3	4794.382	16.064444	54.027	14796.165
4	4773.671	12.529850	38.561	13472.131
5	4686.452	10.074564	28.013	12164.202
6	4592.576	8.186639	19.818	10655.567
7	4512.927	7.352454	16.121	9733.496
8	4357.321	6.548013	12.014	8180.029
9	4225.478	6.334039	9.999	7144.715
10	4156.657	6.428838	8.846	6328.176
11	4062.052	6.568541	8.107	5753.516
12	3889.375	6.353210	7.137	5300.905
13	3680.490	6.251647	6.500	4958.288
14	2646.935	8.611716	8.630	4823.713

TC	WALL PRANDTL	BULK STANTON	BULK PR**0.4	BULK RE**0.8	WALL NU/PR**0.4
1	0.745	0.006296	0.934	2391.947	47.385
2	0.741	0.006390	0.932	2339.450	46.023
3	0.719	0.004410	0.927	2168.299	25.225
4	0.703	0.003525	0.920	2011.634	16.822
5	0.692	0.002893	0.913	1853.817	11.806
6	0.684	0.002396	0.904	1667.482	8.368
7	0.681	0.002175	0.897	1551.012	6.992
8	0.680	0.001964	0.890	1349.596	5.674
9	0.681	0.001911	0.883	1211.122	5.236
10	0.682	0.001947	0.876	1099.064	5.141
11	0.682	0.001991	0.871	1018.466	5.131
12	0.684	0.001925	0.867	953.850	4.786
13	0.685	0.001891	0.864	904.201	4.611
14	0.680	0.002589	0.863	884.515	7.521

TC	VELOCITY (FT/SEC)	MACH NO	PRANDTL NUMBER
1	9.101	0.015	0.842
2	9.336	0.015	0.839
3	10.180	0.016	0.828
4	11.140	0.016	0.812
5	12.352	0.017	0.796
6	14.178	0.018	0.776
7	15.615	0.019	0.761
8	18.959	0.020	0.748
9	22.254	0.022	0.732
10	25.836	0.024	0.718
11	29.170	0.025	0.708
12	32.472	0.027	0.700
13	35.522	0.028	0.693
14	37.170	0.028	0.691

PRESSURE TAP INFORMATION

TAP NUMBERS			BULK REYNOLDS	MOD WALL REYNOLDS	BULK PRANDTL	TW/TB RATIO
2	3	4	9063.9	2143.1	0.754	2.970
3	4	5	7649.0	2038.0	0.740	2.703
4	5	6	6731.2	1995.7	0.725	2.439
5	6	7	6039.5	1950.9	0.713	2.209
6	7	8	5533.4	1974.1	0.704	2.048

TAP NUMBERS			FRICTION FACTOR	BULK F/F BLASIUS	MOD WALL F/F BLASIUS	BULK 16/REYNOLDS
2	3	4	0.009504	1.17378	0.81850	5.38373
3	4	5	0.009436	1.11697	0.80249	4.51077
4	5	6	0.010875	1.24685	0.92006	4.57502
5	6	7	0.012396	1.38322	1.04280	4.67895
6	7	8	0.011261	1.22939	0.95013	3.89442

PARAMETER 1= 1+((TW/TB**.5)/(X/D**.7))
PARAMETER 2= 1+ (1/(X/D**.7))
PARAMETER 3= NU*(TW/TB**.5)/(PAR 1*(PR**.4))
PARAMETER 4= NU*(TW/TB**.5)/(PAR 2*(PR**.4))
PARAMETER 5= GRAETZ NUMBER
PARAMETER 6= (NU/UB**2)(DU/DX)--KAYS
PARAMETER 7= (4/D G**2)(MU/T)(QPP/CP)
PARAMETER 8= (4/H G C)(MU/T)QPP

TC	PARAM 1	PARAM 2	PARAM 3	PARAM 4
1	3.598	2.768	38.808	50.453
2	2.283	1.866	60.756	74.344
3	1.600	1.375	58.185	67.677
4	1.411	1.245	49.786	56.409
5	1.308	1.178	40.565	45.031
6	1.229	1.131	31.326	34.064
7	1.192	1.110	26.409	28.372
8	1.138	1.082	19.991	21.029
9	1.107	1.067	16.409	17.027
10	1.085	1.056	14.150	14.539
11	1.071	1.049	12.622	12.888
12	1.061	1.044	10.930	11.116
13	1.054	1.040	9.752	9.887
14	1.045	1.038	11.464	11.546

TC	PARAM 5	PARAM 6	PARAM 7	PARAM 8
1	0.315E-04	0.189E-07	0.174E-05	0.277E-03
2	0.900E-04	0.164E-06	0.187E-05	0.294E-03
3	0.331E-03	0.161E-06	0.185E-05	0.420E-03
4	0.681E-03	0.156E-06	0.189E-05	0.537E-03
5	0.122E-02	0.156E-06	0.189E-05	0.654E-03
6	0.221E-02	0.154E-06	0.188E-05	0.782E-03
7	0.317E-02	0.152E-06	0.185E-05	0.850E-03
8	0.583E-02	0.146E-06	0.177E-05	0.901E-03
9	0.917E-02	0.140E-06	0.168E-05	0.880E-03
10	0.136E-01	0.133E-06	0.161E-05	0.828E-03
11	0.183E-01	0.126E-06	0.153E-05	0.771E-03
12	0.237E-01	0.118E-06	0.143E-05	0.743E-03
13	0.293E-01	0.107E-06	0.132E-05	0.698E-03
14	0.325E-01	0.378E-08	0.931E-06	0.360E-03

APPENDIX C

UNCERTAINTY ANALYSIS

An analysis was performed for the purpose of predicting the uncertainty in the heat transfer coefficient and the friction factor due to the uncertainty in the experimentally measured quantities. The analysis was conducted according to the technique suggested by Kline and McClintock (1953); uncertainties were attached to the primary measurements based on intuition and instrument specifications, and the propagation of these uncertainties to the calculated quantities was obtained. Table VI contains a list of the uncertainties that were assigned to the experimentally measured quantities and of the uncertainties that were calculated for the results obtained from the measured quantities; the values in Table VI correspond to the downstream region of the tube for run number 44. A comparison of the predicted uncertainties in the heat transfer coefficient and the friction factor with the results displayed graphically in Chapter V indicates that the computed quantities are, in general, within the tolerances specified in Table VI.

Some general comments should be made concerning the prediction of the experimental uncertainties. In the

Table VI Experimental Uncertainties

Measured Quantity	Uncertainty
Voltage	± 0.01%
Current	± 0.25%
Length (Overall)	± 0.04%
Bulk Entry Temperature	± 5.°R
Mass Flow Rate	± 2.%
Tube Diameter	± 1.%
Wall Temperature	± 5.°R
Pressure	± 0.3%
Impulse Function	±10.%

Calculated Quantity	Uncertainty
Radiation Heat Loss	± 5.%
Heat Flux to Gas	± 5.%
Bulk Stagnation Temperature	±32.°R
Bulk Density	± 5.%
Heat Transfer Coefficient	±10.%
Friction Factor	±13.%

interest of convenience, no uncertainties for the gas properties were considered; the properties that were obtained as described in Appendix A were assumed to be precise. Since the perfect gas equation of state was used to compute the density, an uncertainty was calculated for that property and applied to the determination of the uncertainty in the friction factor. The range of the experimental runs was such that the uncertainty in the mass flow rate varied from 1 percent to about 4 percent depending on the position of the float with respect to the flow meter scale for a particular run. It should be noted that the assumption of a 4 percent uncertainty in the mass flow rate produces an uncertainty of 15 percent in the friction factor. Because of the relative precision of the calculation of the local energy generation rate, it was observed that the uncertainty in the heat transfer to the gas was dominated by the uncertainty in the heat losses from the test section. Because the heat transfer to the gas is used in both the calculation of the bulk temperature and the calculation of the heat transfer coefficient, a concerted effort to reduce the uncertainty in the heat loss would manifest itself as a considerable reduction of the uncertainty calculated for the heat transfer coefficient. As experience in the operation of the apparatus and in the accumulation

of experimental data was obtained, a feeling arose among the participating individuals that the data for helium could be expected to have somewhat higher quality than the data for air. This impression was based on the behavior of the various measuring instruments; for example, the condensation problems encountered in the precooled air runs caused, for some runs, severe oscillations of the pressure drop manometers. The performance of the apparatus with helium, however, was in general much more stable.

The dominant factor in the uncertainty of the Nusselt number was the bulk stagnation temperature; the dominant factor in the uncertainty of the friction factor was the impulse function (pressure drop).

APPENDIX D

ELECTRICAL DISCHARGE MACHINING PROCESS

In an attempt to assure good results from the pressure drop measurements, considerable effort was devoted to the drilling of the static pressure tap holes in the wall of the test section. The most common defect in pressure taps is the presence of a burr at the edge of the hole that results from the drilling operation; the burr causes a distortion of the flow stream and erroneous pressure measurements. The hole size is also a factor; the diameter of the pressure tap hole should, in general, be less than ten percent of the tube diameter.

The pressure tap holes associated with the present work were drilled with an Elox Electrical Discharge machine. The configuration of the pressure taps was discussed in Chapter III, and it was stated that the holes were drilled after the pressure tap tubes had been brazed to the test section (see Figure 1). Prior to the machining of the test section, several models were constructed using the same materials, and various drilling techniques were used to obtain sample holes. The sides of the models were cut away, and the holes were examined from the inside with a metallurgical microscope. The

electrical discharge process was found to yield consistently better results than the other techniques that were tested.

The conventional electrical discharge process made use of an electrode of brass tubing through which a continuous flow of dielectric oil was maintained for cooling and chip removal. Since the available electrode tubing was larger than the desired hole size, an electrode made from 0.005 inch diameter tungsten wire was used; oil flow was maintained over the surface of the wire. In operation, the spindle of the machine moved the electrode downward until a spark jumped from the electrode to the test section wall; the spindle then withdrew and the cycle was repeated. A sleeve of Teflon tubing was provided for the inside of the pressure tap tube in order to prevent wandering of the electrode tip and the possibility of the occurrence of a spark between the electrode and the pressure tap tubing. Considerable practice on the part of the operator was obtained before the drilling of the actual test section was attempted; specific details of the technique, such as capacitor settings, spindle settings, and insulation configurations, were recorded in the files of the Energy, Mass, and Momentum Transfer Laboratory.

The development of the drilling technique suggested several improvements that could be made in the general area of pressure tap construction. It was noticed that the localized heating required for the brazing operation caused temporary distortions of the test section tubing, and permanent changes in the flow area at the tap location were possible. A furnace brazing process might alleviate this problem, but a jig of the test section material would be required in order to maintain the proper relationship between the test section and the pressure tap tubes. A means of inspecting the inside of the test section would be most desirable; recent developments in the area of fiber optics suggest that internal inspection might be possible. Another contribution to the construction of pressure taps would be the development of honing, polishing, and measuring techniques applicable to the completed test section.

NOMENCLATURE

English Symbols

A	area
c	speed of sound
c_p	specific heat at constant pressure
D	tube diameter
g_c	dimensional constant 32.174 (lbm) (ft) / (lbf) (sec^2)
h	heat transfer coefficient
H	enthalpy
k	thermal conductivity
K	acceleration parameter, $\frac{\nu}{u_\infty^2} \frac{du_\infty}{dx}$
K_ϕ	transition parameter, $\frac{4}{G^2 D} \frac{\mu}{T} \frac{q''}{c_p}$
l	length
$\dot{m}$	mass flow rate
p	pressure
q	heat transfer rate
q'	lineal heat transfer rate
q''	heat flux
r	coordinate in radial direction
R	tube radius

T	temperature
t'	temperature difference
u	velocity in axial or x direction
$\bar{u}$	mean velocity
x	coordinate
y	coordinate
Y	parameter of Bankston, et. al. (1966)

Greek Symbols

α	expansion coefficient
ε	unit thermal expansion
θ	momentum thickness, defined in Chapter V
μ	absolute viscosity
ν	kinematic viscosity
ρ	density
τ	shear stress
χ	parameter of Back, et. al. (1964)

Dimensionless Groups

C_f	skin friction coefficient, $\tau_w/[\rho u_\infty^2/2g_c]$
f	friction factor, $\tau_w/[\rho u_b^2/2g_c]$
Nu	Nusselt number, hD/k
Pr	Prandtl number, $\mu c_p/k$
Re	Reynolds number, $\rho\bar{u}D/\mu$ or $4\dot{m}/\pi\mu D$

Re_θ Reynolds number based on momentum thickness, $\rho\bar{u}\theta/\mu$

Subscripts

b evaluated at bulk temperature

cp constant properties

c "critical" condition

cl centerline

e edge of boundary layer

o stagnation conditions

w wall

∞ free stream condition

LIST OF REFERENCES

Ambrok, G. S. (1957) "Approximate Solution of Equations for the Thermal Boundary Layer with Variation in Boundary Layer Structure." Soviet Physics, 2(II), 1979.

Back, L. H. and R. A. Seban. (1967) "Flow and Heat Transfer in a Turbulent Boundary Layer with Large Acceleration Parameter." Heat Transfer and Fluid Mechanics Institute, Stanford University Press.

Back, L. H., P. F. Massier and R. F. Cuffel. (1966) "Some Observation on Reduction of Turbulent Boundary-Layer Heat Transfer in Nozzles." AIAA J., 4, 2226.

Back, L. H., P. F. Massier and H. L. Gier. (1964) "Convective Heat Transfer in a Convergent-Divergent Nozzle." Int. J. Heat and Mass Transfer, 7, 549.

Bankston, C. A. (1965) "Fluid Friction, Heat Transfer, Turbulence, and Interchannel Flow Stability in the Transition from Turbulent to Laminar Flow in Tubes." D. Sc. Dissertation, University of New Mexico.

Bankston, C. A., W. L. Sibbitt and V. J. Skoglund. (1966) "Stability of Gas Flow Distribution Among Parallel Heated Channels." AIAA 2nd Propulsion Joint Specialist Conference, AIAA Paper 66-589.

Barnes, J. F. (1960) "An Experimental Investigation of Heat Transfer from the Inside Surface of a Hot Smooth Tube to Air, Helium and Carbon Dioxide." Pyestock, Hants (Great Britain), N.G.T.E.:R. 241.

Boldman, D. R., J. F. Schmidt and R. C. Ehlers. (1967) "Effect of Uncooled Inlet Length and Nozzle Convergence Angle on the Turbulent Boundary Layer and Heat Transfer in Conical Nozzles Operating with Air." J. Heat Transfer, 89, 341.

Cannon, J. C. (1965) "Heat Transfer from a Fluid Flowing Inside a Rotating Cylinder." Ph.D. Thesis, Mechanical Engineering Department, Stanford University.

Cooper, L. R. (1967) "Immersion Gold Plating of Inconel 600." EMMT Lab-TM-7, Aerospace and Mechanical Engineering Department, University of Arizona.

Cremers, C. J. and E. R. G. Eckert. (1962) "Hot-Wire Measurements of Turbulence Correlations in a Triangular Duct." J. Applied Mechanics, 19, 609.

Davenport, M. E. and G. Leppert. (1965) "The Effect of Transverse Temperature Gradients on the Heat Transfer and Friction for Laminar Flow of Gases." J. Heat Transfer, 87, 191.

Davenport, M. E., P. M. Magee and G. Leppert. (1962) "Thermocouple Attachment to a Direct Current Heater." J. Heat Transfer, 84, 187.

Eckert, E. R. G. and R. M. Drake. (1959) Heat and Mass Transfer, 2nd Ed., McGraw-Hill Book Company.

Eckert, E. R. G. and T. F. Irvine, Jr. (1956) "Flow in Corners of Passages with Non-Circular Cross-Sections." Trans. ASME, 78, 709.

Eckert, E. R. G. and T. F. Irvine, Jr. (1960) "Pressure Drop and Heat Transfer in a Duct with Triangular Cross Section," J. Heat Transfer, 82, 125.

Franklin Institute. (1961) Thermodynamic Properties of Helium and Molecular Nitrogen. Preliminary draft, tables prepared by the Franklin Institute for the U.S. Atomic Energy Commission. NYO 9786.

Hatton, A. P. (1965) "Heat Transfer through the Turbulent Incompressible Boundary Layer in the Presence of Moderate Pressure Gradient." Int. J. Heat and Mass Transfer, 8, 1469.

Hess, W. G. (1965) "Thermocouple Conduction Error with Radiation Heat Loss." M.S. Thesis, Aerospace and Mechanical Engineering Department, The University of Arizona.

Hilsenrath, J., et. al. (1960) Tables of Thermodynamic and Transport Properties of Air, Argon, Carbon Dioxide, Carbon Monoxide, Hydrogen, Nitrogen, Oxygen, and Steam. Pergamon Press. Also NBS Circular 564.

Hottel, H. C. and A. F. Sarofim. (1967) Radiative Transfer. McGraw-Hill Book Company.

Humble, L. V., W. H. Lowdermilk and L. G. Desmon. (1951) "Measurements of Average Heat Transfer Coefficients for Subsonic Flow of Air in Smooth Tubes at High Surface and Fluid Temperatures." NACA Report 1020.

Kays, W. M. (1966) Convective Heat and Mass Transfer. McGraw-Hill Book Company.

Kline, S. J. (1967) "Observed Structure Features in Turbulent and Transitional Boundary Layers," Fluid Mechanics of Internal Flow, G. Souran, ed., Elsevier Publishing Company.

Kline, S. J. and F. A. McClintock. (1953) "The Description of Uncertainties in Single Sample Experiments." Mechanical Engineering, 75, 38.

Launder, B. E. (1964) "Laminarization of the Turbulent Boundary Layer by Acceleration." Massachusetts Institute of Technology Gas Turbine Laboratory, Report No. 77.

McCarthy, J. R. and H. Wolf. (1960) "The Heat Transfer Characteristics of Gaseous Hydrogen and Helium." Rocketdyne, Canoga Park, California, RR-60-12.

McEligot, D. M. (1963) "The Effect of Large Temperature Gradients on Turbulent Flow of Gases in the Downstream Regions of Tubes." Ph.D. Dissertation, Stanford University. (TID-19446).

McEligot, D. M., P. M. Magee and G. Leppert. (1964) "Effect of Large Temperature Gradients on Convective Heat Transfer: The Downstream Region." J. Heat Transfer, 87, 67.

McEligot, D. M., L. W. Ormand and H. C. Perkins, Jr. (1966) "Internal Low Reynolds Number Turbulent and Transitional Gas Flow with Heat Transfer." J. Heat Transfer, 88, 239.

Moretti, P. M. and W. M. Kays. (1964) "Heat Transfer through an Incompressible Turbulent Boundary Layer with Varying Free-Stream Velocity and Varying Surface Temperature." Thermosciences Division, Mechanical Engineering Department, Stanford University, PG-1.

Moretti, P. M. and W. M. Kays. (1965) "Heat Transfer to a Turbulent Boundary Layer with Varying Free-Stream Velocity and Varying Surface Temperature - An Experimental Study." Int. J. Heat and Mass Transfer, 8, 1187.

Perkins, H. C. and P. M. Worsoe-Schmidt. (1965) "Turbulent Heat and Momentum Transfer for Gases in a Circular Tube at Wall-to-Bulk Temperature Ratios to Seven." Int. J. Heat and Mass Transfer, 8, 1011.

Persh, J. (1956) "A Study of Boundary Layer Transition from Laminar to Turbulent Flow." NAVORD Report No. 4339.

Preston, J. H. (1958) "The Minimum Reynolds Number for a Turbulent Boundary Layer and the Selection of a Transition Device." J. of Fluid Mech., 3, 373.

Reynolds, H. C. (1968) "Internal Low Reynolds Number Turbulent Heat Transfer." Ph.D. Dissertation, The University of Arizona.

Richards, B. E. and J. L. Stollery. (1966) "Further Experiments on Transition Reversal at Hypersonic Speeds." AIAA J., 4,2224.

Schlichting, H. (1960) Boundary Layer Theory, 4th Ed. McGraw-Hill Book Company.

Schlichting, H. and A. Ulrich. (1942) "Zur Berechnung des Umschlages Laminar-Turbulent." Jahrbuch d. dt-Luftfahrtforschung I, 8.

Schraub, F. A. and S. J. Kline. (1965) "A Study of the Structure of the Turbulent Boundary Layer with and without Longitudinal Pressure Gradients." Thermo-sciences Division, Mechanical Engineering Department, Stanford University, Report MD-12.

Senoo, Y. (1958a) "The Boundary Layer on the End Wall of a Turbine Nozzle Cascade." J. Heat Transfer, 80, 1711.

Senoo, Y. (1958b) "Three-Dimensional Laminar Boundary Layer in Curved Channel with Acceleration." J. Heat Transfer, 80, 1721.

Sergienko, A. H. and V. K. Gretsov. (1959) "Transition from a Turbulent into a Laminar Boundary Layer." S. S. Doklady, 4, 275.

Sibulkin, M. (1962) "Transition from Turbulent to Laminar Pipe Flow." The Physics of Fluids, 5, 280.

Spitler, J. V., Jr. (1967) "Data Reduction for a High Temperature Gas Loop (Air)." Master's Report, Aerospace and Mechanical Engineering Department, The University of Arizona.

Sternberg, J. (1954) "Transition from a Turbulent to a Laminar Boundary Layer." Ballistics Research Laboratory Report No. 906.

Svehla, R. A. (1962) "Estimated Viscosities and Thermal Conductivities of Gases at High Temperatures." NASA TR-R-132.

Wilson, M. P. (1960) "Thermodynamic and Transport Properties of Helium." General Dynamics, GA-1355.

Wisniewski, R. J. and J. R. Jack. (1961) "Recent Studies on the Effect of Cooling on Boundary-Layer Transition at Mach 4." J. of the Aerospace Sciences, March, 1961, 250.

Worsoe-Schmidt, P. M. and G. Leppert. (1965) "Heat Transfer and Friction for Laminar Flow of Gases in a Circular Tube at High Heating Rates." Int. J. Heat and Mass Transfer, 8, 1281.